

AD-766 508

INVESTIGATION OF BILINEAR THERMOVISCOE-
LASTIC BEHAVIOR OF ROCKS

James S. Lai

Utah University

Prepared for:

Bureau of Mines

10 June 1973

DISTRIBUTED BY:

NTIS

National Technical Information Service
U. S. DEPARTMENT OF COMMERCE
5285 Port Royal Road, Springfield Va. 22151

INVESTIGATION OF BILINEAR THERMOVISCOELASTIC
BEHAVIOR OF ROCKS

by

James S. Lai

Final Report submitted to:

U. S. Department of Interior
Bureau of Mines
Twin Cities Mining Research Center
Twin Cities, Minnesota

Contract No. H0220009

Reproduced by
NATIONAL TECHNICAL
INFORMATION SERVICE
U.S. Department of Commerce
Springfield, VA. 22151

June 1973



Civil Engineering Department
College of Engineering
University of Utah
Salt Lake City, Utah 84112

DISTRIBUTION STATEMENT A

Approved for public release;
Distribution Unlimited

AD 766508

FINAL REPORT

APRA Order Number: 1579

Contract Number H0220009

Program Code Number: 2F10

Principal Investigator and
Telephone Number:

J. S. Lai, (801) 581-6813
(801) 581-6931

Name of Contractor:
University of Utah

Effective Date of Contract:
1 January 1972

Short Title of Work:
Investigation of Bilinear Thermovisco-
elastic Behavior of Rocks

Contract Expiration Date:
31 May 1973

Amount of Contract:
\$ 36,800.00

Sponsored by

Advanced Research Project Agency
ARPA Order No. 1579, Amend. No. 3
Program Code 2F10

The views and conclusions contained in this document are those of the authors and should not be interpreted as necessarily representing the official policies, either expressed or implied, of the Advanced Research Project Agency or the U. S. Government.

FORWARD

This research was supported by the Advanced Research Project Agency of the Department of Defense and was monitored by Dr. John B. Cheung of the Twin Cities Mining Research Center, U.S. Bureau of Mines under Contract No. H0220009.

CONTENTS

FIGURES

TABLES

SUMMARY

1.	INTRODUCTION	1
2.	BILINEAR ELASTIC AND VISCOELASTIC THEORIES	6
2.1	Bilinear Elastic Constitutive Relations	7
2.2	Bilinear Viscoelastic Constitutive Relations	21
2.3	Beam Under Pure Bending	25
2.4	Formulation of Plane Stress Problems	34
2.5	Stress Analysis of a Circular Opening Under Internal Pressure	37
2.6	Solution of a Circular Disk Under Diametral Compression	42
	Finite Difference Approximation	42
	Orthotropic Plate Solution Using Finite Element Techniques	48
	Comparison Between Linear, Bilinear and Orthotropic Solutions	48
3.	EXPERIMENTAL INVESTIGATION	50
3.1	Materials and Specimens	50
3.2	Compression Apparatus and Testing Procedures	50
3.3	Tension Apparatus and Testing Procedures	56
3.4	Diametral Compression and Beam Bending Testing Apparatus and Procedures	60
3.5	Experimental Results of Charcoal Granite	61
	Compression Tests	61
	Tension Tests	85

AD-766508
3200.8 (Att 1 to Encl 1)
Mar 7, 66

Unclassified

Security Classification

DOCUMENT CONTROL DATA - R & D		
(Security classification of title, body of abstract and indexing annotation must be entered when the overall report is classified)		
1. ORIGINATING ACTIVITY (Corporate author) Civil Engineering Department University of Utah Salt Lake City, Utah 84112		20. REPORT SECURITY CLASSIFICATION Unclassified
2. REPORT TITLE Investigation of Bilinear Thermoviscoelastic Behavior of Rocks -- Final Report		20. GROUP
4. DESCRIPTIVE NOTES (Type of report and inclusive dates) Final Report (1 January - 31 May 1973)		
5. AUTHOR(S) (First name, middle initial, last name) Dr. James S. Lai		
6. REPORT DATE June 10, 1973	70. TOTAL NO. OF PAGES 112 117	70. NO. OF REFS 22
10. CONTRACT OR GRANT NO. HO220009	90. ORIGINATOR'S REPORT NUMBER(S)	
8. PROJECT NO. ARPA Order No. 1579	90. OTHER REPORT NO(S) (Any other numbers that may be assigned this report)	
9. PROGRAM CODE NO. 2F10		
10. DISTRIBUTION STATEMENT Unlimited		
11. SUPPLEMENTARY NOTES		12. SPONSORING MILITARY ACTIVITY Advanced Research Project Agency Washington, D.C. 20401
13. ABSTRACT <p>The objective of the work reported herein was to investigate the effect of temperature on the elastic and viscoelastic properties of charcoal granite and Dresser basalt under uniaxial tension and compressions. Also, the effect of the difference in tensile and compressive properties on the stress analysis, in general, and on the stress and strain distribution of a beam under bending and a disk under diametral compression, in particular, were analyzed.</p> <p>Experimental results indicate that at higher temperature both materials exhibit time dependency while at low temperature the time-dependency is negligible.</p> <p>Both the experimental and theoretical analyses obtained in this study will add to the understanding of the time-dependent properties of rocks and the effect of these time-dependent properties of rocks to the stability of underground structures, particularly under a severely high temperature environment.</p>		

DD FORM 1473
1 NOV 64

Unclassified

Security Classification

Unclassified

Security Classification

3200.8 (Att 1 to Encl 1)
Mar 7, 66

14. KEY WORDS	LINK A		LINK B		LINK C	
	ROLE	WT	ROLE	WT	ROLE	WT
Bilinearity						
Thermoviscoelasticity						
Creep of rocks						
Time-temperature Superposition Principle						
Beam						
Diametral Compression						
Bilinear elasticity						
Bilinear viscoelasticity						
Creep Compliance						
Charcoal granite						
Dresser basalt						

Unclassified

Security Classification

2

11

CONTENTS (Continued)

3.6	Experimental Results of Dresser Basalt	87
	Compression Tests	87
	Tension Tests	92
3.7	Diametral Compression and Beam Bending Test Results	93
4.	CONCLUSIONS	99
	REFERENCES	100

FIGURES

1.	Linear Elastic and Bilinear Elastic Stress-Strain Relations	8
2.	Uniaxial Tension and Compression; and Definition of E_r , E_c , ν_T , ν_c	9
3.	Triaxial Principal Stress State	11
4.	Stress and Strain Criteria of Bilinear Stress-Strain Relations	14
5.	Transformation of Stress Components	18
6.	Definitions of $J_T(t)$, $J_c(t)$, $\nu_T(t)$, $\nu_c(t)$	23
7.	Simply Supported Beam Under Pure Bending	26
8.	(a) Strain Distributions and Location of Neutral Axes of Linear and Bilinear Viscoelastic Beams Under Pure Bending	32
	(b) Stress Distributions of Linear and Bilinear Viscoelastic Beam Under Pure Bending	33
9.	Thick Walled Cylinder Under Internal Pressure	38
10.	A Circular Disk Under Diametral Compression	43
11.	A Square Grid Laid Upon the First Quadrant of the Circular Disk	46
12.	Comparison of Linear, Bilinear and Orthotropic Solutions of A Disk Under Diametral Compression	47
13.	Compression Apparatus	52
14.	Schematic Diagram of Compression Test Apparatus	53
15.	Tension Apparatus	57
16.	Tension Apparatus (Schematic Diagram)	58
17.	Tension Grip	59
18.	Test Program for Charcoal Granite in Compression	62
19.	Axial Stress-Strain Relations for Charcoal Granite	63
20.	Determination of Threshold Stress and Strain for Charcoal Granite	65
21.	Threshold Stress vs. Temperature	66
22.	Poisson's Ratio vs. Temperature for Charcoal Granite	67

FIGURES (Continued)

23. Creep Strains vs. Time Under Multi-Step Loading	69
24. Creep Strains vs. Time Under Multi-Steps Loading	70
25. Irrecoverable Strain vs. Temperature for Charcoal Granite	72
26. Initial Strain vs. Temperature for Charcoal Granite	73
27. Stress-Strain Relation of An Ideal Locking Material	74
28. A Compression Model for Charcoal Granite	75
29. Comparison of the Theoretical Prediction vs. Experimental Results	77
30. Comparison of the Theoretical Prediction vs. Experimental Results	78
31. Comparison of the Theoretical Prediction vs. Experimental Results	79
32. Comparison of the Theoretical Prediction vs. Experimental Results	80
33. Comparison of the Theoretical Prediction vs. Experimental Results	81
34. Comparison of the Theoretical Prediction vs. Experimental Results	82
35. Comparison of the Theoretical Prediction vs. Experimental Results	83
36. Comparison of the Theoretical Prediction vs. Experimental Results	84
37. Tensile Young's Modulus vs. Temperature for Charcoal Granite	86
38. Creep Curves for Dresser Basalt Under Compressive Stresses	89
39. Creep Curves for Dresser Basalt Under Compressive Stresses	90
40. Compression Elastic Modulus of Dresser Basalt at vs. Temperature	91
41. Log-Log Plots of Creep Curves for Dresser Basalt Under Compressive Stresses	93
42. Tensile Creep Curves of Dresser Basalt	94
43. Diametral Compression Test Results (Charcoal Granite)	96
44. Diametral Compression Test Results (Charcoal Granite)	97
45. Beam Test Results (Charcoal Granite)	98

TABLES

1. Young's Moduli in Tension and Compression	5
2. Material Properties	51
3. Compression Creep Test Program and Results for Dresser Basalt	88

SUMMARY

The objective of the work reported herein was to investigate the effect of temperature on the elastic and viscoelastic properties of charcoal granite and Dresser basalt under uniaxial tension and compression. Also, the effect of the difference in tensile and compressive properties on the stress analysis, in general, and on the stress and strain distribution of a beam under bending and a disk under diametral compression, in particular, were analyzed.

Uniaxial compressive and tensile tests on charcoal granite and Dresser basalt at elevated temperatures were conducted. For charcoal granite under uniaxial compression, the results indicate that at lower temperature (75°F to 500°F) the stress-strain relations are time-independent; above that, the stress-strain relations become time-dependent. Under uniaxial tension, charcoal granite is elastic though the elastic modulus depends on temperature. Results of uniaxial tension and compression tests on Dresser basalt indicate that both the tensile and compressive stress-strain relations exhibit time-dependency only at higher temperature (about 450°F).

A general bilinear elastic and viscoelastic theories were formulated and some interesting results as the consequence of the bilinearity were obtained. Three boundary value problems, a beam under pure bending, a circular opening under internal pressure and a disk under diametral compression were analyzed. The results indicate that when tensile modulus is smaller than the compressive modulus, the critical tensile stresses in these problems tend to be decreasing.

Diametral compression and bending tests were conducted on charcoal granite. The experimental results of maximum tensile and compressive strain in the beam and the tensile and compressive strains at the center of the disk seem can be predicted from the linear elastic solutions.

The results obtained in this study will add to the understanding of the time-dependent properties of rocks and the effect of the time-dependent properties of rocks to the stability of the underground structures, particularly under severe high temperature environment.

1.0 INTRODUCTION

The requirement for improving the safety of underground structures for obtaining minerals deep in the earth such as mine pillars, for the economic storage of food, chemicals, medical supplies, etc., for the civil work such as dams, subways, transportation tunnels, and for underground military installations, a better understanding of the fundamental mechanical properties of rocks is needed. In general, rocks are considered to be an elastic material under relatively short duration of loading at normal temperatures. The creep behavior of rock appears to be significant under loading which acts over a long period of time or for short as well as long term loading under elevated temperature. Therefore, if underground structures are expected to be in service for a long period, the time and temperature dependent properties of rock materials need to be investigated more thoroughly.

Many tests have been performed on a large number of rock types under different loading and environmental conditions in an attempt to determine the time-dependent deformation and to develop the constitutive equation relating strain as a function of stress state, time, temperature and other related variables such as water content, loading rate, etc. It is found that most of the observed creep test results for a number of rock types can be expressed in the following form:

$$\epsilon = \epsilon_e + \epsilon_c + Bt$$

where ϵ_e is the elastic strain, Bt is the steady-state creep and ϵ_c is the transient or primary creep. Tertiary creep is not included because laboratory studies indicate that its duration is usually so short that, once it is initiated, failure cannot be arrested. Griggs [1]* indicated that the transient creep in Solenhofen limestone specimen, loaded for 550 days in uniaxial

*Numbers in brackets refer to references.

compression at approximately 50% of its crushing strength, was logarithmic and could be expressed by

$$\epsilon = (6.1 + 5.21 \log t) 10^{-5}$$

Not only is tertiary creep not included but also a term for steady state creep was either absent or negligible. However, under confined pressure, it was found that the creep rate in the same limestone should include a steady state term and the departure from strictly logarithmic creep was observed within 10 minutes after start of the test. However, in relating to the design of rock structure, this duration is too short to be considered. Höfer [2] measured the lateral deformation in pillars in a number of German potash (halite plus sylvite) mines and showed that the lateral deformation rate was constant for periods ranging from 63 days to nearly 10 years and strain rates up to 4 per cent per year. Micro-seismic investigation indicated however that there is a period of accelerated movement of in-situ rock preceding failure [3]. This period may range from a few hours to several weeks depending on the size of the rock. Thus it can be interpreted that in-situ rock exhibits varying degrees of transient creep, steady-state creep and tertiary creep.

Results from previous reports [1,4,5,6] indicated that the time-dependent behavior of rock is strongly affected by temperature. Hokao [7] measured the change of the strength and Young's modulus, in tension and compression, of rocks caused by temperature changes. Photomicrographs indicated that decrease in the strength at elevated temperature might be caused by the expansion of minerals, especially the quartz component at its α - β

transition temperature, in which many cracks were being observed. Le Comte [5] performed creep experiments at constant load on polycrystalline halite and showed that it is also possible to induce large permanent strain without confining pressure provided that the temperature is sufficiently high. Byerlee [8] indicated that at higher confining pressure and at elevated temperature, intracrystalline deformation mechanisms can also occur. In the study of the short time thermoviscoelastic behavior of Charcoal granite and Dresser basalt at elevated temperatures (up to 1000°C), Fischer and Cheung [9] found that the creep compliance data could be treated as a thermorheologically simple material in which time-temperature superposition principle is applicable.

In uniaxial compressive, creep tests of rocks, many researchers [10,11, 12,13] observed that rocks deformed more in the initial stage of loading. Brace [11] showed that the strain-stress behavior of rock is strongly nonlinear at low stress. Morgenstern [13] found, for sandstone, that when the sum of the principal stresses is greater than about 1600 psi, the modulus of rigidity becomes a constant and the stress-strain relation is nonlinear when the stress is below that level. A similar stress-strain relation was mentioned by Prager [14] from testing living soft tissues, granular materials and show which deform more freely under small stress until a certain strain level is reached after which the stiffness of the materials increase rapidly.

Most creep results available for rock are from compression tests. There have been very few results of creep in tension. It is known that the tensile strength of rocks is very small in comparison to its compressive strength and that the modulus of rocks in tension is different from that in creep compression. Also, the time-dependent properties of rocks under tensile

stress are relatively unknown. Although many rock structures are designed such that stress states in an entire structure are compressioned, situations do occur in which part of the structure is subjected to tensile stress, and, under this situation tensile properties of rocks are extremely important.

If the stress-strain relations under tension and compression are different, the conventional linear elastic and/or linear viscoelastic solutions of various boundary value problems relating to the rock structures can introduce erratic results as indicated by Haimson and Tharp [15]. Under this condition, the bilinear behavior, in which the tensile modulus (E_T) and compressive modulus (E_C) are considered to be different, should be incorporated in the theoretical analysis. The tensile and compressive Young's moduli of certain rock types are shown in Table I.

Very little literature can be found at the present time in the area of bilinear analyses. Ambartsumyan and Khachatryan [16] have presented the basic formulations of bilinear elastic theory. Herrmann [17], Haimson and Tharp [15] and Blatz and Levinson [18] investigated the problem of thick-walled cylinders.

The objective of the research carried out herein are:

- (1) Experimental investigations of the time and temperature dependent properties of rocks with emphasis on investigating the different response under tensile and compressive stresses;
- (2) Theoretical investigation of the stress-strain distribution of a beam, a diametrically loaded disc of rocks using bilinear stress-strain relations; and
- (3) Comparison of the theoretical predictions of the beam and the diametrically loaded disc with the experimental results.

TABLE I - YOUNG'S MODULI IN TENSION AND COMPRESSION

Rock Type	E_t (10^6 psi)	E_c (10^6 psi)	$\phi^2 = E_t/E_c$
Westerly granite ⁸	2.5	10.5	0.24
Austin limestone ⁶	1.7	2.3	0.74
Carthage limestone ⁶	5.1	9.2	0.55
Indiana limestone ⁶	1.6	3.9	0.41
Indiana limestone ⁷	2.5	4.9	0.51
Georgia marble ⁸	3.4	6.1	0.56
Tennessee marble ⁸	7.7	11.1	0.69
Russian marble ⁸	1.3	3.0	0.43
Star Mine quartzite ⁸	11.0	11.0	1.00
Arizona sandstone ⁶	1.7	6.6	0.26
Berea sandstone ⁹			0.50
Millsap sandstone ⁶	0.1	1.9	0.05
Tennessee sandstone ⁶	0.2	2.4	0.08
Russian sandstone ¹	1.7	8.3	0.21

2.0 BILINEAR ELASTIC AND VISCOELASTIC THEORIES

The constitutive relations governing an isotropic linear elastic material can be expressed by the following equations:

$$\sigma_{ij} = \lambda \epsilon_{kk} \delta_{ij} + 2G \epsilon_{ij} \quad (1)$$

The constant λ and G are called Lamé's constants, where

$$G = \frac{E}{2(1+\nu)} \quad (2)$$

is the modulus of elasticity in shear, E is the elastic modulus (Young's modulus), ν is the Poisson's ratio, and

$$\lambda = \frac{E\nu}{(1+\nu)(1-2\nu)} = \frac{2G}{1-2\nu} \quad (3)$$

Inverting (1) to solve for the strain tensor ϵ_{ij} yields

$$\epsilon_{ij} = \frac{1+\nu}{E} \sigma_{ij} - \frac{\nu}{E} \sigma_{kk} \delta_{ij} \quad (4)$$

It can be shown, such as (3) and (4) that there are only two material constants for a linear elastic material.

For (isotropic) linear viscoelastic materials, the following governing constitutive relations can be obtained:

$$\sigma_{ij}(t) = 3\delta_{ij} \int_0^t K(t-\xi) \frac{\partial \epsilon_{kk}(\xi)}{\partial \xi} d\xi + 2 \int_0^t G(t-\xi) \frac{\partial \epsilon_{ij}(\xi)}{\partial \xi} d\xi \quad (5)$$

or alternatively,

$$\epsilon_{ij}(t) = \delta_{ij} \int_0^t J_1(t-\xi) \frac{\partial \sigma_{kk}(\xi)}{\partial \xi} d\xi + \int_0^t J_2(t-\xi) \frac{\partial \sigma_{ij}(\xi)}{\partial \xi} d\xi \quad (6)$$

Again, there are only two independent time functions $K(t)$, $G(t)$, or $J_1(t)$ and $J_2(t)$ or their equivalent forms for a linear viscoelastic material.

Equation (1), implies that under the infinitesimal uniaxial tension and compression strain, the magnitude of the stress output are the same. This fundamental assumption has been verified experimentally to be true or nearly so for most of the materials. Based on this assumption, theories of linear elasticity and linear viscoelasticity have been developed.

Strictly speaking, however, almost every material behaves differently in tension and compression. This is particularly true for composite materials, such as rocks, concrete, soil, asphalt concrete, solid propellants, etc., as the mechanisms of deformation induced by tensile and compressive stresses are different. Therefore, the stress-strain relations under tension and compression are different. Because of this, the linear elastic and viscoelastic theories which assume a unique modulus for tension and compression may not be able to describe the stress and strain distribution accurately.

It is the objective of this chapter to explore the theoretical implications of bilinearity derived from the behavior of materials. The term "bi-linear" is used in this report to refer to the behavior of materials having different linear stress-strain relations under tension and compression, see Figure 1.

2.1 Bilinear Elastic Constitutive Relations

For a bilinear elastic material subjected to uniaxial tension and compression tests as shown in Figure 2, four material constants E_T , E_C , ν_T , and ν_C are obtained. These four constants are defined as follows:

$$\begin{aligned} E_T &= \frac{\sigma_T}{\epsilon_T} \\ E_C &= \frac{\sigma_C}{\epsilon_C} \\ \nu_T &= - \left[\frac{b_T - b_0}{b_0} \right] / \epsilon_T \\ \nu_C &= - \left[\frac{b_C - b_0}{b_0} \right] / \epsilon_C \end{aligned} \tag{7}$$

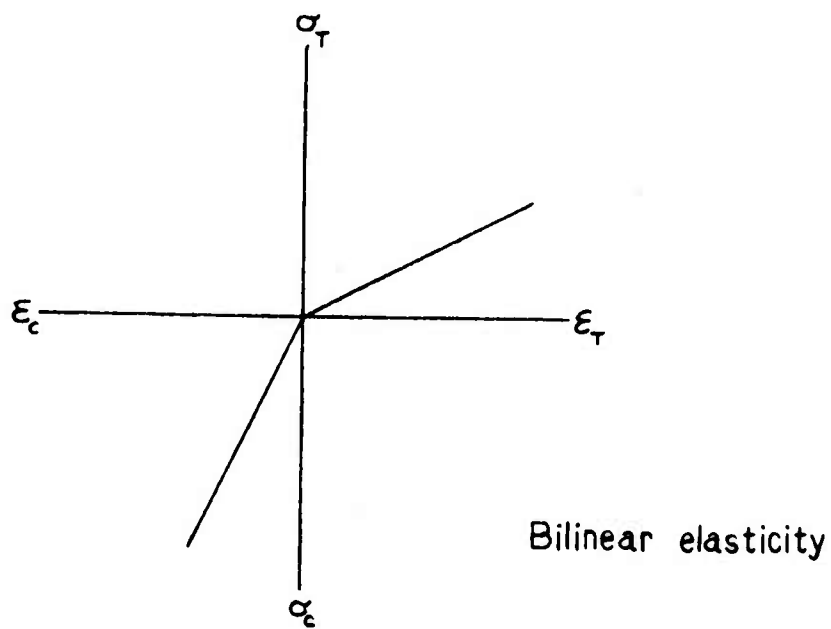
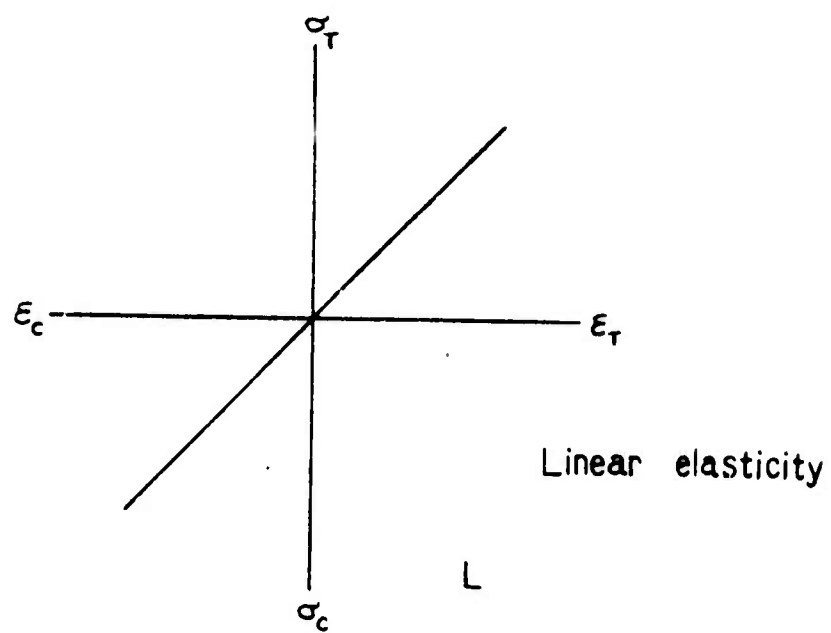
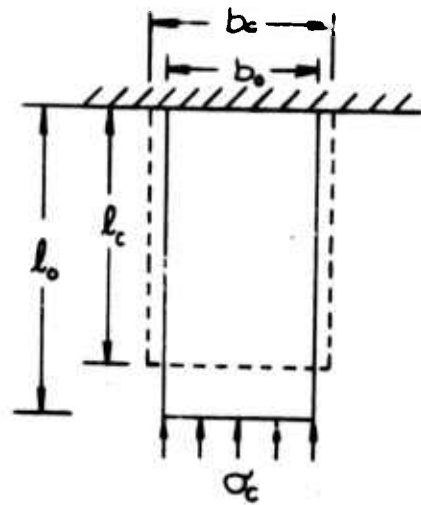
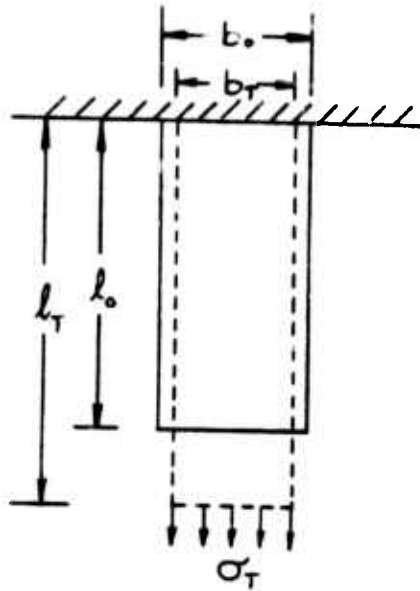


FIGURE 1 Linear Elastic and Bilinear Elastic Stress-Strain Relations



$$\epsilon_T = \frac{l_T - l_0}{l_0}$$

$$\epsilon'_T = \frac{b_T - b_0}{b_0}$$

$$E_T = \frac{\sigma_T}{\epsilon_T}$$

$$\nu_T = -\frac{\epsilon'_T}{\epsilon_T}$$

$$\epsilon_c = \frac{l_c - l_0}{l_0}$$

$$\epsilon'_c = \frac{b_c - b_0}{b_0}$$

$$E_c = \frac{\sigma_c}{\epsilon_c}$$

$$\nu_c = -\frac{\epsilon'_c}{\epsilon_c}$$

FIGURE 2 Uniaxial Tension and Compression; and Definitions of E_T , E_c , ν_T , ν_c

where subscript T and c denote for tension and compression respectively. For linear elastic materials, as mentioned at the beginning of the chapter, there are only two material constants, say E and ν , and the other material constants can be expressed in terms of these two constants. For example, (2) relates the shear modulus G to E and ν . Similarly, for bi-linear elastic materials, the other material constants associated with different stress states may be expressed in terms of the four constants defined in (7). Before going into such details, the derivation of the bilinear stress-strain relations under triaxial principal stress states is in order. Let σ_1 , σ_2 and σ_3 be the principal stresses at a given material point of the body as shown in Figure 3. Due to the fact that the principal stresses σ_1 , σ_2 and σ_3 at any point can be either positive or negative, the deformed body may be divided essentially into four zones with their corresponding stress-strain relations given in the following:

(1) Zone (I): $\sigma_1 > 0$, $\sigma_2 > 0$, $\sigma_3 > 0$

$$\epsilon_1 = \frac{1+\nu_T}{E_T} \sigma_1 - \frac{\nu_T}{E_T} (\sigma_1 + \sigma_2 + \sigma_3) , \text{ permutation 1, 2, 3,}$$

$$\epsilon_1 + \epsilon_2 + \epsilon_3 = \frac{1-2\nu_T}{E_T} (\sigma_1 + \sigma_2 + \sigma_3) = \frac{(\sigma_1 + \sigma_2 + \sigma_3)}{3K_T} \quad (8a,b,c)$$

$$\text{where } 3K_T = \frac{E_T}{1-2\nu_T} \quad (8d)$$

(2) Zone (II): $\sigma_1 > 0$, $\sigma_2 > 0$, $\sigma_3 < 0$

$$\epsilon_1 = \frac{\sigma_1}{E_T} - \frac{\nu_T}{E_T} \sigma_2 - \frac{\nu_c}{E_c} \sigma_3 \quad (9a)$$

$$\epsilon_2 = -\frac{\nu_T \sigma_1}{E_T} + \frac{\sigma_2}{E_T} - \frac{\nu_c}{E_c} \sigma_3 \quad (9b)$$

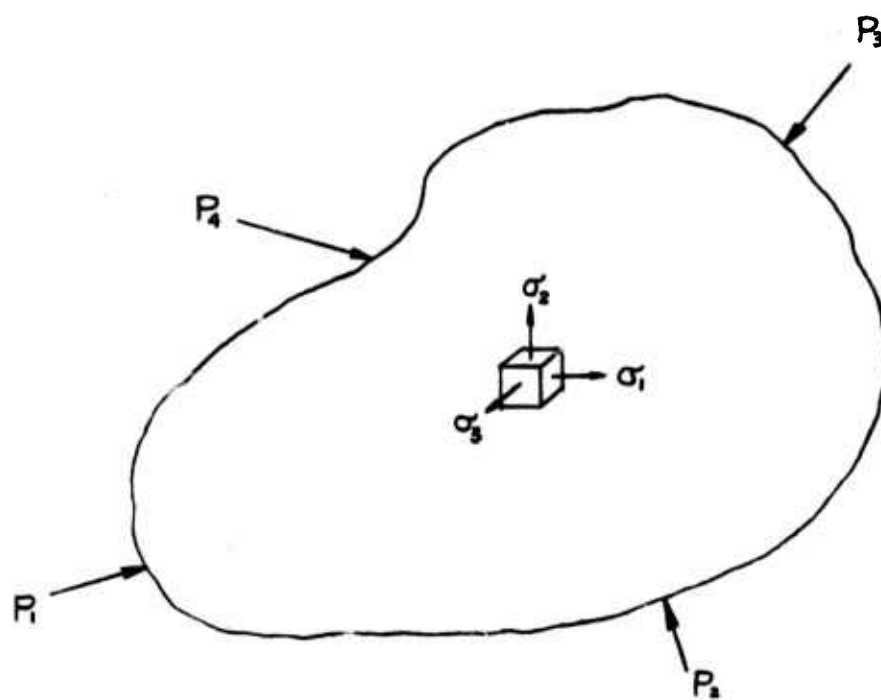


FIGURE 3 Triaxial Principal Stress State

$$\epsilon_3 = -\frac{\nu_T \sigma_1}{E_T} - \frac{\nu_T \sigma_2}{E_T} + \frac{\sigma_3}{E_C} \quad (9c)$$

$$\begin{aligned} \epsilon_1 + \epsilon_2 + \epsilon_3 &= \frac{1-2\nu_T}{E_T} (\sigma_1 + \sigma_2 + \sigma_3) + \left(\frac{1}{E_C} - \frac{1}{E_T} + \frac{2\nu_T}{E_T} - \frac{2\nu_C}{E_C} \right) \sigma_3 \\ &= \frac{1-2\nu_T}{E_T} (\sigma_1 + \sigma_2 + \sigma_3) + \left(\frac{1}{E_C} - \frac{1}{E_T} \right) \sigma_3 \end{aligned} \quad (9d)$$

where $\frac{\nu_T}{E_T} = \frac{\nu_C}{E_C}$

(3) Zone (III): $\sigma_1 > 0$, $\sigma_2 < 0$, $\sigma_3 < 0$

$$\epsilon_1 = \frac{\sigma_1}{E_T} - \frac{\nu_C \sigma_2}{E_C} - \frac{\nu_C}{E_C} \sigma_3 \quad (10a)$$

$$\epsilon_2 = -\frac{\nu_T \sigma_1}{E_T} + \frac{\sigma_2}{E_C} - \frac{\nu_C}{E_C} \sigma_3 \quad (10b)$$

$$\epsilon_3 = -\frac{\nu_T \sigma_1}{E_T} - \frac{\nu_C}{E_C} \sigma_2 + \frac{\sigma_3}{E_C} \quad (10c)$$

$$\begin{aligned} \epsilon_1 + \epsilon_2 + \epsilon_3 &= \frac{1-2\nu_C}{E_C} (\sigma_1 + \sigma_2 + \sigma_3) + \left(\frac{1}{E_T} - \frac{1}{E_C} + \frac{2\nu_C}{E_C} - \frac{2\nu_T}{E_T} \right) \sigma_1 \\ &= \frac{1-2\nu_C}{E_C} (\sigma_1 + \sigma_2 + \sigma_3) + \left(\frac{1}{E_T} - \frac{1}{E_C} \right) \sigma_1 \end{aligned} \quad (10d)$$

(4) Zone (IV): $\sigma_1 < 0$, $\sigma_2 < 0$, $\sigma_3 < 0$

$$\epsilon_1 = \frac{1+\nu_C}{E_C} \sigma_1 - \frac{\nu_C}{E_C} (\sigma_1 + \sigma_2 + \sigma_3), \text{ permutation } 1, 2, 3 \quad (11a,b,c)$$

$$\epsilon_1 + \epsilon_2 + \epsilon_3 = \frac{1-2\nu_C}{E_C} (\sigma_1 + \sigma_2 + \sigma_3) = \frac{(\sigma_1 + \sigma_2 + \sigma_3)}{3K_C} \quad (11d)$$

where $3K_C = \frac{E_C}{1-2\nu_C}$

$\frac{\nu_C}{E_C} = \frac{\nu_T}{E_T}$ can be argued from the postulation of the strain-energy density function.

This shows that the designated zones based upon stress and strain are not necessarily the same. In other words, "bi-linearity" has two definitions; one is based upon stress and the other one is based upon strain. These two definitions are illustrated in Figure 4. In Figure 4a, whenever the stress-strain curve crosses the zero stress points, the slope (modulus) changes from E_C to E_T or E_T to E_C . In Figure 3b, the modulus will change whenever the stress-strain curve crosses the zero strain points. Biaxial tests are required in order to determine which one of the criteria will fit closer to the actual behavior of a given material. Perhaps an even more general bi-linear state can exist in which the "cross-over" point can occur at stress and strain anywhere.

In our study we will concentrate on the more restricted case in which the cross-over point occurs at the zero stress state; that is, the stress-strain relation shown in Figure 4a.

In the stress zone I and IV, the stress-strain relations (8a,b,c,d) and (11a,b,c,d) are identical to the stress-strain relations of linear elasticity (4), except E_T , ν_C and E_C , ν_C are used respectively, for tension and compression. Therefore, the basic equations, the stress analysis techniques and the results from linear elasticity can be used directly in these two stress zones. In the stress zones II and III, however, the stress-strain relations are different from (4) and that is where the bi-linear elastic theory deviates from the linear elastic theory.

Solving (8), (9), (10) and (11), for stress components after simplifying yields:

(1) Zone (I)

$$\sigma_1 = \frac{E_T}{1+\nu_T} \epsilon_1 + \frac{E_T \nu_T}{(1+\nu_T)(1-2\nu_T)} (\epsilon_1 + \epsilon_2 + \epsilon_3)$$

permutation 1, 2, 3 (12a,b,c)

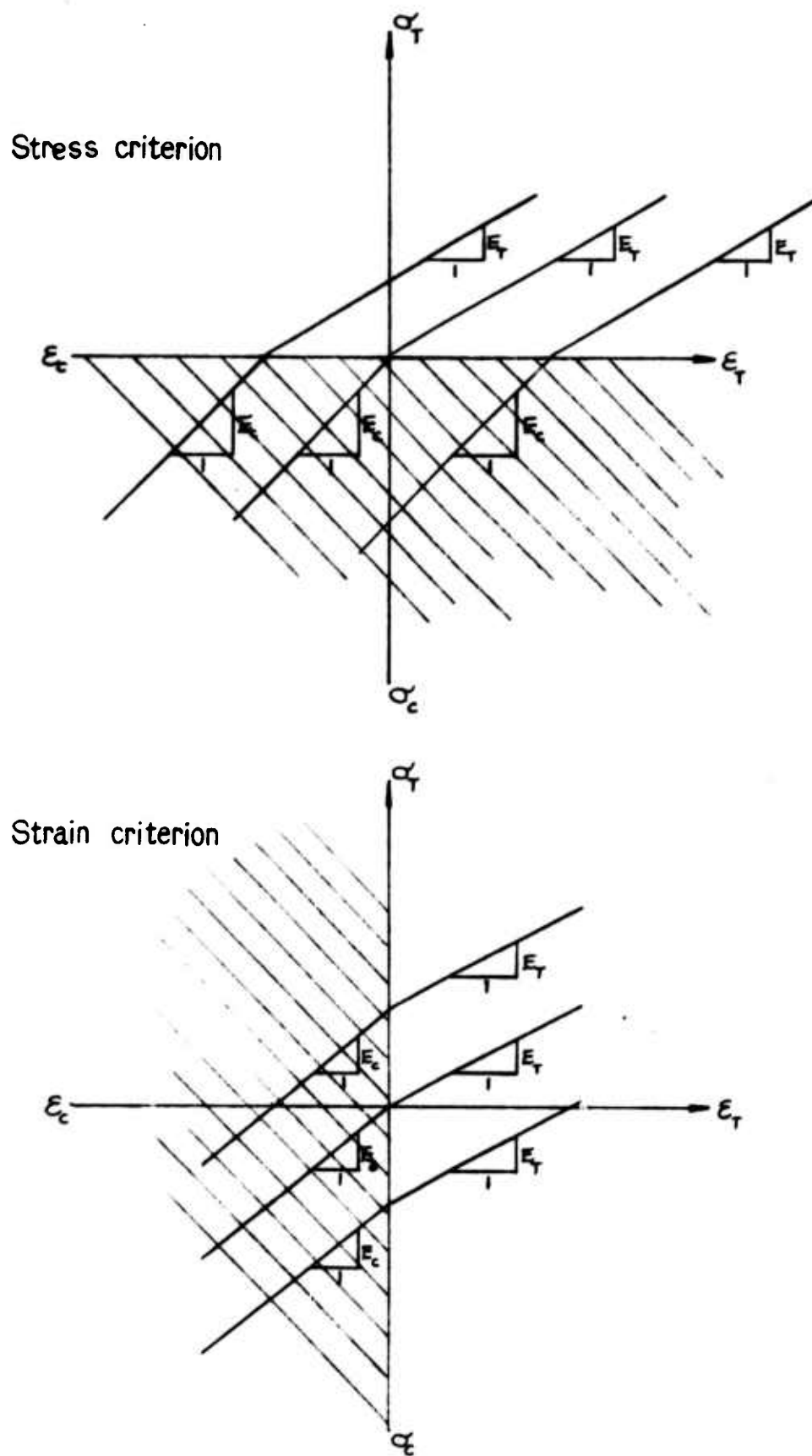


FIGURE 4 Stress and Strain Criteria of Bilinear Stress-Strain Relations

(2) Zone (II): $\sigma_1 > 0$, $\sigma_2 > 0$, $\sigma_3 < 0$

$$\sigma_1 = \frac{E_T}{(1+\nu_T)(1-\nu_T-2\nu_T\nu_c)} [(1-\nu_T\nu_c)\epsilon_1 + \nu_T(1+\nu_c)\epsilon_2 + \nu_c(1+\nu_T)\epsilon_3] \quad (13a)$$

$$\sigma_2 = \frac{E_T}{(1+\nu_T)(1-\nu_T-2\nu_T\nu_c)} [\nu_T(1+\nu_c)\epsilon_1 + (1-\nu_T\nu_c)\epsilon_2 + \nu_c(1+\nu_T)\epsilon_3] \quad (13b)$$

$$\sigma_3 = \frac{E_c}{(1-\nu_T-2\nu_T\nu_c)} [\nu_T(\epsilon_1+\epsilon_2+\epsilon_3) + (1-2\nu_T)\epsilon_3] \quad (13c)$$

(3) Zone (III): $\sigma_1 > 0$, $\sigma_2 < 0$, $\sigma_3 < 0$

$$\sigma_1 = \frac{E_T}{(1-\nu_c-2\nu_T\nu_c)} [\nu_c(\epsilon_1+\epsilon_2+\epsilon_3) + (1-2\nu_c)\epsilon_1] \quad (14a)$$

$$\sigma_2 = \frac{E_T}{(1+\nu_c)(1-\nu_c-2\nu_T\nu_c)} [\nu_T(1+\nu_c)\epsilon_1 + (1-\nu_T\nu_c)\epsilon_2 + \nu_c(1+\nu_T)\epsilon_3] \quad (14b)$$

$$\sigma_3 = \frac{E_c}{(1+\nu_c)(1-\nu_c-2\nu_T\nu_c)} [\nu_T(1+\nu_c)\epsilon_1 + \nu_c(1+\nu_T)\epsilon_2 + (1-\nu_T\nu_c)\epsilon_3] \quad (14c)$$

(4) Zone (IV): $\sigma_1 < 0$, $\sigma_2 < 0$, $\sigma_3 < 0$

$$\sigma_1 = \frac{E_c}{1+\nu_c} \epsilon_1 + \frac{E_c\nu_c}{(1+\nu_c)(1-2\nu_c)} (\epsilon_1+\epsilon_2+\epsilon_3)$$

permutation 1, 2, 3 (15a,b,c)

Notice that the four zones specified above are based on the sign of the principal stresses. The corresponding principal strains ϵ_1 , ϵ_2 , ϵ_3 , however, do not have to have the same sign combination. For example, in Zone 1, the ϵ_1 could be in compression if σ_2 and/or σ_3 are much larger than σ_1 .

Once the stress-strain relations have been established under principal stress states, the stress-strain relations under general stress state can be derived by applying the method of transformation. For the sake of simplicity, the plane **stress** state ($\sigma_3 = 0$) instead of a general three-dimensional stress state is considered in the following. In this case there are only three zones: (1) $\sigma_1 > 0, \sigma_2 > 0, \sigma_3 = 0$; (2) $\sigma_1 > 0, \sigma_2 < 0, \sigma_3 = 0$; (3) $\sigma_1 < 0, \sigma_2 < 0, \sigma_3 = 0$. Zone (1) and Zone (3) are identical to the linear elastic problem provided E_T, ν_T and E_C, ν_C are used instead of E and ν in Zone (1) and Zone (3), respectively. Hence, only the general stress-strain relations in Zone (2) are to be derived in the following:

$$\epsilon_1 = \frac{1}{E_T} \sigma_1 - \frac{\nu_C}{E_C} \sigma_2 \quad (17a)$$

$$\epsilon_2 = -\frac{\nu_T}{E_T} \sigma_1 + \frac{1}{E_C} \sigma_2 \quad (17b)$$

$$\epsilon_3 = -\frac{\nu_T}{E_T} \sigma_1 - \frac{\nu_C}{E_C} \sigma_2 = -\frac{\nu_T}{E_T}(\sigma_1 + \sigma_2) = -\frac{\nu_C}{E_C}(\sigma_1 + \sigma_2) \quad (17c)$$

In order to obtain the general stress-strain relations between $\epsilon_x, \epsilon_y, \gamma_{xy}$ as the function of $\sigma_x, \sigma_y, \tau_{xy}$, from the principal stress-strain relations of (17), the following procedures will be taken. From the geometric relation the transformation will be performed to obtain the strain $\epsilon_x, \epsilon_y, \gamma_{xy}$ with respect to x-y axes as the function of ϵ_1 and ϵ_2 with respect to the principal axes 1 and 2 and the results are shown in the following:

$$2\epsilon_x = (\epsilon_1 + \epsilon_2) + (\epsilon_1 - \epsilon_2) \cos 2\psi \quad (18a)$$

$$2\epsilon_y = (\epsilon_1 + \epsilon_2) - (\epsilon_1 - \epsilon_2) \cos 2\psi \quad (18b)$$

$$2\epsilon_{xy} = -(\epsilon_1 - \epsilon_2) \sin 2\psi \quad (18c)$$

and
$$\sigma_1 = \frac{\sigma_x + \sigma_y}{2} + \frac{\sigma_x - \sigma_y}{2} \cos 2\psi + \sigma_{xy} \sin 2\psi = \frac{\sigma_x + \sigma_y}{2} + \frac{Q}{2} \quad (19a)$$

$$\sigma_2 = \frac{\sigma_x + \sigma_y}{2} - \frac{\sigma_x - \sigma_y}{2} \cos 2\psi - \sigma_{xy} \sin 2\psi = \frac{\sigma_x + \sigma_y}{2} - \frac{Q}{2} \quad (19b)$$

where

$$2\psi(x,y) = \tan^{-1} \frac{2\tau_{xy}}{\sigma_x - \sigma_y} = \frac{\epsilon_{xy}}{\epsilon_x - \epsilon_y} \quad (20)$$

is the principal direction as shown in Figure 5 for stress and strain because of isotropy. Substituting (19a), (19b) into (17a) and (17b) and the resulting equation into (18a), (19b) and (19c), yield the stress-strain relation in x-y coordinates as follows:

$$\epsilon_1 = \frac{1}{E_T} \left[\frac{\sigma_x + \sigma_y}{2} + \frac{Q}{2} \right] + \frac{\nu_c}{E_c} \left[\frac{\sigma_x + \sigma_y}{2} - \frac{Q}{2} \right] \quad (21a)$$

$$\epsilon_2 = \frac{\nu_T}{E_T} \left[\frac{\sigma_x + \sigma_y}{2} + \frac{Q}{2} \right] + \frac{1}{E_c} \left[\frac{\sigma_x + \sigma_y}{2} - \frac{Q}{2} \right] \quad (21b)$$

$$\epsilon_1 + \epsilon_2 = \left[\frac{1}{E_T} \frac{1+\phi^2}{2} - \frac{\nu_T}{E_T} \right] (\sigma_x + \sigma_y) + \frac{1}{E_T} \left(\frac{1+\phi^2}{2} \right) Q \quad (21c)$$

$$\epsilon_1 - \epsilon_2 = \frac{1}{E_T} \frac{(1-\phi^2)}{2} (\sigma_x + \sigma_y) + \left(\frac{1}{E_T} \frac{1+\phi^2}{2} + \frac{\nu_c}{E_c} \right) Q \quad (21d)$$

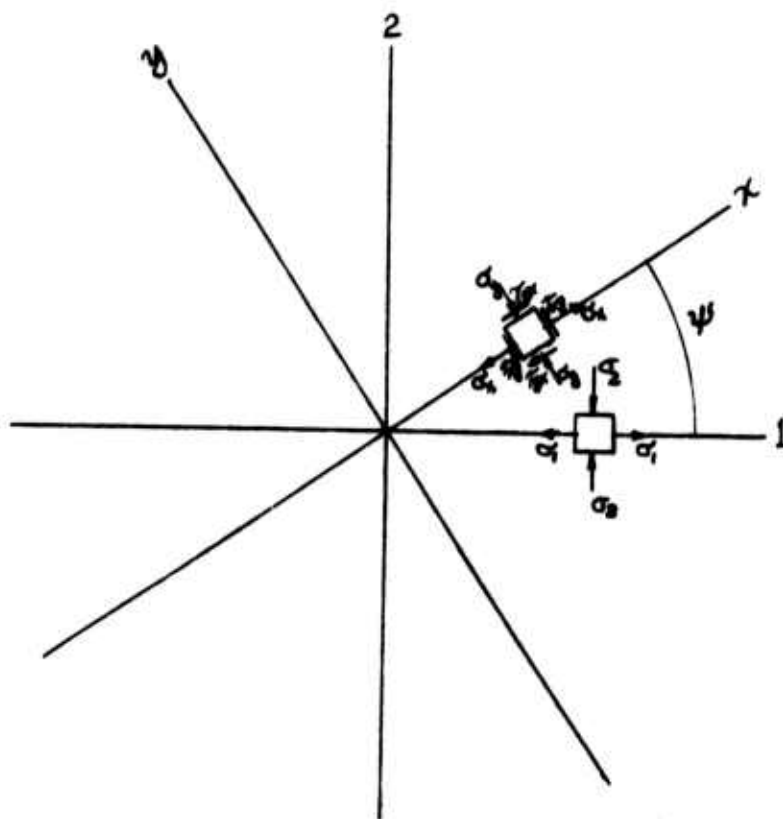


FIGURE 5 Transformation of Stress Components

$$\begin{aligned}
2\epsilon_x = & \left(\frac{1}{E_T} \frac{1+\phi^2}{2} - \frac{\nu_T}{E_T} - \frac{1}{E_T} \frac{1-\phi^2}{2} \cos 2\psi \right) (\sigma_x + \sigma_y) \\
& + \left(\frac{1}{E_T} \frac{1-\phi^2}{2} + \frac{1}{E_T} \frac{1+\phi^2}{2} \cos 2\psi - \frac{\nu_T}{E_T} \cos 2\psi \right) [(\sigma_x - \sigma_y) \cos 2\psi \\
& + 2\sigma_{xy} \sin 2\psi] \quad (22a)
\end{aligned}$$

$$\begin{aligned}
2\epsilon_y = & \left(\frac{1}{E_T} \frac{1+\phi^2}{2} - \frac{\nu_T}{E_T} - \frac{1}{E_T} \frac{1-\phi^2}{2} \cos 2\psi \right) (\sigma_x - \sigma_y) + \left(\frac{1}{E_T} \frac{1-\phi^2}{2} - \frac{1}{E_T} \frac{1+\phi^2}{2} \cos 2\psi \right. \\
& \left. - \frac{\nu_T}{E_T} \cos 2\psi \right) [(\sigma_x - \sigma_y) \cos 2\psi + 2\sigma_{xy} \sin 2\psi] \quad (22b)
\end{aligned}$$

$$\begin{aligned}
2\epsilon_{xy} = & -\frac{1}{E_T} \frac{1-\phi^2}{2} (\sigma_x - \sigma_y) \sin 2\psi \\
& - \left(\frac{1}{E_T} \frac{1-\phi^2}{2} + \frac{\nu_T}{E_T} \right) [(\sigma_x - \sigma_y) \cos 2\psi + 2\sigma_{xy} \sin 2\psi] \sin 2\psi
\end{aligned}$$

where $\phi^2 = \frac{E_T}{E_C}$ (22c)

Inserting (20) into (22), after rearranging terms, yields

$$\epsilon_x = \frac{1}{E_T} \frac{1+\phi^2}{2} \sigma_x - \frac{\nu_T}{E_T} \sigma_y + \frac{1}{E_T} \frac{1-\phi^2}{4} \frac{(\sigma_x^2 - \sigma_y^2) + Q^2}{Q} \quad (23a)$$

$$\epsilon_y = -\frac{\nu_T}{E_T} \sigma_x + \frac{1}{E_T} \frac{1+\phi^2}{2} \sigma_y + \frac{1}{E_T} \frac{1-\phi^2}{4} \frac{-(\sigma_x^2 - \sigma_y^2) + Q^2}{Q} \quad (23b)$$

$$\epsilon_z = \epsilon_3 = -\frac{\nu_T}{E_T} (\sigma_x + \sigma_y) \quad (23c)$$

$$\epsilon_{xy} = \frac{1}{E_T} \left(\frac{1+\phi^2}{2} + \nu_T \right) (2\sigma_{xy}) + \frac{1}{E_T} \frac{1-\phi^2}{2} \frac{(\sigma_x + \sigma_y) \sigma_{xy}}{Q} \quad (23d)$$

$$\epsilon_x + \epsilon_y + \epsilon_z = \frac{1}{E_T} \left(\frac{1+\phi^2}{2} - 2\nu_T \right) (\sigma_x + \sigma_y) + \frac{1}{E_T} \frac{1-\phi^2}{2} Q$$

where $Q^2 = (\sigma_x - \sigma_y)^2 + (2\sigma_{xy})^2$ (23e)

Equation (23a, b, c, d, e) contain essentially two parts: the linear and nonlinear parts. The linear part is essentially identical to the corresponding linear elastic stress-strain relation provided the coefficients are modified to take into consideration the bilinear elastic moduli. It can be shown easily that (23a---e) become the familiar constitutive equations of linear elasticity by imposing the conditions of $E_T = E_C = E$, $\nu_T = \nu_C = \nu$, $\phi^2 = E_T/E_C = 1$. Imposing this condition into (23a---e) the nonlinear stress terms vanish. Equation (23a---e) point out several interesting features. The deviatoric stress-strain relations (23d) and the dilational stress-strain relations (23e) are not separable. Under pure shear stress state, which is equivalent to $|\sigma_1| = |\sigma_2|$,

$$\epsilon_x = \frac{1}{E_T} \frac{1-\phi^2}{2} \sigma_{xy} \quad (24a)$$

$$\epsilon_y = \frac{1}{E_T} \frac{1-\phi^2}{2} \sigma_{xy} \quad (24b)$$

$$\epsilon_z = 0 \quad (24b1)$$

$$\epsilon_{xy} = \frac{1}{E_T} \left(\frac{1+\phi^2}{2} + \nu_T \right) (2\sigma_{xy}) \quad (24c)$$

$$= \left(\frac{1}{E_T} + \frac{1}{E_C} + \frac{\nu_T}{E_T} + \frac{\nu_C}{E_C} \right) \sigma_{xy}$$

$$\epsilon_x + \epsilon_y + \epsilon_z = \frac{1}{E_T} (1-\phi^2) (2\sigma_{xy}) = \left(\frac{1}{E_T} - \frac{1}{E_C} \right) (2\sigma_{xy}) \quad (24d)$$

The axial stresses are induced as given in (24a) and (24b) and the shear strain is linearly proportional to shear stress. Eq. (24d) also indicates that applying pure shear stress would induce volume change. The volume will increase if $E_T < E_C$ and decrease if $E_T > E_C$. Furthermore, the shear modulus can be obtained from (24c) as follows

$$\mu = \frac{\sigma_{xy}}{\epsilon_{xy}} = \frac{1}{\left(\frac{1+\nu_T}{E_T} + \frac{1+\nu_C}{E_C} \right)} \quad (25)$$

2.2 Bilinear Viscoelastic Constitutive Relations

Referring to (5), (6), and (17a, b) the bilinear viscoelastic constitutive equations under biaxial tension and compression stress state, $\sigma_1(t) > 0$ and $\sigma_2(t) < 0$, can be written in the following form

$$\epsilon_1(t) = \int_0^t J_T(t-\xi) \dot{\sigma}_1(\xi) d\xi - \int_0^t J_C(t-\xi) \nu_C(t-\xi) \dot{\sigma}_2(\xi) d\xi \quad (26a)$$

$$\epsilon_2(t) = - \int_0^t J_T(t-\xi) \nu_T(t-\xi) \dot{\sigma}_1(\xi) d\xi + \int_0^t J_C(t-\xi) \dot{\sigma}_2(\xi) d\xi \quad (26b)$$

Under constant stresses input,

$$\sigma_1(t) = \sigma_1 H(t)$$

$$\sigma_2(t) = \sigma_2 H(t)$$

where σ_1 and σ_2 are independent on time and $H(t)$ is the Heavyside unit junction, (26a, b) become

$$\epsilon_1(t) = J_T(t) \sigma_1 - J_C(t) \nu_C(t) \sigma_2 \quad (27a)$$

$$\epsilon_2(t) = - J_T(t) \nu_T(t) \sigma_1 + J_C(t) \sigma_2 \quad (27b)$$

J_T , J_C , ν_T and ν_C are defined as follows

$$J_T(t) = \frac{\epsilon_T(t)}{\sigma_T} \quad (28a)$$

$$J_C(t) = \frac{\epsilon_C(t)}{\sigma_C} \quad (28b)$$

$$\nu_T(t) = - \epsilon_T'(t) / \epsilon_T(t) \quad (28c)$$

$$\nu_c(t) = - \epsilon_c'(t) / \epsilon_c(t) \quad (28d)$$

$$J_T(t) \nu_T(t) = - \epsilon_T'(t) / \sigma_T^0 \quad (28e)$$

$$J_C(t) \nu_C(t) = - \epsilon_C'(t) / \sigma_C^0 \quad (28f)$$

These terms are shown in Fig. 6.

Taking the Laplace transformations of (26a, b) with respect to time yield the following results

$$\bar{\epsilon}_1(s) = s \bar{J}_T(s) \bar{\sigma}_1(s) - \overline{s J_C(s) \nu_C(s)} \sigma_2(s) \quad (29a)$$

$$\bar{\epsilon}_2(s) = - s \overline{J_T(s) \nu_T(s)} \sigma_1(s) + s \bar{J}_C(s) \bar{\sigma}_2(s) \quad (29b)$$

where a superscript slash over a symbol indicates that the quantity has been transformed and s is the transformed variable. Again, for the postulation of the strain-energy density function

$$\overline{J_T(s) \nu_T(s)} = \overline{J_C(s) \nu_C(s)} \quad (30a)$$

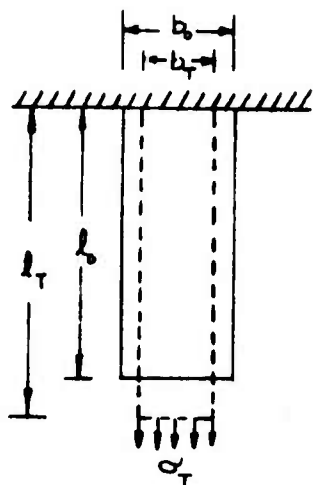
and the inverse Laplace transformation of (30a) becomes

$$J_T(t) \nu_T(t) = J_C(t) \nu_C(t) = J_{TC}(t) \quad (30b)$$

Under uniaxial tension and compression, (26a, b) become

$$\epsilon_T(t) = \int_0^t J_T(t-\xi) \dot{\sigma}_T(\xi) d\xi \quad (31a)$$

$$\epsilon_C(t) = \int_0^t J_C(t-\xi) \dot{\sigma}_C(\xi) d\xi \quad (31b)$$



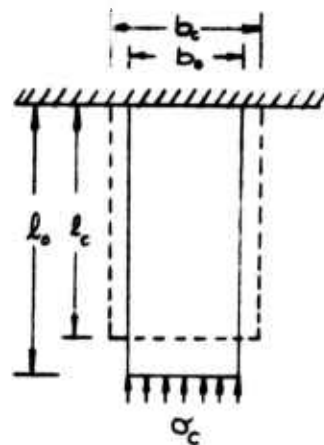
$$\epsilon_T(t) = [l_T(t) - l_0] / l_0$$

$$\epsilon'_T(t) = [b_T(t) - b_0] / b_0$$

$$J_T(t) = \epsilon_T(t) / \sigma_T$$

$$\nu_T(t) = -\epsilon'_T(t) / \epsilon_T(t)$$

$$J_T(t) \nu_T(t) = -\epsilon'_T(t) / \sigma_T$$



$$\epsilon_c(t) = [l_c(t) - l_0] / l_0$$

$$\epsilon'_c(t) = [b_c(t) - b_0] / b_0$$

$$J_c(t) = \epsilon_c(t) / \sigma_c$$

$$\nu_c(t) = -\epsilon'_c(t) / \epsilon_c(t)$$

$$J_c(t) \nu_c(t) = -\epsilon'_c(t) / \sigma_c$$

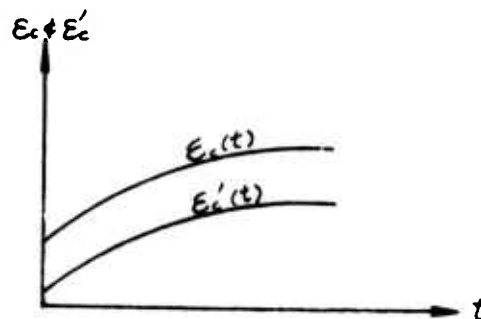
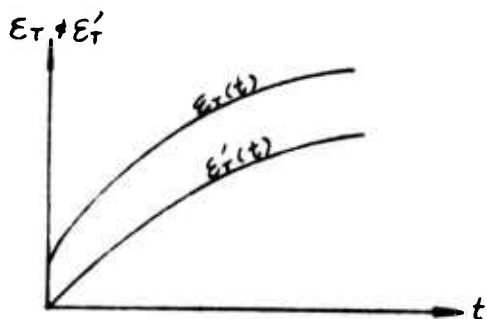
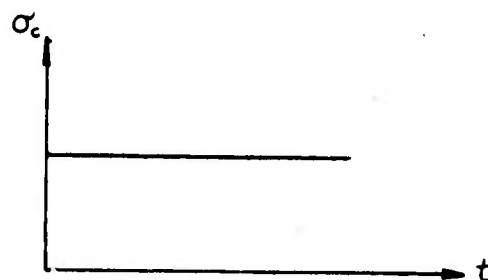
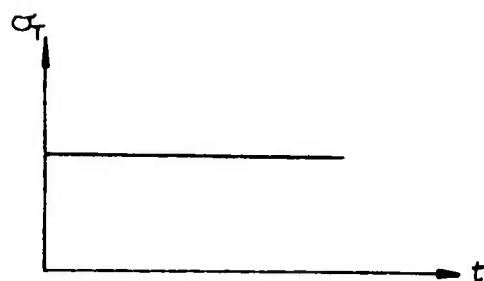


FIGURE 6 Definitions of $J_T(t)$, $J_c(t)$, $\nu_T(t)$, $\nu_c(t)$

for creep formulation and the corresponding constitutive relation for relaxation formulation can be written as follows

$$\sigma_T(t) = \int_0^t E_T(t-\xi) \dot{\epsilon}_T(\xi) d\xi \quad (32a)$$

$$\sigma_C(t) = \int_0^t E_C(t-\xi) \dot{\epsilon}_C(\xi) d\xi \quad (32b)$$

where $E_T(t)$ and $E_C(t)$ are the stress relaxation moduli for tension and compression. Applying the Leplace transform to (31a) and (32a) yield

$$\bar{\epsilon}_T(s) = s \bar{J}_T(s) \bar{\sigma}_T(s) \quad (33a)$$

$$\bar{\sigma}_T(s) = s \bar{E}_T(s) \bar{\epsilon}_T(s) \quad (33b)$$

Eliminating σ_T and ϵ_T from (33a, b) yield

$$\bar{J}_T(s) \bar{E}_T(s) = \frac{1}{s} \quad (34)$$

Applying the inverse Laplace transforms to (34) yields

$$\int_0^t J_T(t-\xi) E(\xi) d\xi = t \quad (35)$$

Similarly, J_C and E_C are related by

$$\int_0^t J_C(t-\xi) E_C(\xi) d\xi = t \quad (36)$$

Thus, from (35) and (36), the relaxation modulus can be determined if the corresponding creep compliance is given and vice versa.

By using the elastic viscoelastic corresponding principle to the bilinear viscoelastic problem, many results derived in Section 2.1 for bilinear elastic theory can be used directly to the bilinear viscoelastic theory.

2.3 Beam Under Pure Bending

In the previous sections, the constitutive relations governing the bilinear elastic and viscoelastic materials have been presented. The next step will be to show how these constitutive relations may be used to solve stress analysis problems in bilinear elastic and viscoelastic materials. In this section the stress analysis of a simple beam under pure bending will be discussed. The following assumptions are made for the analyses of the problem : (a) plane sections before bending remain plane after bending, (b) bilinear viscoelastic stress-strain relations of (26a, b) and (30b) hold, (c) the effect due to shear is negligible.

A simply supported bilinear viscoelastic beam as shown in Fig. 7 is subjected to a known pure bending moment $M(t)$ and the stress and strain distributions and the deflection are sought. Assumption (a) that plane sections before bending remain plane after bending implies that strains are linearly proportional to the distance from the neutral axis whose location is to be determined. Therefore

$$\epsilon(t, y) = k(t)y \quad (37)$$

where ϵ represents the axial strain, positive for tension and negative for compression, y is the distance measured positive downward from the neutral axis and k is the curvature.

Assumption (b) implies that (31a, b) or (32a, b) can be used to represent the constitutive relations under tension and compression. Inserting (37)

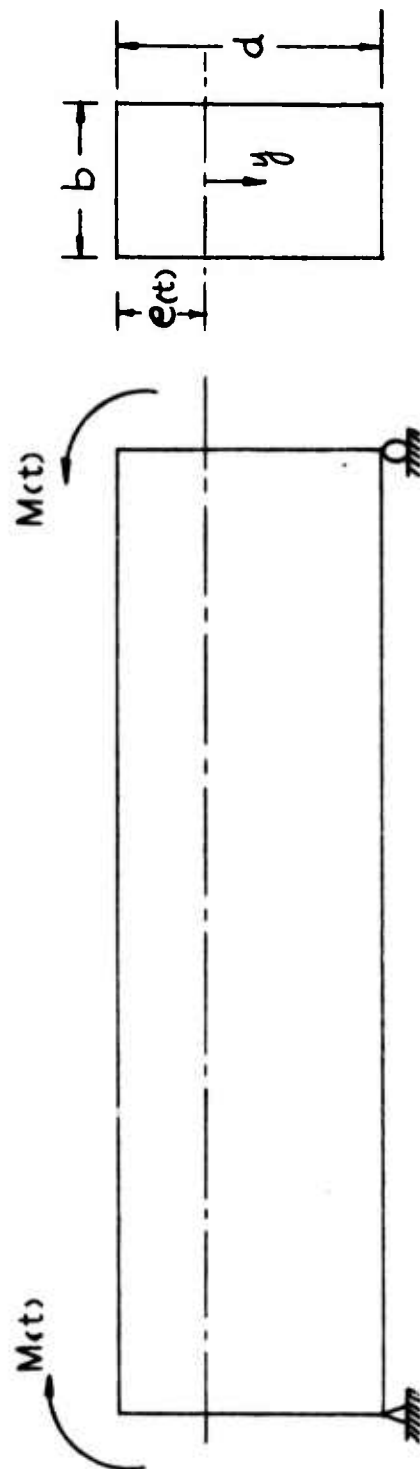


FIGURE 7 Simply Supported Beam Under Pure Bending

into (32a, b) yields

$$\sigma_T(t) = y \int_0^t E_T(t-\xi) \dot{k}(\xi) d\xi, \quad y > 0 \quad (38a)$$

$$\sigma_C(t) = y \int_0^t E_C(t-\xi) \dot{k}(\xi) d\xi, \quad y < 0 \quad (38b)$$

The equilibrium conditions yield the following relations

$$\int_A \sigma dA = 0 \quad (39)$$

$$\int_A \sigma_y dA = M(t) \quad (40)$$

Equation (39) is the balance of the resultant force of the axial stress on the cross section of the beam and (40) is the balance of the internal moment of the axial stress on the cross section of a portion of the beam with the external applied moment $M(t)$ on the same portion. In (37), (40), A signifies the area of the cross-section. Inserting (38a), (38b) into (39) and (40), yields two simultaneous equations for two unknowns, curvature $K(t)$, and position of the neutral axis $e(t)$. For a rectangular beam of width b and depth d these equations are

$$b \int_0^{-e(t)} \sigma_C(t, y) dy + b \int_0^{[d-e(t)]} \sigma_T(t, y) dy$$

or

$$b \int_{-e(t)}^0 \left[\int_0^t E_C(t-\xi) \dot{k}(\xi) d\xi \right] y dy + b \int_0^{+[d-e(t)]} \left[\int_0^t E_T(t-\xi) \dot{k}(\xi) d\xi \right] (y) dy = 0 \quad (41)$$

and

$$b \int_{-e(t)}^0 \left[\int_0^t E_c(t-\xi) \dot{k}(\xi) d\xi \right] y^2 dy + b \int_0^{[d-e(t)]} \left[\int_0^t E_T(t-\xi) \dot{k}(\xi) d\xi \right] y^2 dy = M(t), \quad (42)$$

where $e(t)$ represents the position of the neutral axis as measured from the top surface. Integrating of (41) and (42) with respect to y yield

$$- \frac{b e(t)^2}{2} \int_0^t E_c(t-\xi) \dot{k}(\xi) d\xi + \frac{b [d-e(t)]^2}{2} \int_0^t E_T(t-\xi) \dot{k}(\xi) d\xi = 0 \quad (43)$$

and

$$\frac{1}{3} b e(t)^3 \int_0^t E_c(t-\xi) \dot{k}(\xi) d\xi + \frac{b [d-e(t)]^3}{3} \int_0^t E_T(t-\xi) \dot{k}(\xi) d\xi = M(t) \quad (44)$$

Equations (43) and (44) are two coupled integral equations for two unknowns, the position of the neutral axis $e(t)$ and the curvature $k(t)$. The solution of $e(t)$ and $k(t)$ from (43) and (44) can be attained by means of numerical method which will be used in the future. There are several special cases in which exact solutions can be obtained. For example, if the tensile and compressive creep compliances and relaxation modulus have the following relation

$$E_c(t) = a_0^2 E_T(t)$$

or

$$J_c(t) = \frac{1}{a_0^2} J_T(t) \quad (45)$$

where a_0^2 is a constant. Equation (45) implies that, although both tensile and compressive properties are time dependent, the ratio between E_T and E_c are constant. Inserting (45) into (43) after integration yields

$$\frac{b}{2} \left\{ [d-e(t)]^2 - a_0^2 e(t)^2 \right\} \int_0^t E_T(t-\xi) \dot{k}(\xi) d\xi = 0 \quad (46)$$

Since $E_T(t)$ is an arbitrary function and $k(t)$ is not zero, (46) implies

$$[d - e(t)]^2 - a_0^2 e(t)^2 = 0 \quad (47a)$$

or

$$e(t) = \frac{d}{1+a_0} \quad (47b)$$

Inserting (47b) into (44) yields

$$\frac{bd^3}{3} \left(\frac{a_0}{1+a_0} \right)^2 \int_0^t E_T(t-\xi) \dot{k}(\xi) d\xi = M(t) \quad (48)$$

Applying Laplace transformation to (48)

$$\left[\frac{bd^3}{3} \left(\frac{a_0}{1+a_0} \right)^2 \right] s \bar{E}_T(s) \bar{k}(s) = \bar{M}(s)$$

and using (34), yields the solution of the curvature in the Laplace transform domain as follows

$$\frac{bd^3}{3} \left(\frac{a_0}{1+a_0} \right)^2 \bar{k}(s) = s \bar{M}(s) \bar{J}_T(s) \quad (49)$$

Taking the inversion of (49) yields

$$\frac{bd^3}{3} \left(\frac{a_0}{1+a_0} \right)^2 k(t) = \int_0^t J_T(t-\xi) \dot{M}(\xi) d\xi \quad (50)$$

or

$$k(t) = \frac{1}{I_e} \int_0^t J_T(t-\xi) \dot{M}(\xi) d\xi \quad (50a)$$

where

$$I_e = \frac{bd^3}{3} \left(\frac{a_0}{1+a_0} \right)^2$$

is the moment of inertia of the rectangular cross-section with respect to the neutral axis. The strain distribution can be obtained by inserting (50a) into (37)

$$\epsilon(t, y) = \frac{y}{I_e} \int_0^t J_T(t-\xi) M(\xi) d\xi \quad (51)$$

and the stress distribution can be obtained by substituting (50a) into (38a) and (38b) in the Laplace transform domain and then applying the inverse Laplace transform which yields

$$\sigma_T(t) = \frac{M(t)y}{I_e}, \quad y < 0 \quad (52a)$$

$$\sigma_C(t) = \frac{a_0^2 M(t)y}{I_e}, \quad y < 0 \quad (52b)$$

For small deflections the strain, ϵ , and deflection, w , are related by the following equation

$$\epsilon(t, y) = y \frac{d^2 w(t, x)}{dx^2} \quad (53)$$

(see any book on strength of materials.)

Inserting (51) into (53) yields

$$\frac{d^2 w(t, x)}{dx^2} = k(t) = \frac{1}{I_e} \int_0^t J_T(t-\xi) \dot{M}(\xi) d\xi \quad (54)$$

Thus, the deflection can be calculated from (54) for a given set of boundary conditions and given $J_T(t)$ and $a_0^2 = \frac{J_T(t)}{J_C(t)}$.

The effect of bilinearity can be shown from this simple analysis. For example, three beams having identical geometry and subjected to the same bending moment M_0 and assuming that the material properties for the three beams are as follows

$$\text{Beam \#1} \quad J_C = J, \quad J_T = J, \quad a_0^2 = 1,$$

$$\text{Beam \#2} \quad J_C = \frac{1}{4} J, \quad J_T = J, \quad a_0^2 = 4,$$

$$\text{Beam \#3} \quad J_C = J, \quad J_T = 4J, \quad a_0^2 = 4,$$

Inserting these material properties into (47b), (50a) and (51) and normalizing the strains by assuming that the maximum tensile and compressive strain for beam #1 equal ± 1 , the resultant neutral axes and the normalized strain distributions of the beams are shown in Figure 8a. For Beam #3 where the tensile creep compliance is four times proportionally larger than Beam #1, and the compressive creep compliance remains the same as that of Beam #1, the resultant maximum tensile strain at the bottom of Beam #3 is three times the corresponding maximum tensile strain in Beam #1, and the maximum compressive strain in Beam #3 is 1.5 the maximum compressive strain in Beam #1. The maximum tensile stress in Beam #3 is actually reduced as shown in Figure 8b. These results point out the fact that in interpreting the bending test results of bilinear elastic or viscoelastic materials care must be exercised, particularly in evaluating the tensile strength from flexure test.

The actual theoretical and experimental results of the strains of beams under pure bending are shown in Section 3.7.

Beam #1 $J_c = J, J_t = J$

Beam #2 $J_c = \frac{1}{4}J, J_t = J$

Beam #3 $J_c = J, J_t = 4J$

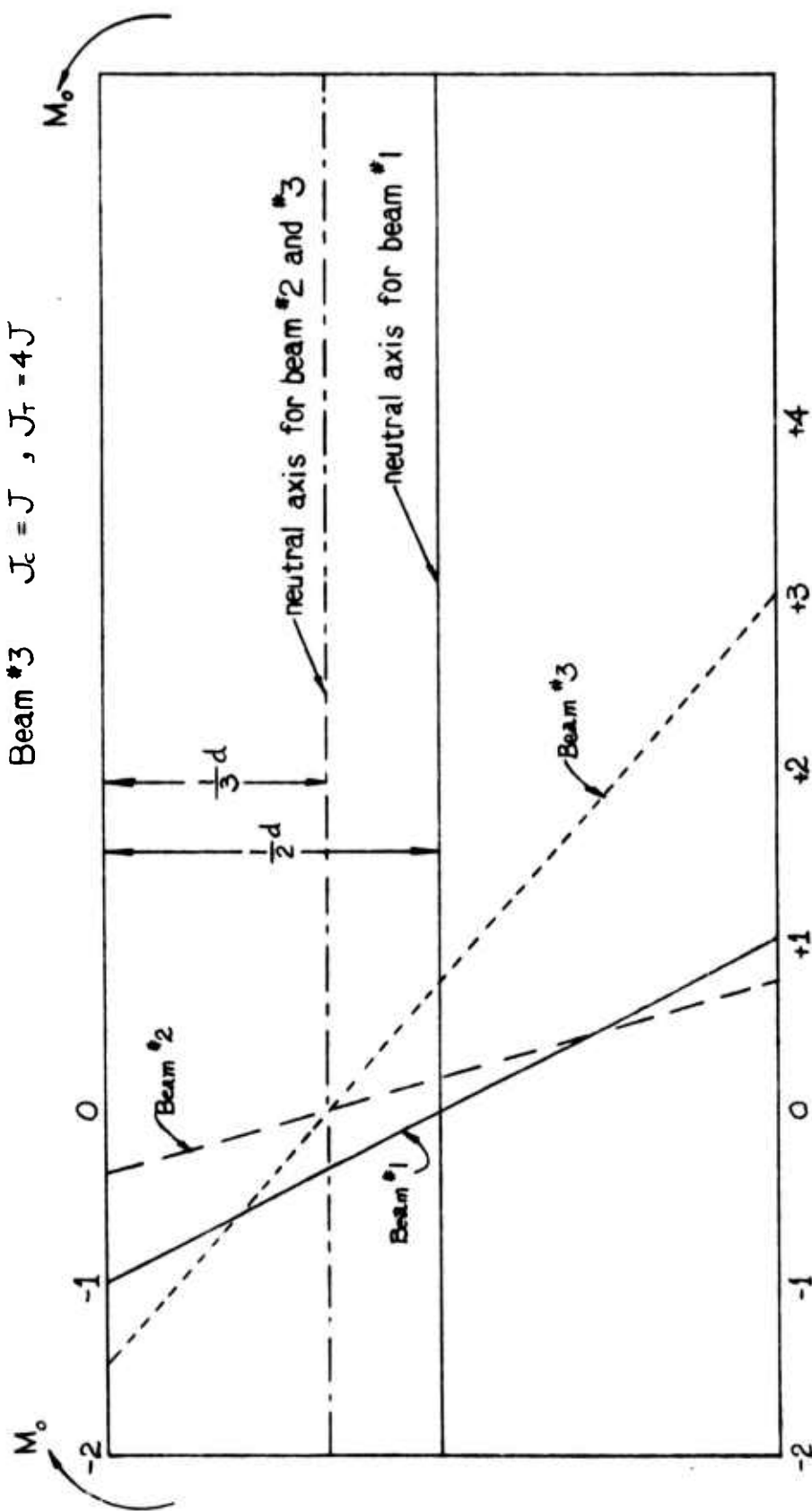


FIGURE 8 (a) Strain Distributions and the Location of Neutral Axes of Linear and Bilinear Viscoelastic Beams Under Pure Bending

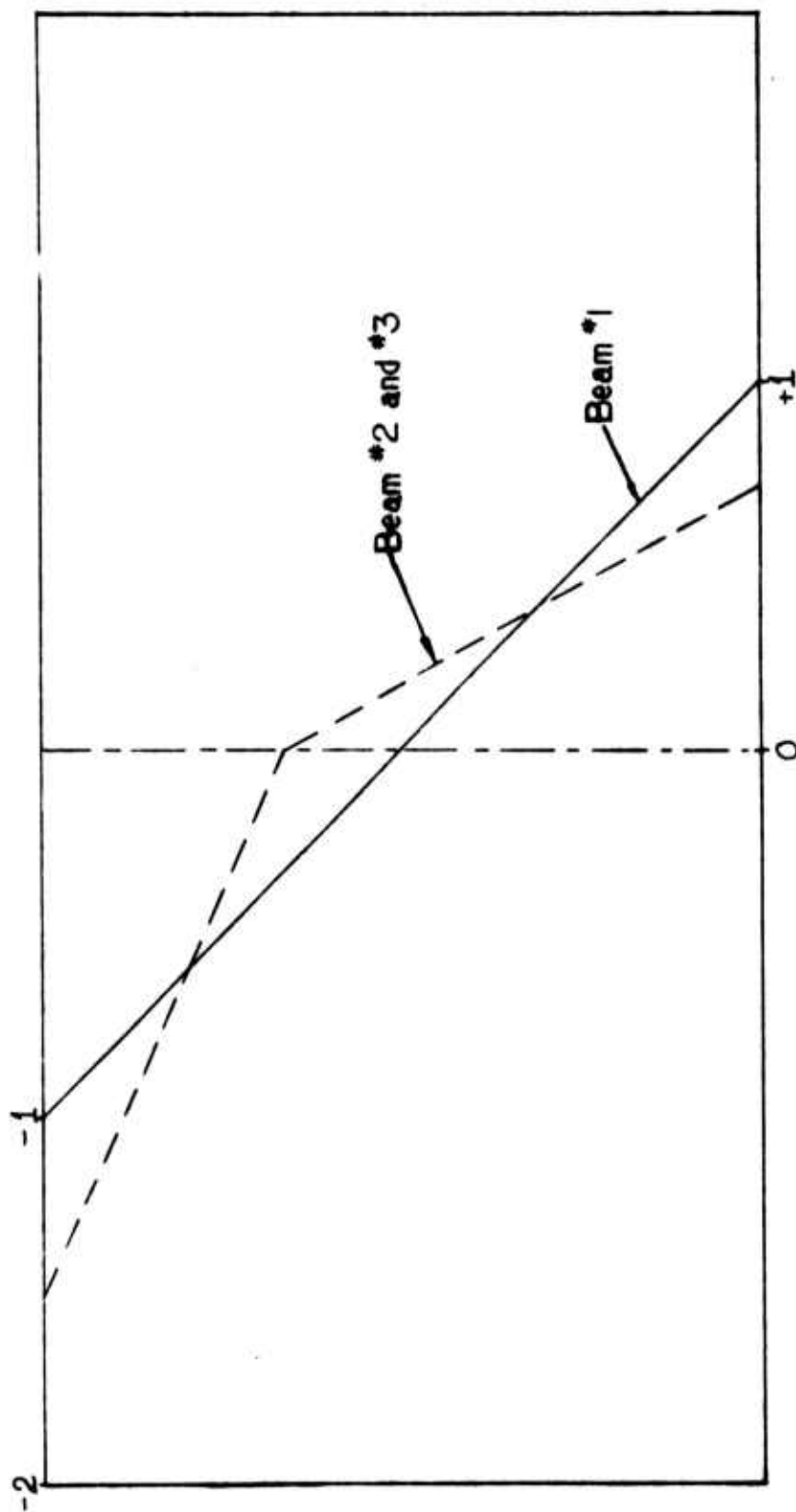


FIGURE 8 (b) Stress Distributions of Linear and Bilinear Viscoelastic Beams Under Pure Bending

2.4 Formulation of Plane Stress Problems

In the analysis of stress and deformation, three kinds of equations are needed; equilibrium equations, kinematic (compatibility) equations and constitutive equations of the material, plus the boundary conditions. The first two kinds of equations are the same for linear elastic as well as for bilinear elastic problems. The main feature which differentiates the bilinear elastic from linear elastic problems is in the constitutive equations. In the following, the governing equations used in the solution of stress analysis problems for bilinear elastic material are formulated briefly.

(A) Equilibrium Equations

$$\frac{\partial \sigma_x}{\partial x} + \frac{\partial \tau_{xy}}{\partial y} = 0 \quad (55a)$$

$$\frac{\partial \tau_{xy}}{\partial x} + \frac{\partial \sigma_y}{\partial y} = 0 \quad (55b)$$

(B) Compatibility Equations

$$\frac{\partial^2 \epsilon_x}{\partial y^2} + \frac{\partial^2 \epsilon_y}{\partial x^2} = \frac{\partial^2 \epsilon_{xy}}{\partial x \partial y} \quad (56)$$

(C) Bilinear Constitutive Equations

(C-1) Region 1 $\sigma_1 > 0$, $\sigma_2 > 0$

$$\epsilon_x = \frac{1}{E_T} [\sigma_x - \nu_T \sigma_y] \quad (57a)$$

$$\epsilon_y = \frac{1}{E_T} [\sigma_y - \nu_T \sigma_x] \quad (57b)$$

$$\epsilon_{xy} = \frac{2(1+\nu_T)}{E_T} \tau_{xy} \quad (57c)$$

(C-2) Region 2 $\sigma_1 > 0$, $\sigma_2 < 0$

$$\epsilon_x = \frac{1}{E_T} \frac{1+\phi^2}{2} \sigma_x - \frac{\nu_T}{E_T} \sigma_y + \frac{1-\phi^2}{4} \frac{(\sigma_x^2 - \sigma_y^2) + Q^2}{Q} \quad (23a)$$

$$\epsilon_y = -\frac{\nu_T}{E_T} \sigma_x + \frac{1}{E_T} \frac{1+\phi^2}{2} \sigma_y + \frac{1-\phi^2}{4} \frac{(\sigma_y^2 - \sigma_x^2) + Q^2}{Q} \quad (23b)$$

$$\epsilon_{xy} = \frac{1}{E_T} \left(\frac{1+\phi^2}{2} + \nu_T \right) (2\tau_{xy}) - \frac{1-\phi^2}{2} \frac{(\sigma_x + \sigma_y) \sigma_{xy}}{Q} \quad (23c)$$

$$Q^2 = (\sigma_x - \sigma_y)^2 + (2\sigma_{xy})^2 \quad (23d)$$

(C-3) Region 3 $\sigma_1 < 0$, $\sigma_2 < 0$

$$\epsilon_x = \frac{1}{E_C} [\sigma_x - \nu_C \sigma_y] \quad (58a)$$

$$\epsilon_y = \frac{1}{E_C} [\sigma_y - \nu_C \sigma_x] \quad (58b)$$

$$\epsilon_{xy} = \frac{2(1+\nu_C)}{E_C} \tau_{xy} \quad (59c)$$

Because of the difference in the constitutive equations in these three regions, the characteristic of the solutions for each region will be different. In regions 1 and 3, the constitutive equations (57) and (58) are identical to linear elastic problems, provided that E_T , ν_T and E_C , ν_C respectively, are used in regions 1 and 3 instead of E and ν . Therefore in these two regions the characteristics of the solutions should be similar to that of the linear elastic solution. For example, introducing a stress function as defined in the following:

$$\sigma_x = \frac{\partial^2 \psi}{\partial y^2} \quad (59a)$$

$$\sigma_y = \frac{\partial^2 \psi}{\partial x^2} \quad (59b)$$

$$\tau_{xy} = - \frac{\partial^2 \psi}{\partial x \partial y} \quad (59c)$$

It can be shown readily that the solution of a two-dimensional problem in these two regions reduce to finding a bi-harmonic function,

$$\frac{\partial^4 \psi}{\partial x^4} + 2 \frac{\partial^4 \psi}{\partial x^2 \partial y^2} + \frac{\partial^4 \psi}{\partial y^4} = 0 \quad , \quad (60)$$

which satisfies appropriate boundary conditions.

In region 2, however, the solution will be much more difficult due to the nonlinear constitutive equations in this region. Methods of solving the problem in this region will be discussed in detail in the next section.

The difficulty in solving the problem in region 2 is only a part of the whole problem in solving a general plane stress problem for a bi-linear elastic material. If the boundaries separating these three different types of regions are known, in prior, then in principle the solution on each region can proceed independently and the solution in each region should satisfy both the prescribed exterior boundary conditions and the stress and strain across the interface between two regions must be continuous. Unfortunately, the boundaries separating these three different types of regions are not known in prior to most problems. This will further complicate the solution of a general plane stress problem.

2.5 Stress Analysis of a Circular Opening under Internal Pressure

Due to the fact that the geometry of the boundary and the loading are axially symmetric, the solution of this class of problem can be formulated by means of polar coordinates (r, θ) and that the solution should depend only on r . Furthermore, as shown in Figure 9, the whole body can be separated into two regions. In the inner region (region 1) the radial stress is in compression and the tangential stress is in tension; in the outer region (region 2) both axial and tangential stress are compression. The interface separating these two regions is undetermined but is dependent only on a single parameter ($r = R$) due to the axially symmetric condition. Because of this, the solution of this class of problem becomes possible. Although the solution of this problem is available elsewhere [15, 17, 18], a brief discussion of this problem is presented in this section to illustrate the techniques for solving this type of problem which may help to gain an insight into the solution of the more complex general two dimensional problems one of which is to be discussed in the next section.

The equation of equilibrium for this axially symmetric problem is given by:

$$\frac{d}{dr} \left(\frac{\sigma_{rr}}{r} \right) + \frac{\sigma_{rr} - \sigma_{\theta\theta}}{r} = 0 \quad (61)$$

where σ_{rr} and $\sigma_{\theta\theta}$ are the radial and tangential stresses. In the following, only the plane stress problem ($\sigma_{zz} = 0$) is considered.

The strain-displacement relations are given by

$$\epsilon_{rr} = \frac{du}{dr}, \quad \epsilon_{\theta\theta} = \frac{u}{r} \quad (62)$$

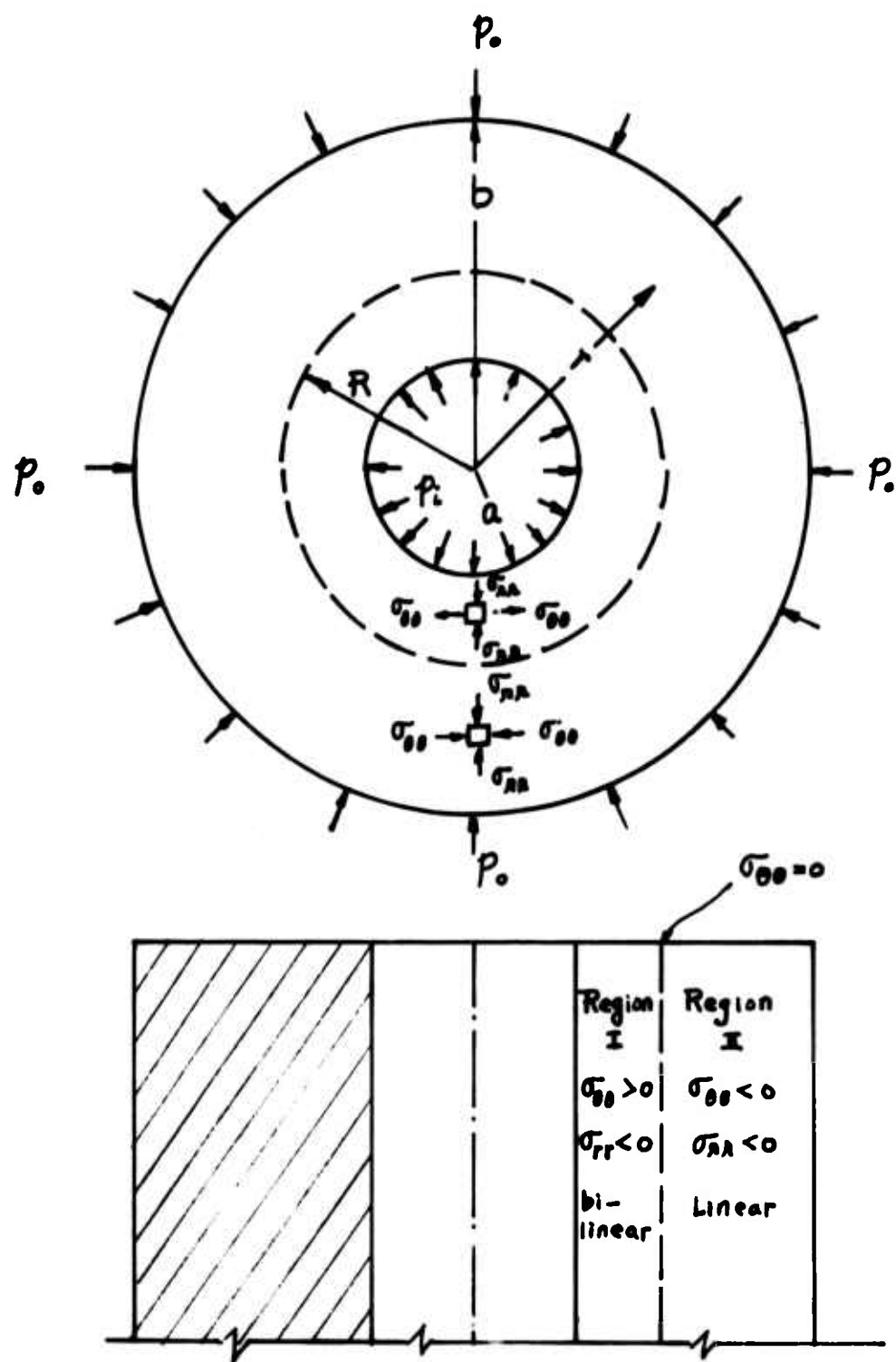


FIGURE 9 Thick Walled Cylinder Under Internal Pressure

where ϵ_{rr} and $\epsilon_{\theta\theta}$ are the radial and tangential strains; u is the radial displacement which depends on r only.

The stress-strain relations for regions I and II are as follows:

Region I:

$$\begin{aligned}\epsilon_{rr} &= \frac{1}{E_c} \sigma_{rr} - \frac{\nu_T}{E_T} \sigma_{\theta\theta} \\ \epsilon_{\theta\theta} &= -\frac{\nu_c}{E_c} \sigma_{rr} + \frac{1}{E_T} \sigma_{\theta\theta}\end{aligned}\quad (63)$$

Region II:

$$\begin{aligned}\epsilon_{rr} &= \frac{1}{E_c} [\sigma_{rr} - \nu_c \sigma_{\theta\theta}] \\ \epsilon_{\theta\theta} &= \frac{1}{E_c} [\sigma_{\theta\theta} - \nu_c \sigma_{rr}]\end{aligned}\quad (64)$$

For Region I, solving stresses σ_{rr} , $\sigma_{\theta\theta}$ in terms of strains ϵ_{rr} and $\epsilon_{\theta\theta}$ and using (62), the stress σ_{rr} , $\sigma_{\theta\theta}$ can be expressed in terms of radial displacement u as follows:

$$\begin{aligned}\sigma_{rr} &= \frac{E_c}{1-\nu_c^2 \phi^2} \left[\frac{du}{dr} + \nu_c \phi^2 \frac{u}{r} \right] \\ \sigma_{\theta\theta} &= \frac{\phi^2 E_c}{1-\nu_c^2 \phi^2} \left[\nu_c \frac{du}{dr} + \frac{u}{r} \right]\end{aligned}\quad (65)$$

In (65) the following relations $\frac{\nu_T}{E_T} = \frac{\nu_c}{E_c}$ and $\phi^2 = \frac{E_T}{E_c}$ have been used. Inserting (65) into (61) yields

$$\frac{d^2 u}{dr^2} + \frac{1}{r} \frac{du}{dr} - \phi^2 \frac{u}{r^2} = 0 \quad (66)$$

The general solution of (66) is

$$U(r) = A r^\phi + B r^{-\phi} \quad (67)$$

Inserting (67) into (65) yields the following stresses in Region I

$$\sigma_{rr} = \frac{E_c}{1-\nu_c} \frac{\phi^2}{2} [A(\phi+\nu_c\phi^2) r^{\phi-1} - B(\phi-\nu_c\phi^2) r^{-\phi-1}] \quad (68a)$$

$$\sigma_{\theta\theta} = \frac{\phi^2 E_c}{1-\nu_c} \frac{\phi^2}{2} [A(1+\nu_c\phi) r^{\phi-1} + B(1-\nu_c\phi) r^{-\phi-1}] \quad (68b)$$

The stresses in Region II can be obtained readily from linear elastic solution [19] as follows:

$$\sigma_{rr} = \frac{C}{r^2} + D \quad (69a)$$

$$\sigma_{\theta\theta} = -\frac{C}{r^2} + D \quad (69b)$$

The following boundary conditions are used to determine the four constants A, B, C, D and the interface $r = R$ which separates the two regions.

$$\left. \begin{array}{ll} \sigma_{rr} = -P_i & \text{at } r = a \\ \sigma_{\theta\theta} = 0 & \text{at } r = R \end{array} \right\} \quad (\text{in Region I})$$

$$\left. \begin{array}{ll} \sigma_{\theta\theta} = 0 & \text{at } r = R \\ \sigma_{rr} = -P_o & \text{at } r = b \end{array} \right\} \quad (\text{in Region II})$$

$$\sigma_{rr}^{(I)} = \sigma_{rr}^{(II)} \quad \text{at } r = R \quad (70)$$

In Region I ($r < R$), the following stresses can be obtained:

$$\sigma_{rr} = -P_i \left(\frac{r}{a}\right)^{\phi-1} \frac{\left(\frac{R}{r}\right)^{2\phi} + 1}{\left(\frac{R}{a}\right)^{2\phi} + 1} \quad (71a)$$

$$\sigma_{\theta\theta} = \phi P_i \left(\frac{r}{a}\right)^{\phi-1} \frac{\left(\frac{R}{r}\right)^{2\phi} - 1}{\left(\frac{R}{a}\right)^{2\phi} + 1} \quad (71b)$$

In Region II ($r > R$) the following stresses can be obtained:

$$\sigma_{rr} = -P_o \frac{\left(\frac{R}{r}\right)^2 + 1}{\left(\frac{R}{b}\right)^2 + 1} \quad (71c)$$

$$\sigma_{\theta\theta} = P_o \frac{\left(\frac{R}{r}\right)^2 - 1}{\left(\frac{R}{b}\right)^2 + 1} \quad (71d)$$

where R can be determined from the last boundary conditions.

$$\left(\frac{R}{a}\right)^{\phi-1} \frac{\left(\frac{R}{b}\right)^{2\phi} + 1}{\left(\frac{R}{a}\right)^{2\phi} + 1} = \frac{P_o}{P_i} \quad (71e)$$

As the external boundary become very large in comparison with the internal boundary ($\frac{a}{b} \rightarrow 1$) and $P_o = 0$, the effect of bilinearity on the maximum tangential stress becomes:

$$\sigma_{\theta\theta} = P_i \phi = P_i \sqrt{\frac{E_T}{E_C}} \quad (72)$$

2.6 Solutions of a Circular Disk under Diametral Compression

A circular disk under vertical diametral compression as shown in Figure 10 yields a biaxial tension and compression stress field along the vertical and horizontal diameters. Because of this unique feature, a single test of the disk readily reveals strengths in both tension and compression of the material concerned. This type of test becomes popular particularly for testing the tensile properties of brittle materials.

Although the linear elastic solution of this problem is available [19] the solution of this same problem for bilinear materials is nevertheless very involved. The basic equations for plane stress problems are presented in Section 2.4. Because of the highly nonlinear constitutive equation, (23a, 23b, 23c), in Region II it is doubtful that an exact analytical solution can be obtained. In the following, the solution of the bilinear problem is explored, using:

- (1) a finite difference approximation
- (2) orthotropic plate solution using finite element technique.

Finite Difference Approximation

In formulating the solution it is assumed that the entire region of the disk belongs to stress zone 2, i.e., $\sigma_1 > 0$, $\sigma_2 < 0$, $\sigma_3 = 0$. This assumption is reasonable in light of the linear elastic solution of the same problem.

Substituting the stresses in terms of the stress function as defined in (59a, 59b, 59c) into the bilinear stress-strain relations (23a, 23b, 23c), and then substituting the stress-strain relations into the compatibility equation (56) yields the following fourth order partial differential equation for the stress function

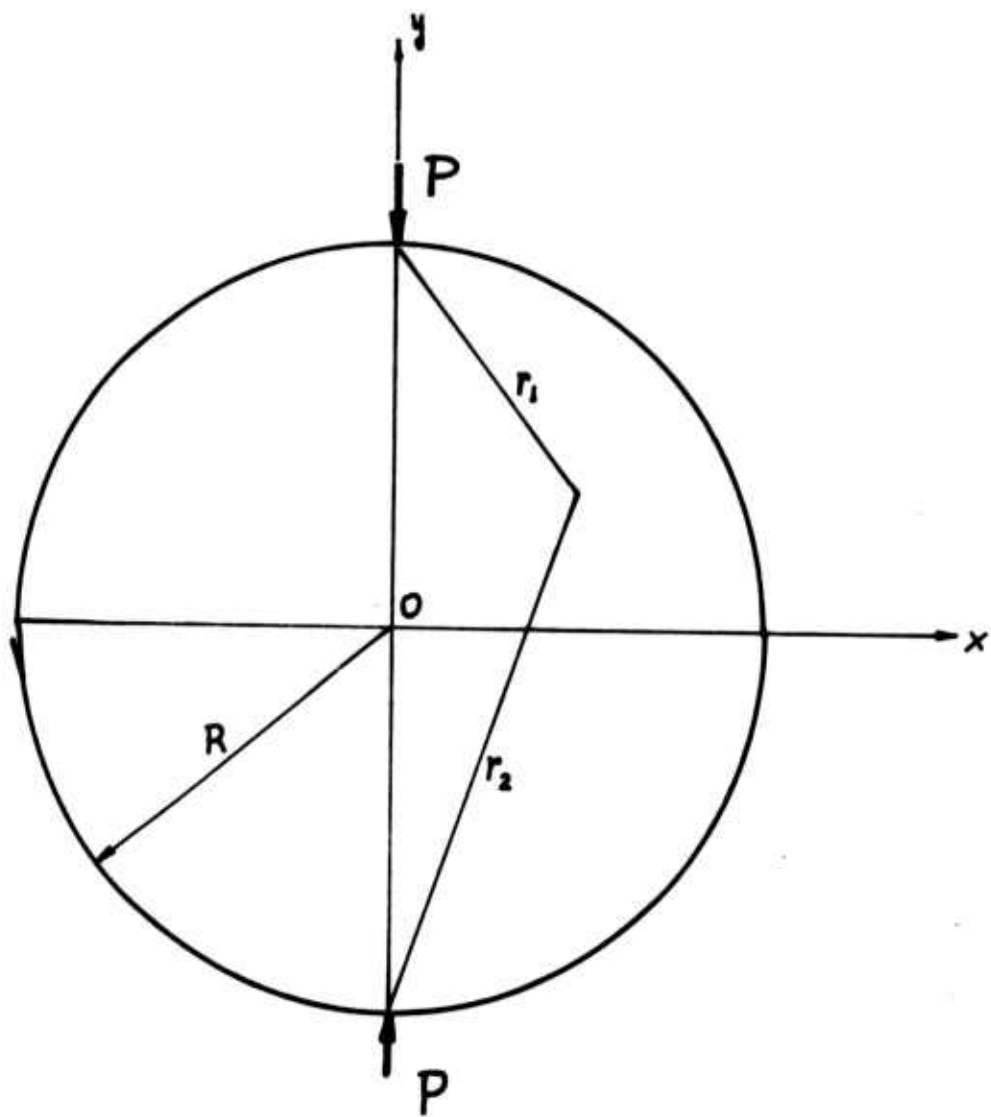


FIGURE 10 A circular Disk Under Diametral Compression

$$\frac{\partial^4 \psi}{\partial x^4} + 2 \frac{\partial^4 \psi}{\partial x^2 \partial y^2} + \frac{\partial^4 \psi}{\partial y^4} = \frac{1}{\nu_T} \frac{1-\phi^2}{4} K_\psi \quad (73)$$

where K_ψ contains all the nonlinear terms

$$K_\psi = \left[\frac{\sigma_x^2 - \sigma_y^2 + Q^2}{Q} \right]_{,yy} + \left[\frac{\sigma_y^2 - \sigma_x^2 + Q^2}{Q} \right]_{,xx} - 2 \left[\frac{(\sigma_x + \sigma_y) \sigma_{xy}}{Q} \right]_{,xy}$$

$$Q^2 = (\sigma_x - \sigma_y)^2 + (2\sigma_{xy})^2 \quad (74)$$

and the stresses σ_x , σ_y and σ_{xy} in (74) have to be expressed in terms of the stress function as defined in (59a, 59b, 59c). When $\phi^2 = 1$, (73) reduces to the biharmonic function and therefore, reduces to the solution of the corresponding linear elastic problem.

Equation (73) is solved by means of successive iteration using finite difference methods

$$\psi_{,xxxx}^{(n)} + 2\psi_{,xxyy}^{(n)} + \psi_{,yyyy}^{(n)} = \frac{1}{\nu_T} \frac{1-\phi^2}{4} K_\psi^{(n-1)} \quad (75)$$

where $K_\psi^{(n-1)}$ is the solution obtained from the iteration.

When $n = 0$, $K_\psi^{(n-1)} = 0$ and (75) reduces to a biharmonic function. Thus, the linear elastic solution of the stresses σ_x^0 , σ_y^0 , σ_{xy}^0 [19] as shown in the following serve as the initial input for the iteration.

$$\sigma_x^0 = -\frac{2P}{\pi} \left[\frac{(R-y)x^2}{r_1^4} + \frac{(R+y)x^2}{r_2^4} - \frac{1}{2R} \right]$$

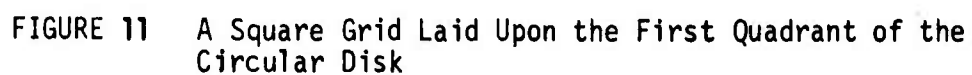
$$\sigma_y^0 = -\frac{2P}{\pi} \left[\frac{(R-y)^3}{r_1^4} + \frac{(R+y)^3}{r_2^4} - \frac{1}{2R} \right]$$

$$\sigma_{xy}^0 = \frac{2P}{\pi} \left[\frac{(R-y)^2 x}{r_1^4} - \frac{(R+y)^2 x}{r_2^4} \right] \quad (76)$$

$$\begin{aligned} r_1^2 &= x^2 + (R-y)^2 \\ r_2^2 &= x^2 + (R+y)^2 \end{aligned} \tag{76}$$

For the purpose of approximating derivatives of the stress function ψ by finite differences, a square grid of size $h = 0.08R$ is laid on one quarter of the circular disk (Figure 11). This gives a total of 135 interior grid points and 26 boundary points. The grid size selected is such that, based on an analysis of the linear elastic case, it yields a fairly good approximation to the derivatives of the stress function by finite differences. Equation (75), which must be valid throughout a circular disk under diametral compression, is written for each of the 135 interior grid points, by way of approximating the derivatives of the stress function by finite difference. For those interior points close to the boundary the distances between adjacent points may not be equal. In such cases, different derivation of finite difference equations for the irregular grid has to be used [20].

The following iterative process is used to solve (75). First, material properties and the numerical values of the linear elastic solution (76) are substituted into (74) and then to the right hand side of (75) for each of the 135 equations corresponding to the 135 grids. Thus, the solution of the problem reduces to the solution of 135 simultaneous linear equations with zero stress boundary conditions. This set of equations is solved using the Gauss-Seidel iterative method [21]. The result from the first iteration is then used to construct a new stress field for the disk. This stress field is substituted into (74) for calculating the K_ψ for each grid and the process is repeated until the ratio of the difference of the tensile stress at the center from the successive iterations to the tensile stress is less than one percent. The results are shown in Figure 12.



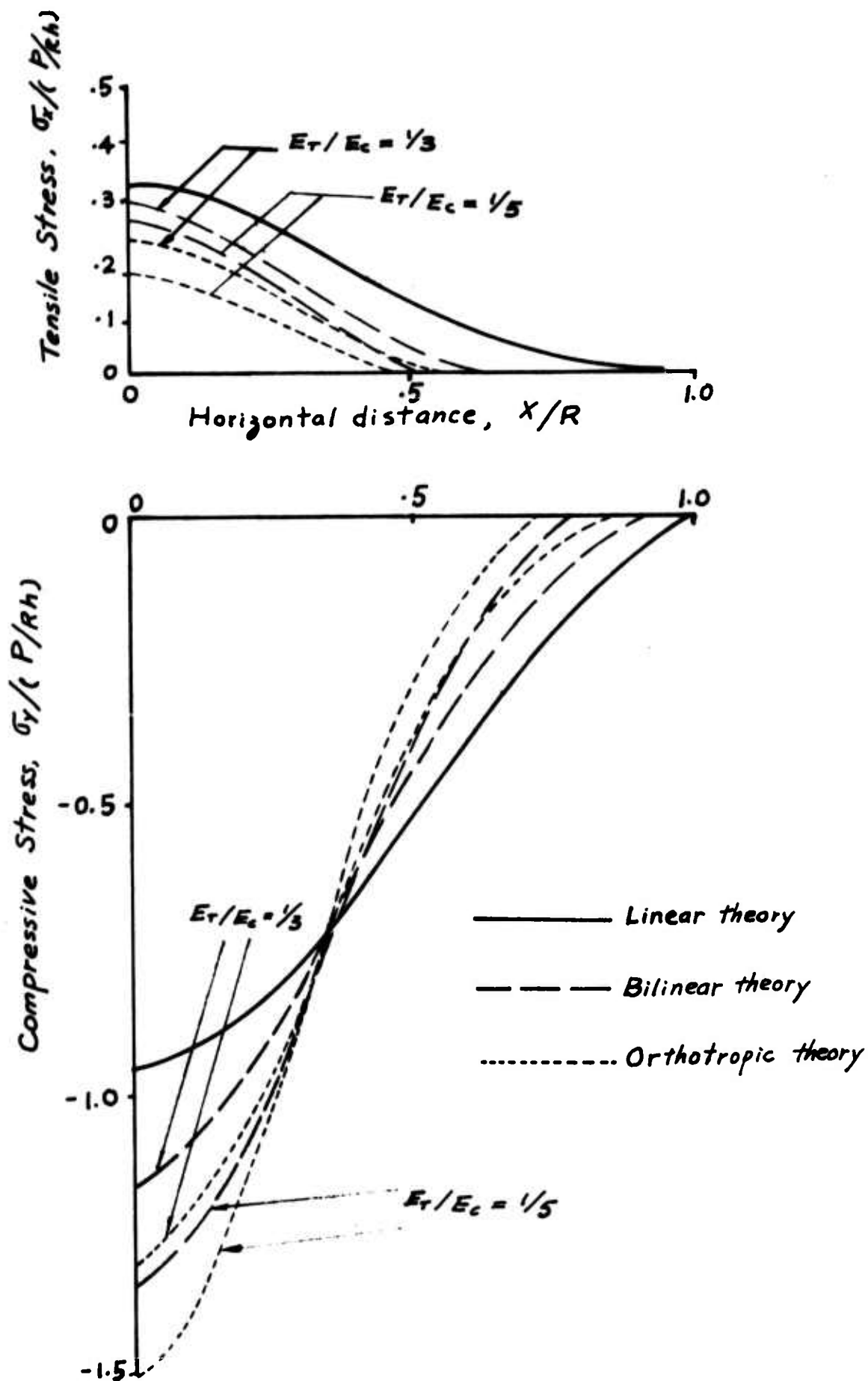


FIGURE 12 Comparison of Linear, Bilinear and Orthotropic Solutions of A Disk Under Diametral Compression

Orthotropic Plate Solution using Finite Element Techniques

If the circular disk is an orthotropic plate having moduli of E_T in the horizontal direction and of E_C in the vertical direction, the stress-strain relations become

$$\epsilon_x = \frac{1}{E_T} \sigma_x - \frac{\nu_C}{E_C} \sigma_y$$

$$\epsilon_y = -\frac{\nu_T}{E_T} \sigma_x + \frac{1}{E_C} \sigma_y$$

$$\epsilon_{xy} = \frac{\tau_{xy}}{G} = \left(\frac{1}{E_T} + \frac{1}{E_C} + \frac{\nu_T}{E_T} + \frac{\nu_C}{E_C} \right) \tau_{xy}$$

and the corresponding compatibility equation in terms of stress function becomes

$$\frac{\partial^4 \psi}{\partial x^4} + (1+\phi^2) \frac{\partial^4 \psi}{\partial x^2 \partial y^2} + \frac{\partial^4 \psi}{\partial y^4} = 0$$

Making use of Wilson's computer program [22], the solution of an orthotropic circular plate under diametral compression is obtained and plotted in Figure 12 for compression.

Comparison Between Linear, Bilinear and Orthotropic Solutions

The linear elastic solution [19], the bilinear and orthotropic solutions obtained in this section are shown in Figure 12. For $E_T < E_C$, the tensile stresses at the center and along the horizontal diameter of the disk in the bilinear solution and orthotropic solution are both less than the result obtained from the linear elastic solution, through the bilinear elastic solutions lie between the linear elastic and orthotropic

solution. The compressive stresses at the center and along the horizontal diameter are higher than the corresponding stresses obtained from the linear elastic solution. Again, the bilinear elastic solutions lie between the linear elastic and orthotropic solutions.

3.0 EXPERIMENTAL INVESTIGATION

The objectives of the experimental investigation are twofold; (1) to investigate the time and temperature dependent properties of two rock types, Charcoal granite and Diesser basalt, with emphasis on investigating the different response under tensile and compressive stresses, (2) to investigate the strain distributions of beams under bending and disks under diametral compression of the two rock types.

3.1 Materials and Specimens

Two 1' X 1' X 1' blocks of Charcoal granite and one 1' X 1' X 1' block of Dresser basalt used in the tests were supplied by Twin Cities Mining Research Center, Twin Cities, Minnesota. Information pertaining to these two rock types are given in Table 2.

Compression specimens of 1 1/2" diameter and approximately 3 in. long were used. The specimens were cored by a 1 1/2" diamond core drill. Ends were machined parallel to within 0.001 in. The tension specimens of 1.404 in. diameter and approximately 6 1/2 in. long were used. The specimen surfaces were polished.

For the beam bending tests, the specimens used were 3" X 3/4" X 15". For the diametral compression tests, the specimens used were 4 in. diameter and 3/4 in. thick.

3.2 Compression Apparatus and Testing Procedures

An 80,000 pound capacity uniaxial compression testing device was designed and constructed in the course of this study. As shown in Fig. 13, the apparatus consisted of four major parts: a main frame, a hydraulic loading system, a heating device and an axial strain measuring device.

TABLE II - MATERIAL PROPERTIES

	Charcoal Granite	Dresser Basalt
Sources	St. Cloud, Minnesota	Dresser, Wisconsin
Mineral Content (percent by wt)	Fledspar 60% Quartz 16% Hornblende 20% Eiotite 3% Other 1%	Feldspar 50% Augite 40% (including altered material) Magnetite 8% Other 2%
Average Grain Size	0.46 mm	0.10 mm

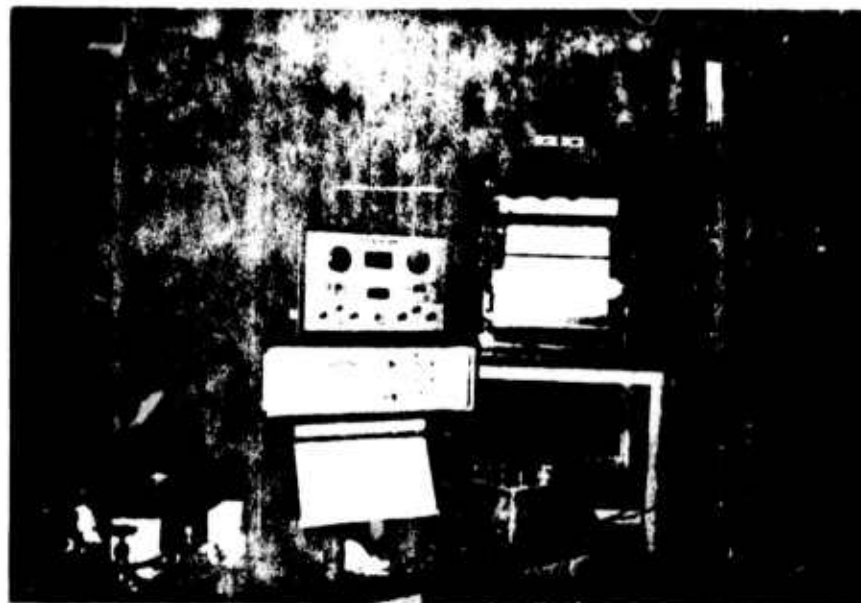


FIGURE 13 Compression Apparatus

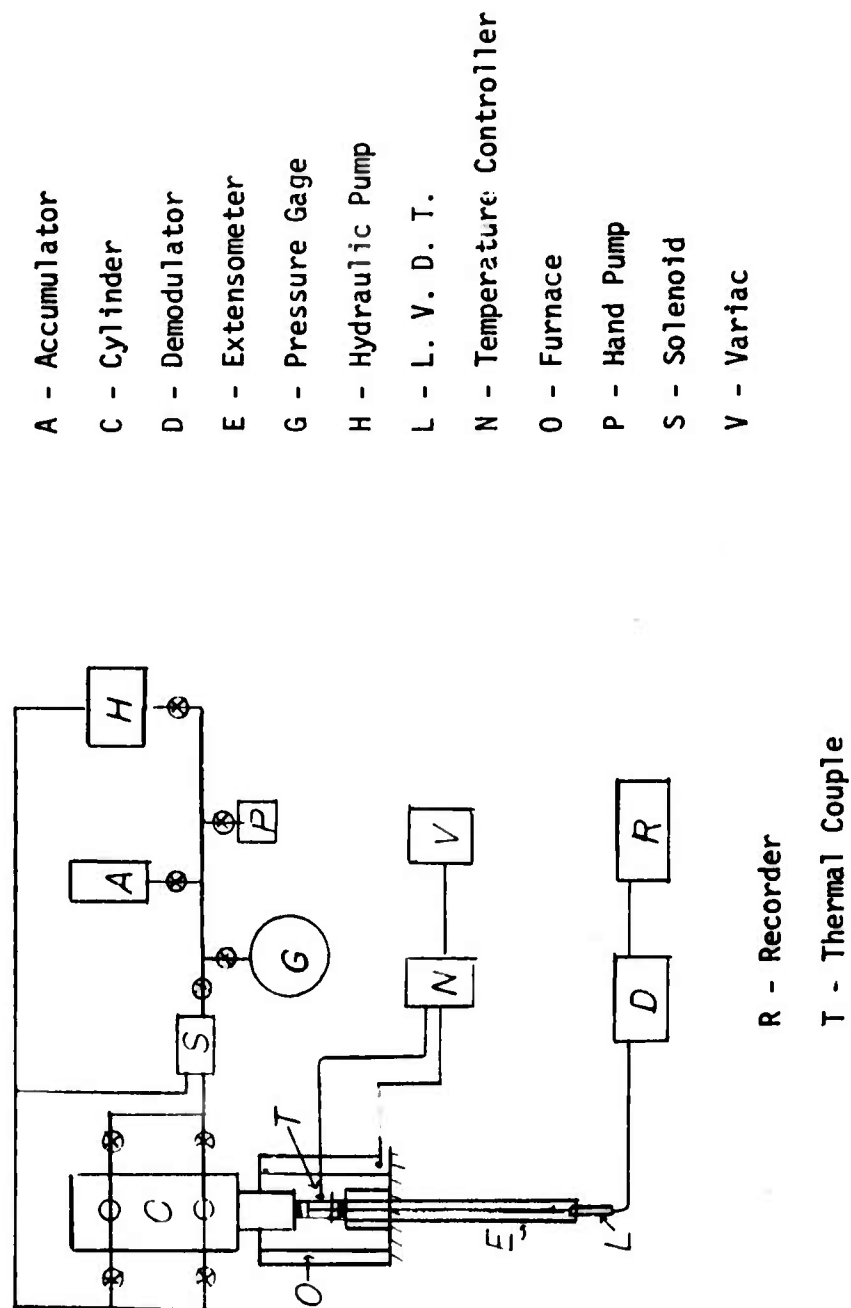


FIGURE 14 Schematic Diagram of Compression Test Apparatus

The hydraulic loading system as shown schematically in Fig. 14 consisted of a hydraulic pump, an accumulator, a solenoid and a double acting cylinder. In addition, a hand pump was also connected to the system. The relationship between the pressure of the system and the load generated from the cylinder was calibrated by a 100,000 pounds capacity proving ring and the total load exerted on the specimen was read directly from a Heise Pressure gage.

In order to perform creep tests above room temperature, a temperature regulating system was used. The specimen was heated in an electric split-tube furnace which was maintained at constant temperature by an API's temperature controller. An iron-constantan thermocouple was used to measure the temperature. Power was supplied at 220 volts through a variac to the furnace. The temperature variation along the gage length was 8°F.

The strain measurement was accomplished by using two pairs of rods attached to the upper and lower gage points of the test specimen to transmit the motion of the gage points to a linear variable displacement transformer (LVDT). The gage length is about 2 1/2 in. Relative motion of the upper and lower gage points during the test caused an output of the LVDT which was directly related to the strain. The output from the LVDT was amplified and demodulated and a permanent record was made by a strip-chart recorder. The sensitivity of strain measurement was 20×10^{-6} in./in. The transverse strain was measured by means of a Micro-Measurement's WK-06-250BP-120 high temperature strain gage. A strain indicator was used to monitor this strain output.

During the set-up the rock specimen was placed between the upper and lower loading heads. To prevent excessive heat transfer through the loading head, which would cause uneven temperature distribution in specimen, two 1/8 in. asbestos sheets and two 1/2 in. thick stainless steel discs were used.

The asbesto sheets were placed directly against the loading heads and the steel discs were placed between the asbesto sheets and specimen ends. This arrangement provided proper insulation to achieve a uniform temperature distribution along the gage length and over the cross section and yet prevented intrusion failure of the rock sample which would have resulted had the asbesto been placed directly against the specimen end.

During each of the tests, the rate of heating was controlled at about 5°F. per minute. After reaching the test temperature, the specimen was maintained at that temperature for about one hour before loading. It was found that the temperature at the center of the specimen reached the test temperature in approximately 30 minutes after the surface reached the test temperature. The temperature was then maintained at selected constant value throughout the duration of the test.

During loading, the hydraulic pump was used to precharge the accumulator first to about 200 psi higher than the desired pressure and then to charge the cylinder. When the desired pressure was reached in the cylinder, the pump was shut off. The accumulator then was used to supply and regulate the pressure in the cylinder. If additional pressure was desired in order to raise the compressive load, the pump was turned on again to precharge the accumulator first; then the same process followed.

In performing the constant stress creep tests, the specimen was loaded in a stepwise manner to each desired creep load within about 30 seconds. Owing to the creep of the specimen, which would cause a slight decrease in pressure, a hand pump was used to adjust and maintain the desired pressure. Although using the accumulator could accomplish the same objective, the use of a hand pump was easier particularly in making a fine adjustment.

In performing the test for determining the Young's modulus and Poisson ratio, the load was increased slowly in small steps and the corresponding axial and transverse strain at each load were recorded. After a linear stress-strain relationship was obtained, the load was then decreased slowly in small steps and the corresponding strain were recorded.

3.3 Tension Apparatus and Testing Procedures

The tension machine was designed to test cylindrical specimens under uniaxial tensile load. The tensile load was produced by dead weights through a 1:20 ratio lever arm. The heating and the axial strain measuring device were identical to the one described in Section 3.2 except the silica glass (vycor) rods, instead of stainless steel rods were used for the extensometer rods. This material has a very low thermal expansion coefficient (about 10^{-12} in./in./°F.) and therefore could minimize the error induced in the tensile strain due to change in temperature of the rods. Figure 15 shows the apparatus and Figure 16 is a schematic diagram of the testing system.

It took a considerable amount of time to resolve the specimen gripping problem. For an enlarged ended specimen, gripping is relatively simple. Unfortunately, for hard rocks such as the ones used in this study, an enlarged ended specimen is very difficult to make and is very costly. For these reasons it was decided to use cylindrical specimens which could be obtained at a relatively low cost as this type of specimen can be obtained directly using a core drill. Gripping of a straight cylinder-type specimen becomes a problem. The problem of gripping was further compounded by high strength and high temperature required during testing. After trying several different types of grips, a friction grip

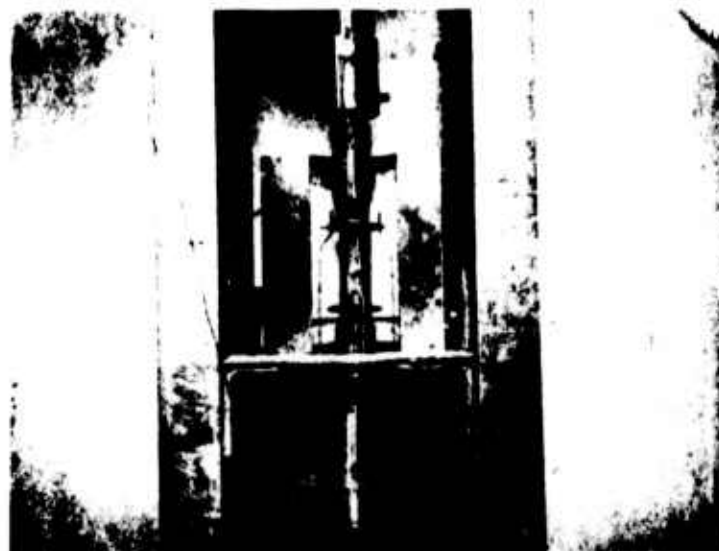


FIG. 15 Tension Apparatus

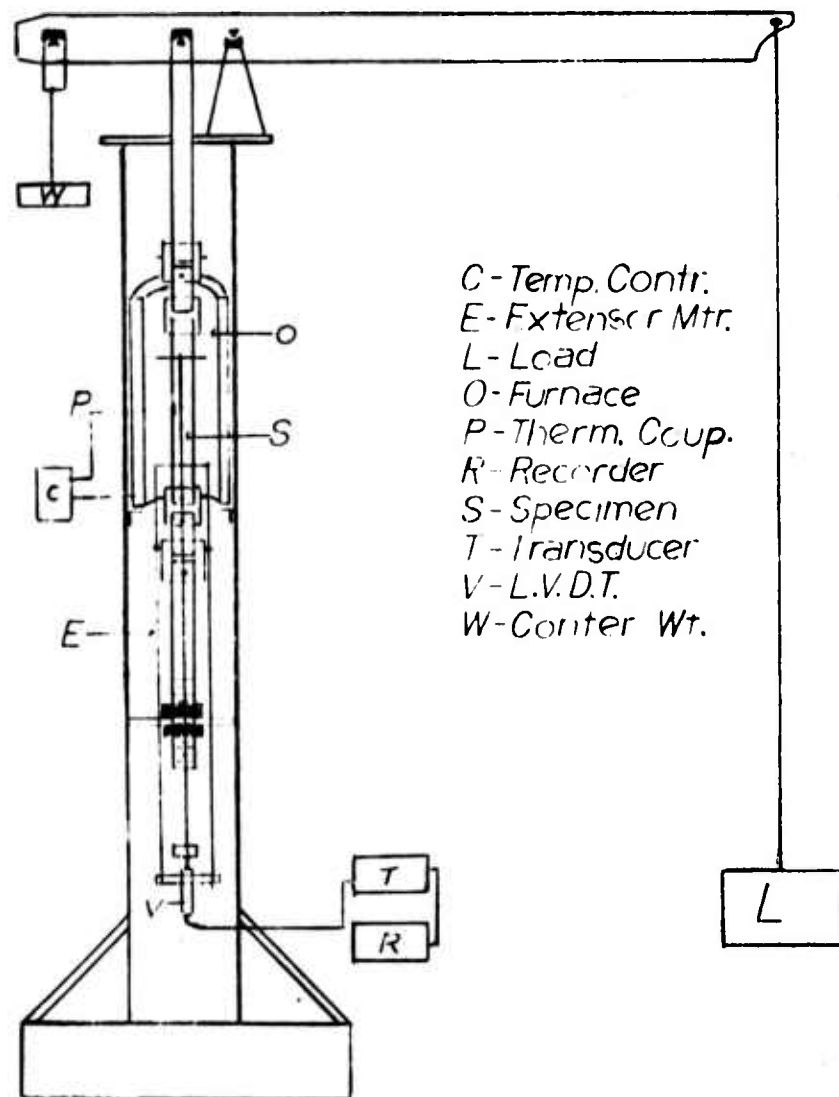


FIG. 16 TENSION APPARATUS (Schematic Diagram)

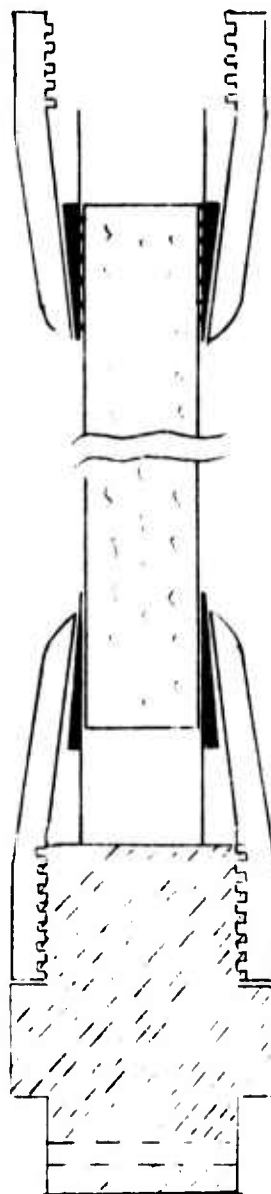
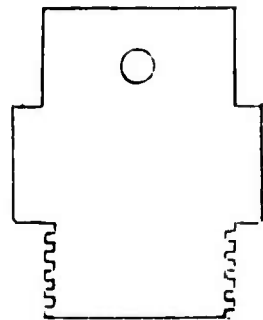


FIGURE 17 Tension Grip

was found to be quite satisfactory. The grip, as shown in Figure 17, consisted of a stainless steel collar, a connecting rod, and a tapered circular spring wedge with diamond spikes welded on the inner side of the spring. When assembled, the inner side of the spring with diamond spikes contacted the lateral surface of the rock specimen around the ends. When tensile loads were applied to the specimen through the grips, the grips had the tendency to slide out inducing lateral pressure against the surface of the rock sample and further tightening the grips on the specimen. This grip design proved to be quite satisfactory. Of the tensile tests conducted using this kind of grip, only a few specimen failed in or near the grips.

During testing, the heating procedure was identical to the one used in the compression tests. The loading procedure was relatively simple, as dead loads were applied to one end of the lever arm.

3.4 Diametral Compressing Bending Testing Apparatus and Procedures

An Instron tester with a temperature chamber was used for carrying out the diametral compression tests and beam bending tests. Although Instron tester is in general a deformation controlled testing machine, the fact that the creep phenomenon is negligibly small for the testing temperature up to 400°F permits one to conduct these tests using this apparatus.

For the diametral compression tests the vertical and horizontal strains at the center of the disk were measured by means of a micro-measurements WK-06-250WT-120 Tee rosette high temperature ° strain gage. The previous uniaxial compression test results indicate that this type of strain gage can be used only up to 450°F, although according to the

manufacturer's specification, this type of gage can be used up to 600°F. Because of this reason, the testing temperature for the diametral compression tests and beam bending tests was held below 400°F.

During the tests, a cross head speed of 0.02 in./min. was used. The load exerted on the specimen as well as the longitudinal and the transverse strain at the center of the disk were simultaneously recorded until maximum load was reached; and the specimens were fractured diametrically.

For the beam bending tests, the maximum tensile strains and the maximum compressive strains of the beam under a two-points loading were measured by means of two strain gages attached to the top and bottom surfaces of the beam.

3.5 Experimental Results of Charcoal Granite

Compression Tests

The compression test program is summarized in Figure 18. These tests consisted of determination of Young's modulus, Poisson's ratio and step loading tests for determining the creep properties. Six tests were conducted, each at a different temperature (73°F, 224°F, 356°F, 451°F, and 819°F), for determining Young's modulus and Poisson's ratio as a function of temperature. The results of the axial stress-strain curves are shown in Figure 19. It can be seen from these stress-strain curves that the material at low stress has lower stiffness than at higher stress. When the stress was increased gradually, the material gradually stiffened as shown in each curve, until a certain stress was reached. Beyond this stress, the stress-strain relation became linear. It was speculated

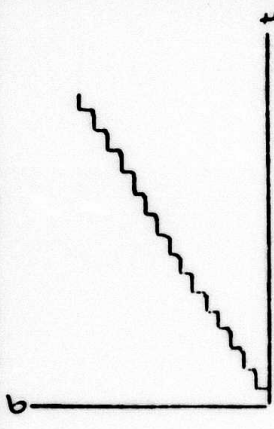
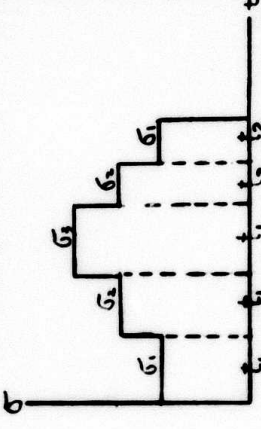
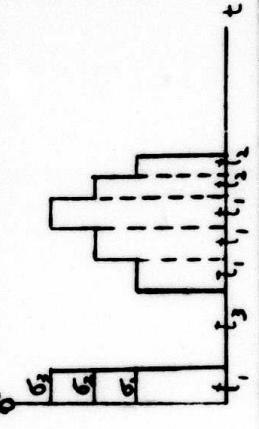
	Loading vs. Time	No. spec. used	Test Temp. °F	
1		6	73 224 356 451 540 819	
2	<div>a</div> 	5	500 550 600 650 700	$\sigma_1 = 10,000 \text{ psi}$ $\sigma_2 = 15,000 \text{ psi}$ $\sigma_3 = 20,000 \text{ psi}$
	<div>b</div> 	3	600	$t_1 = 30 \text{ min.}$ $t_2 = 20 \text{ min.}$ $t_3 = 70 \text{ min.}$

FIGURE 18 Test Program for Charcoal Granite in Compression

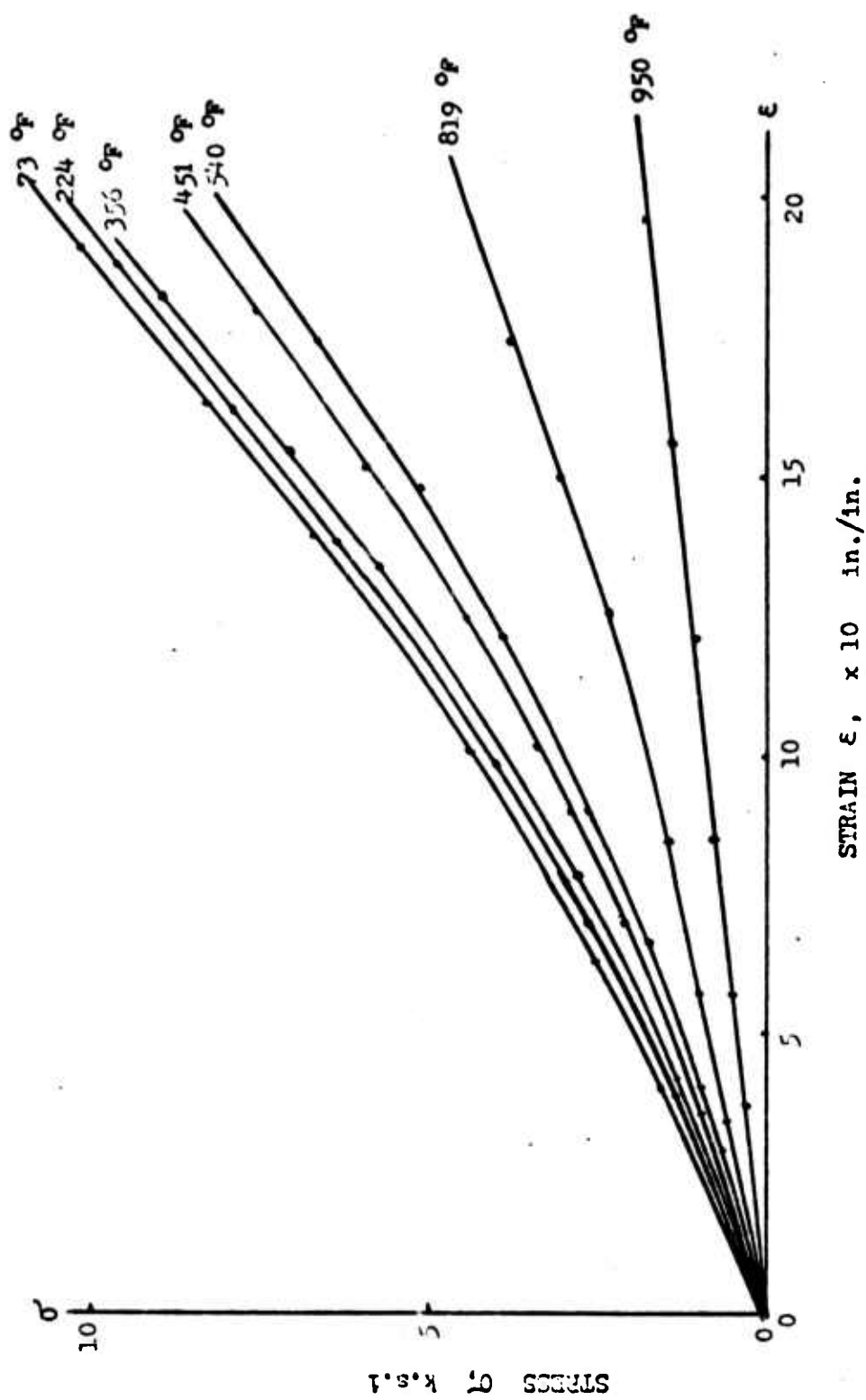


FIGURE 19 Axial Stress-Strain Relations for Charcoal Granite

that the existence of this stress might be due to the "preconsolidation" effect of the material before it was taken from the underground site. Casagrande's technique for predicting the preconsolidation pressure of soil was used to determine the stress and strain at the threshold and the typical result is shown in Figure 20. Plotting threshold stress (σ_0) at each test vs. temperature, as shown in Figure 21, indicated that the threshold stresses were linearly proportional to the temperature. The threshold strains were found to be independent of temperature and had the magnitude of about 0.00084 in./in..

The Young's modulus of the rock was determined from the straight line portion of the stress-strain curves shown in Figure 19. However, because of the fact that not all the strain is completely recoverable, the stress-strain relation should be further divided into recoverable and unrecoverable portions so that a true Young's modulus may be determined from the recoverable portion of the strain. A complete determination of the uniaxial stress-strain relation including recoverable, irrecoverable and time-dependent components is presented later in this section.

The transverse strain during each test was recorded. Two Poisson's ratios were calculated for each test, one Poisson's ratio was obtained from the loading portion of the test results by dividing the total measured transverse strain by the total axial strain; the second Poisson's ratio was obtained from the unloading portion of the test results by dividing the recoverable transverse strain by the recoverable axial strain. These two Poisson's ratios versus test temperature are shown in Fig. 22.

The step loading tests which were used for the determination of time independent as well as time dependent behavior of the material are

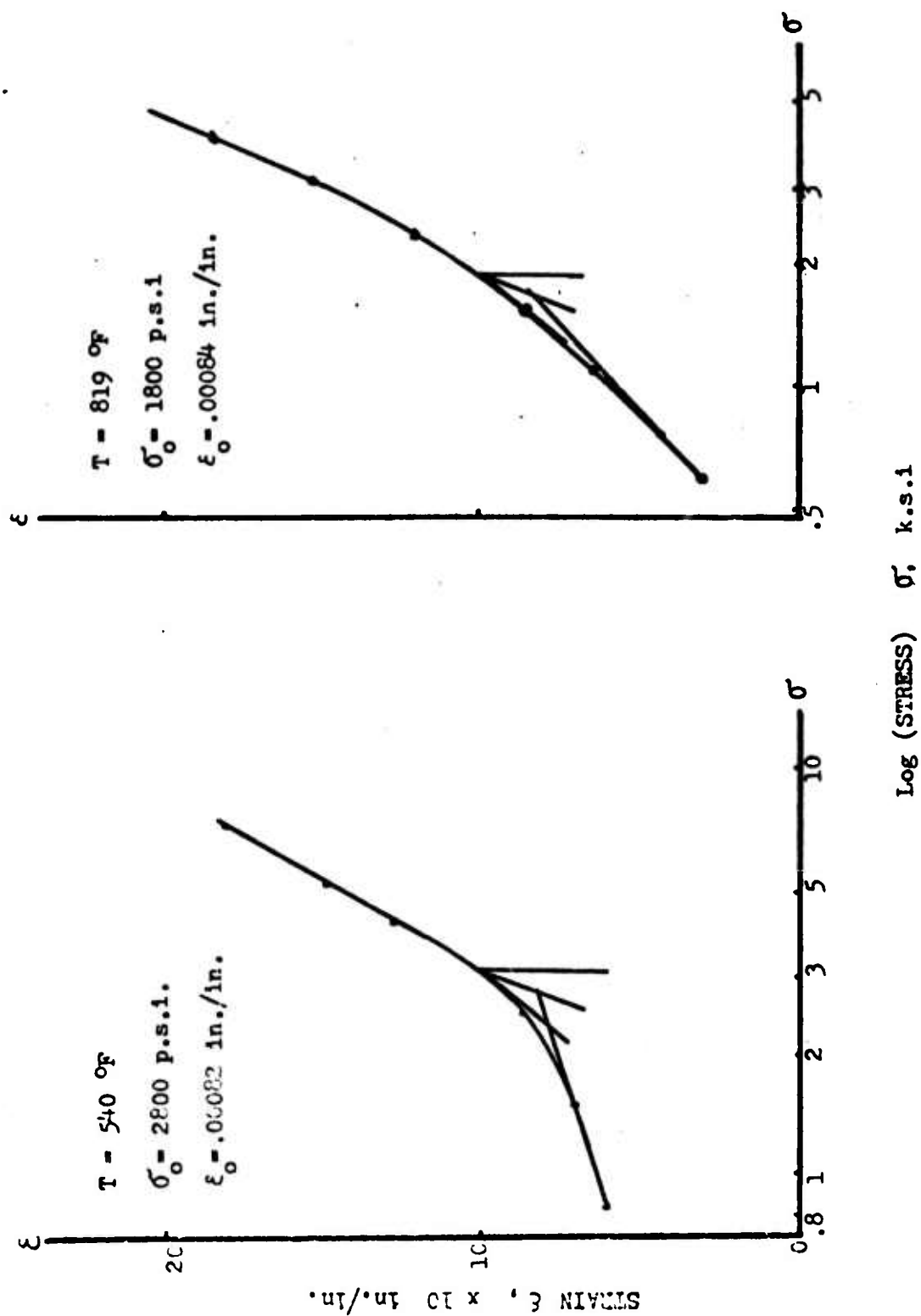


FIGURE 20 Determination of Threshold Stress and Strain for Charcoal Granite

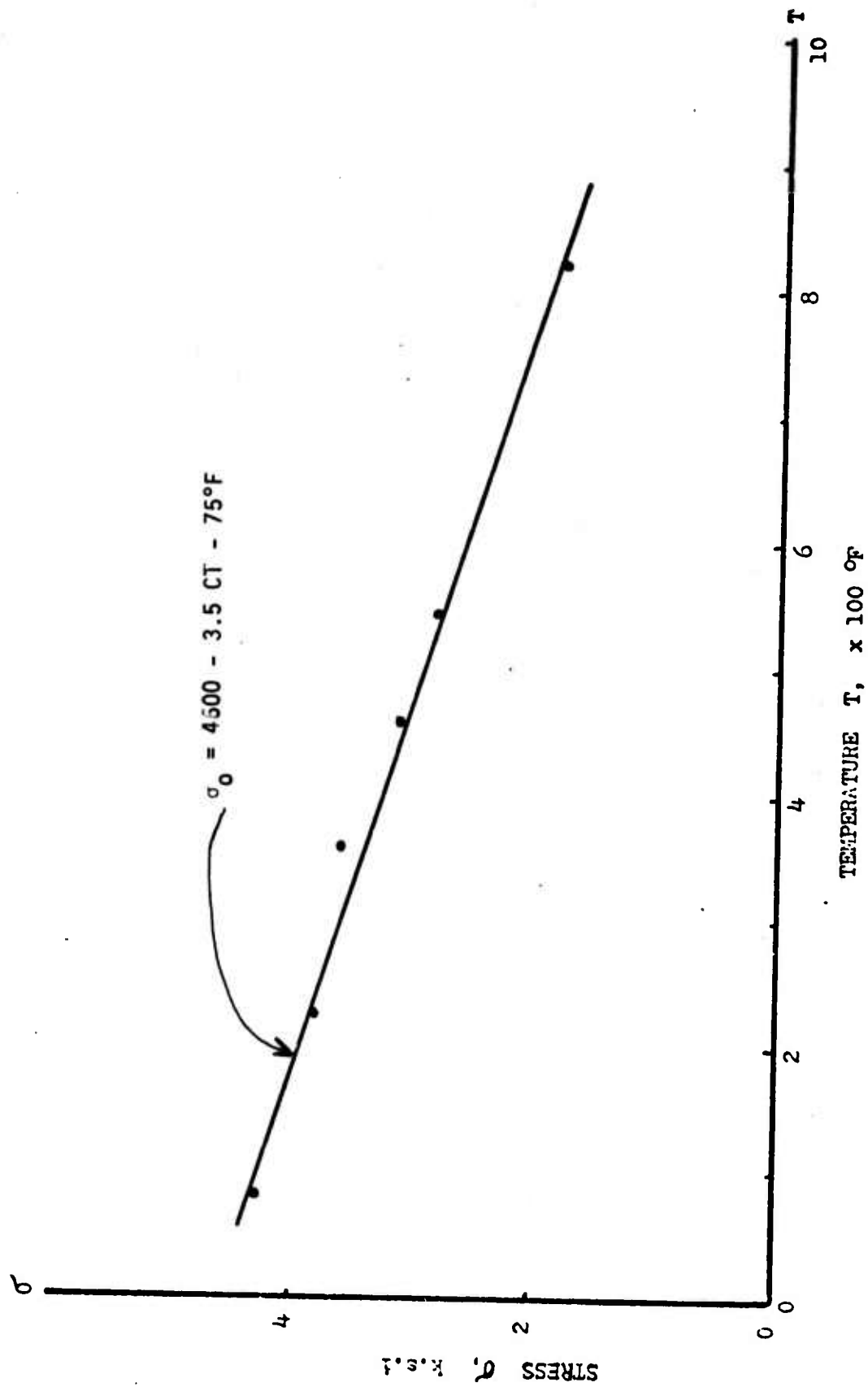


FIGURE 21 Threshold Stress vs. Temperature

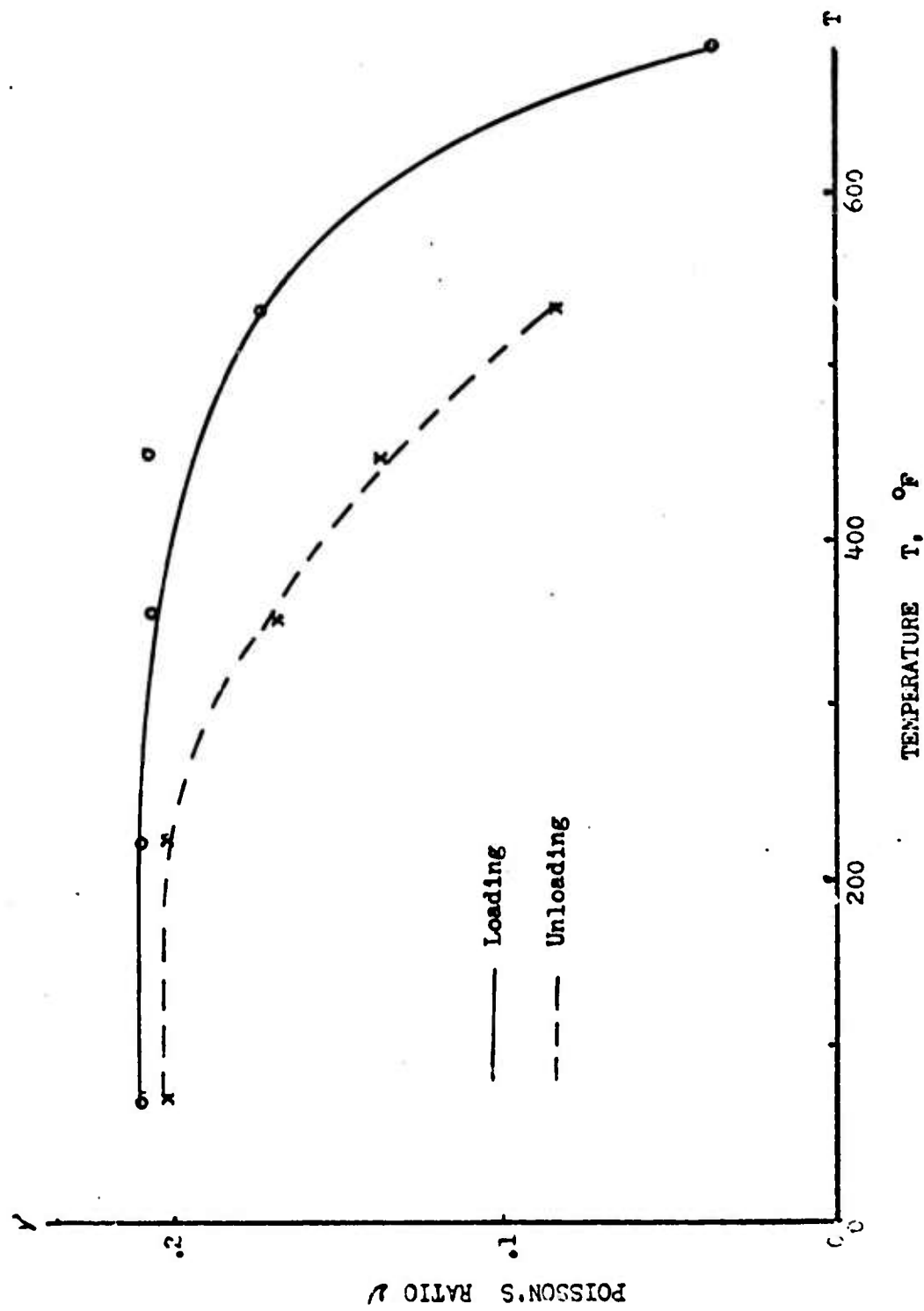


FIGURE 22 Poisson's Ratio vs. Temperature for Charcoal Granite

shown in Figure 18. Two loading histories were used. The first loading history involved a step-wise increasing stress from zero to 10,000 psi, to 15,000 psi, to 20,000 psi and then a reverse of this by decreasing the stress in step-wise from 20,000 psi, to 15,000 psi, to 10,000 psi and to zero. The loading time on each step was 30 minutes and 20 minutes, respectively, for each step-up and step-down period. The results of these tests are shown in Figure 23. The second loading history, as shown in Figure 18, had a single step of loading and unloading followed by a step-up and step-down loading history. The results of these tests are shown in Figure 24.

Results shown in Figure 23 and Figure 24 indicate that Charcoal granite, under uniaxial compressive stress, exhibits time-dependent strain as well as time-independent strain, and also that the time-independent strain consists of recoverable and irrecoverable parts.

From the results of the second testing period and the last testing period (both are under zero stress) shown in Figure 24, it indicated that the irrecoverable strains depend only on the maximum stress level in the entire stress history and are independent on the stress history. The results shown in the last period of Figure 23 indicated that the irrecoverable strains depend on temperature. Also, in Figure 23 by comparison of the difference of the total strains between the first period and the fifth period, and the second and the fourth period (both pairs have the same stress increment can be determined. For example, at 10,000 psi stress increment the irrecoverable strain at different temperatures can be obtained from Figure 23. These are shown in Figure 25. The fact that the results show a linear relation between the irrecoverable strain and the temperature indicates that

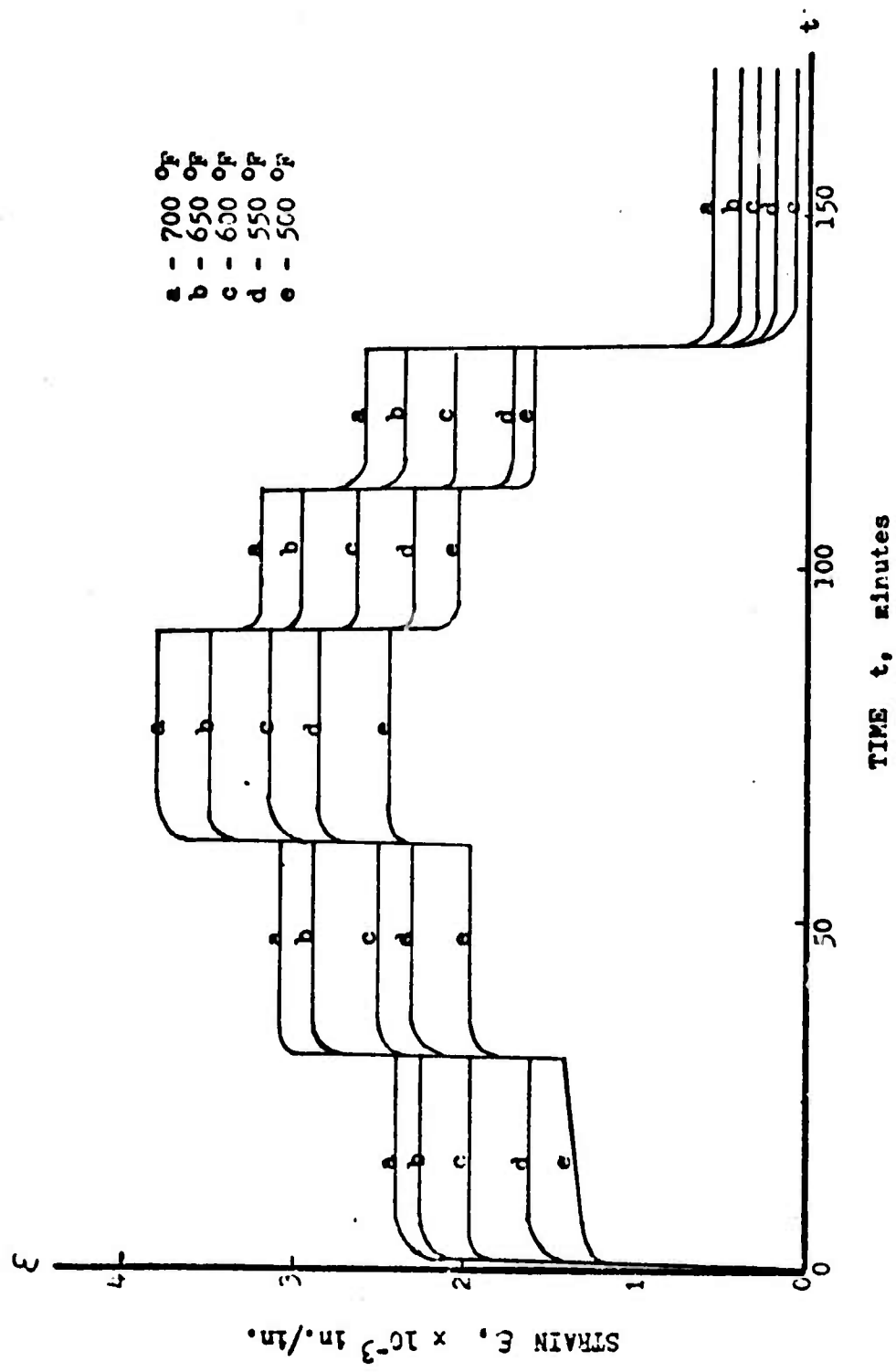


FIGURE 23 Creep Strains vs. Time Under Multi-Steps Loading

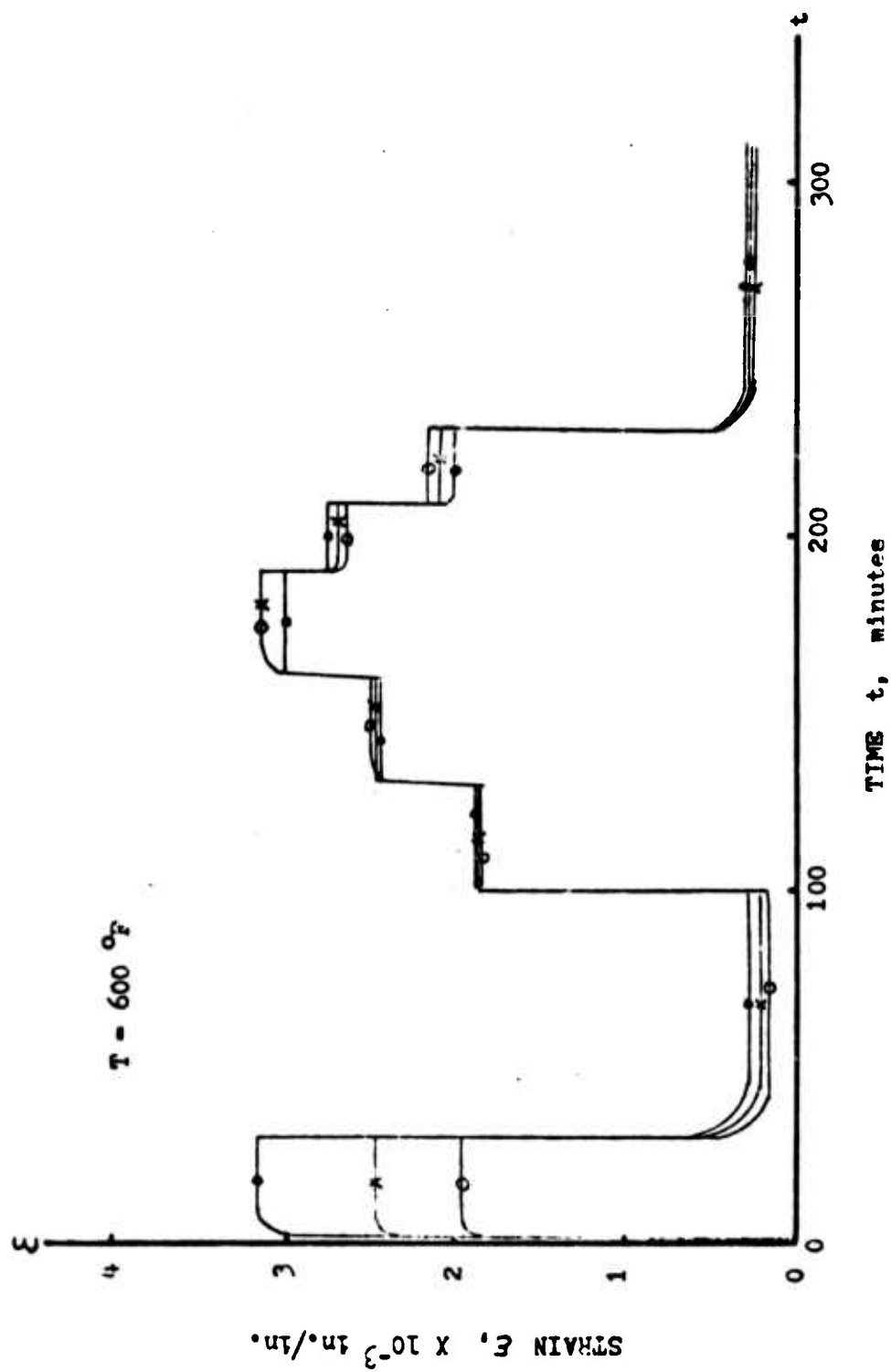


FIGURE 24 Creep Strains vs. Time Under Multi-Steps Loading

$$\epsilon_2 = 1.18 (T - 475) \times 10^{-10} \times \sigma. \quad (77)$$

In this expression it is assumed that when the test temperature, T , is below 475°F there will be no measureable irrecoverable strain.

After separating the irrecoverable strains from the total incremental strains obtained from each loading step, the elastic strain (ϵ_1) and creep strain (ϵ_3) were obtained in the same way. The results are:

$$\epsilon_1 = \sigma / E_1 ; E_1 = 12.5 \times 10^6 \text{ psi} \quad (78)$$

$$\epsilon_3 = \sigma \times (0.011 \times 10^{-6}) \times (T - 475) t^n$$

$$n = 0.214 \quad (79)$$

where t is in minutes and T in °F.

Using the strains ϵ_1 , ϵ_2 and ϵ_3 obtained from the previous procedures, together with total strain obtained in the first step of the tests shown in Figure 23 and Figure 24, it was found that in order to use ϵ_1 , ϵ_2 and ϵ_3 developed in this section to describe the actual stress-strain relation accurately, an initial strain (ϵ_0) had to be added. Using the experimental results from the first period of the test programs shown in Figure 23, and Figure 24, it was found that this strain is dependent on temperature as shown in Figure 26. The following relationship may be obtained:

$$\epsilon_0 = 4.6 \times 10^{-4} + 1.25 \times 10^{-6} (T - 475) \quad (80)$$

where T is °F.

The existence of the initial strain ϵ_0 may be illustrated by Figure 27 and materials having the stress-strain relations of this kind are called "ideal locking material" [14].

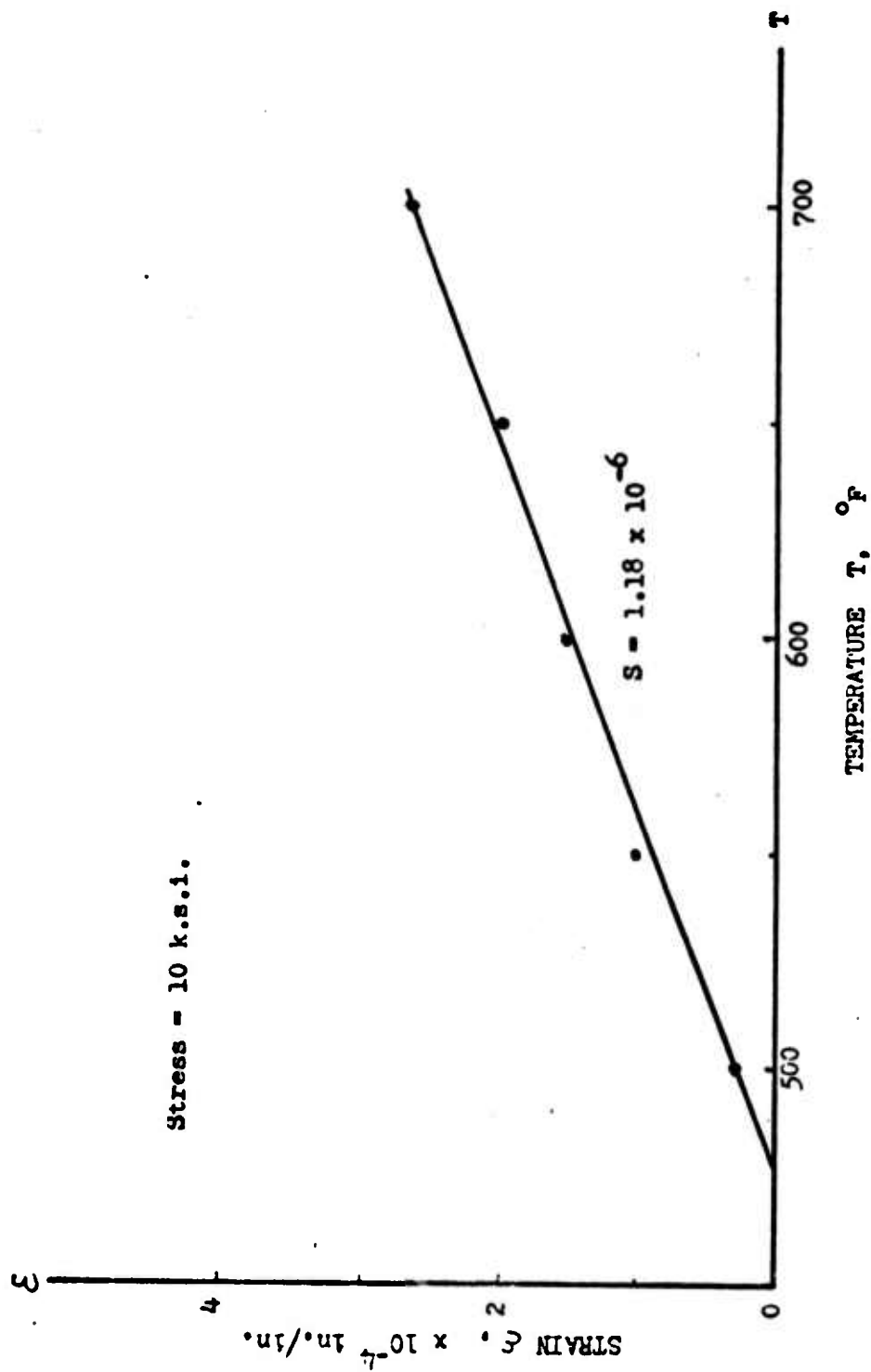


FIGURE 25 Irrecoverable Strain vs. Temperature for Charcoal Granite

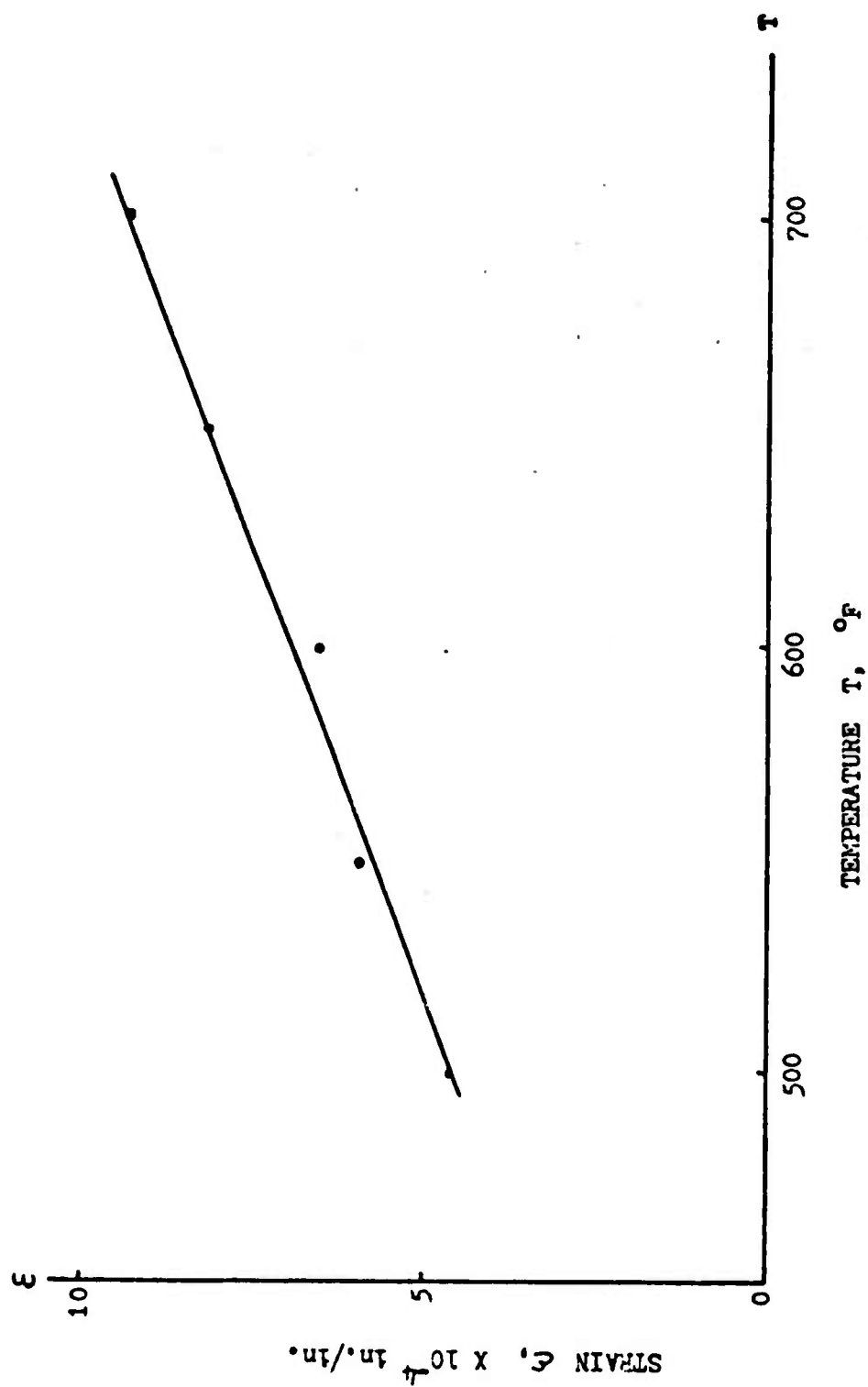


FIG. 26 Initial Strain vs. Temperature for Charcoal Granite

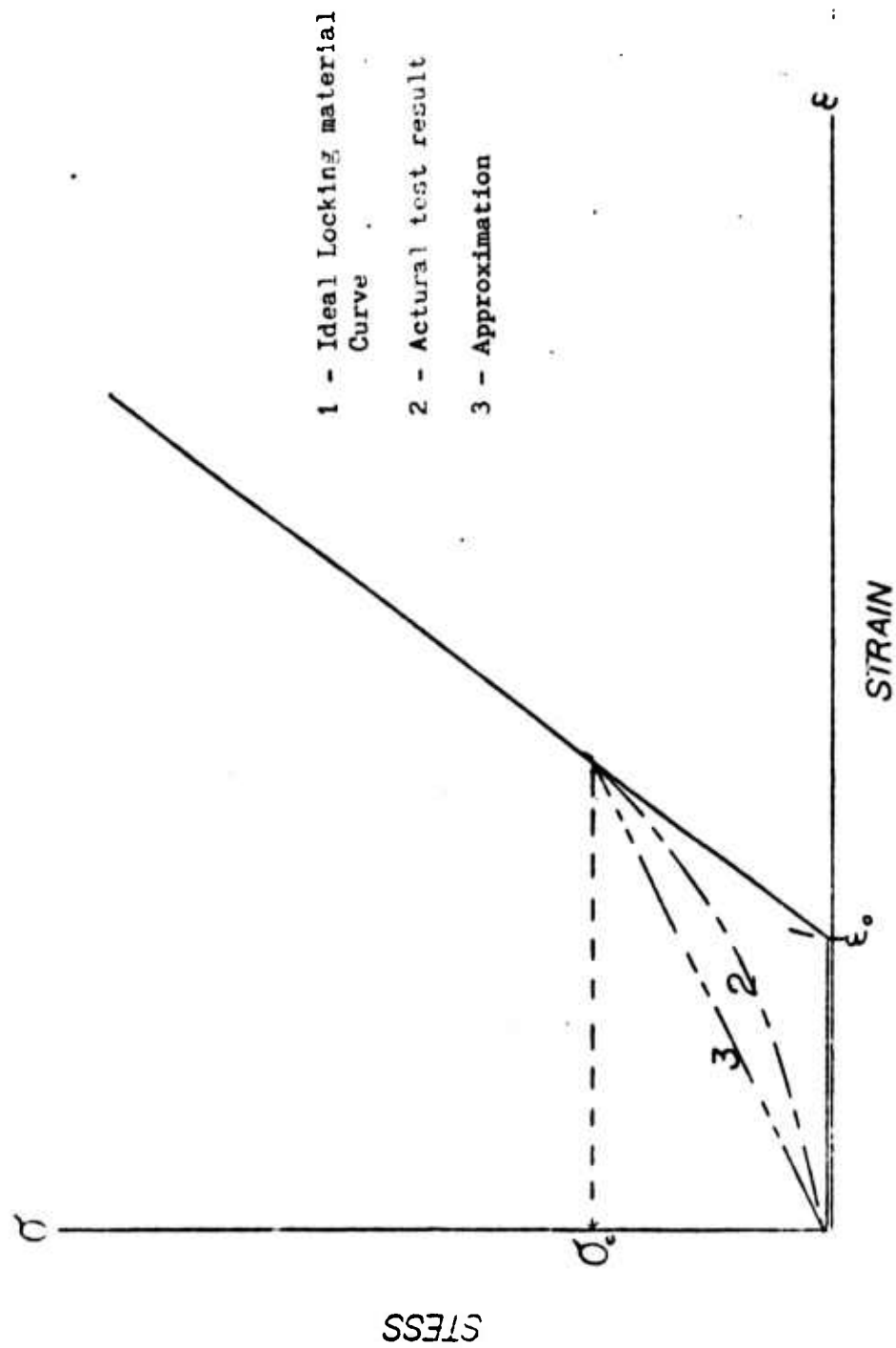


FIG. 27 Stress-strain Relation of An Ideal locking Material



-75-

A mechanical model as shown in Figure 28 was developed to describe the stress-strain relationship of the material under uniaxial compressive stress. This model consisted of four elements: a confined spring with small spring constant resting on a rigid support (which allows the spring to deform to ϵ_0 for stress larger than σ_0), a recoverable spring, an irrecoverable spring and a generalized Maxwell model. These four elements were connected in series. Using this mechanical model the stress-strain relation can be described as:

$$\epsilon = \epsilon_0 + \epsilon_1 + \epsilon_2 + \epsilon_3 ; \text{ for } \sigma \geq \sigma_0 \quad (81)$$

This expression is "exact" when the applied stress is greater than σ_0 .

The following equation may be used to estimate the strain when $\sigma \leq \sigma_0$:

$$\epsilon = (\sigma/\sigma_0) \epsilon_0 + \epsilon_1 + \epsilon_2 + \epsilon_3 \quad (82)$$

where σ_0 , ϵ_0 , ϵ_1 , ϵ_2 and ϵ_3 can be obtained from Equations 77, 78, 79, and 80 respectively.

For both cases, during unloading, the strain can be obtained from Equation 81 and Equation 82 provided that $\epsilon_2 = 0$.

The predication of the strain responses of the material, under multi-step uniaxial compressive stress at different temperatures using Equation 81, are shown by the dashed lines in Figure 29 to Figure 36. The results compare very favorably with the experimental results (in solid line).

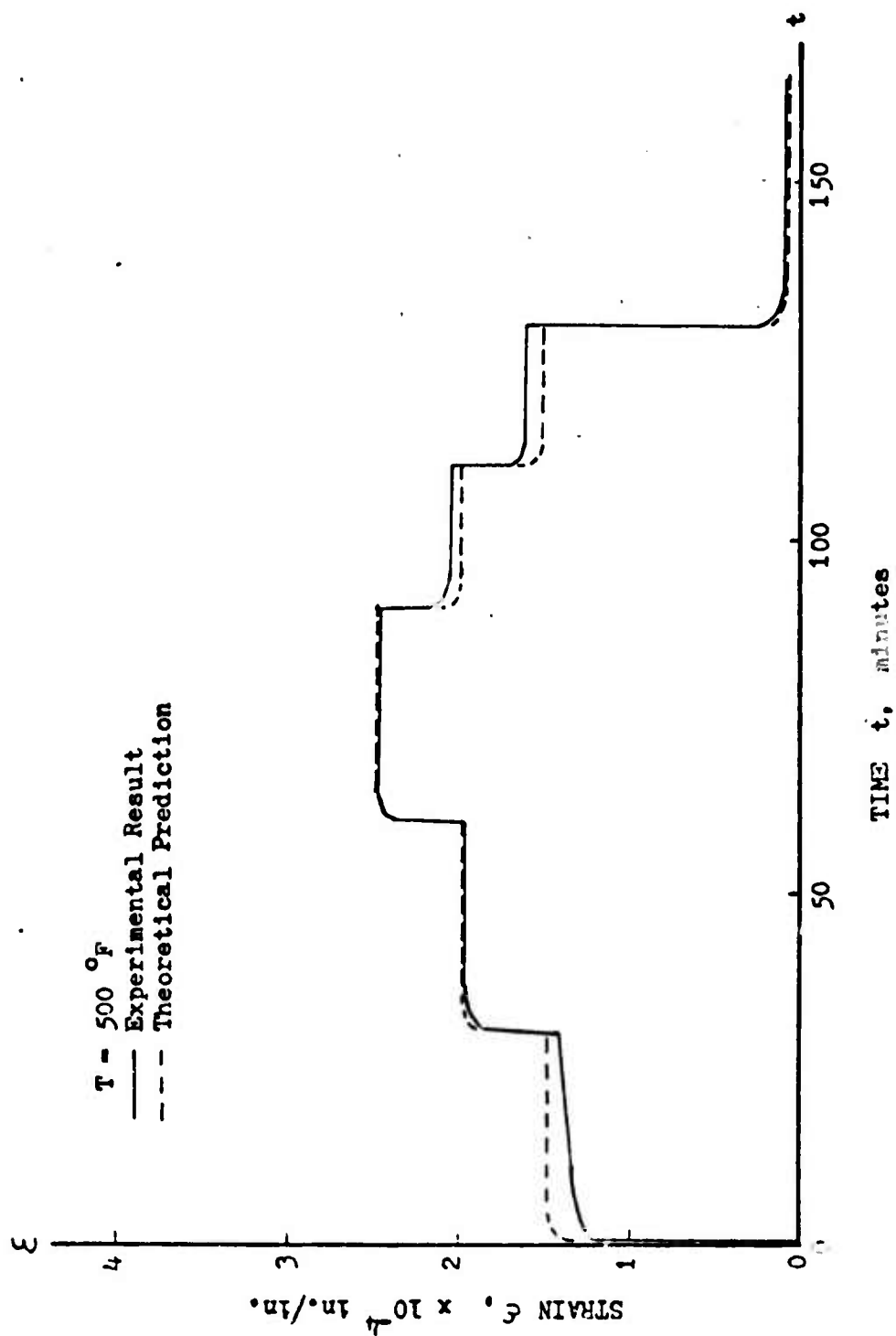


FIG. 29 Comparison of the Theoretical Prediction vs. Experimental Result

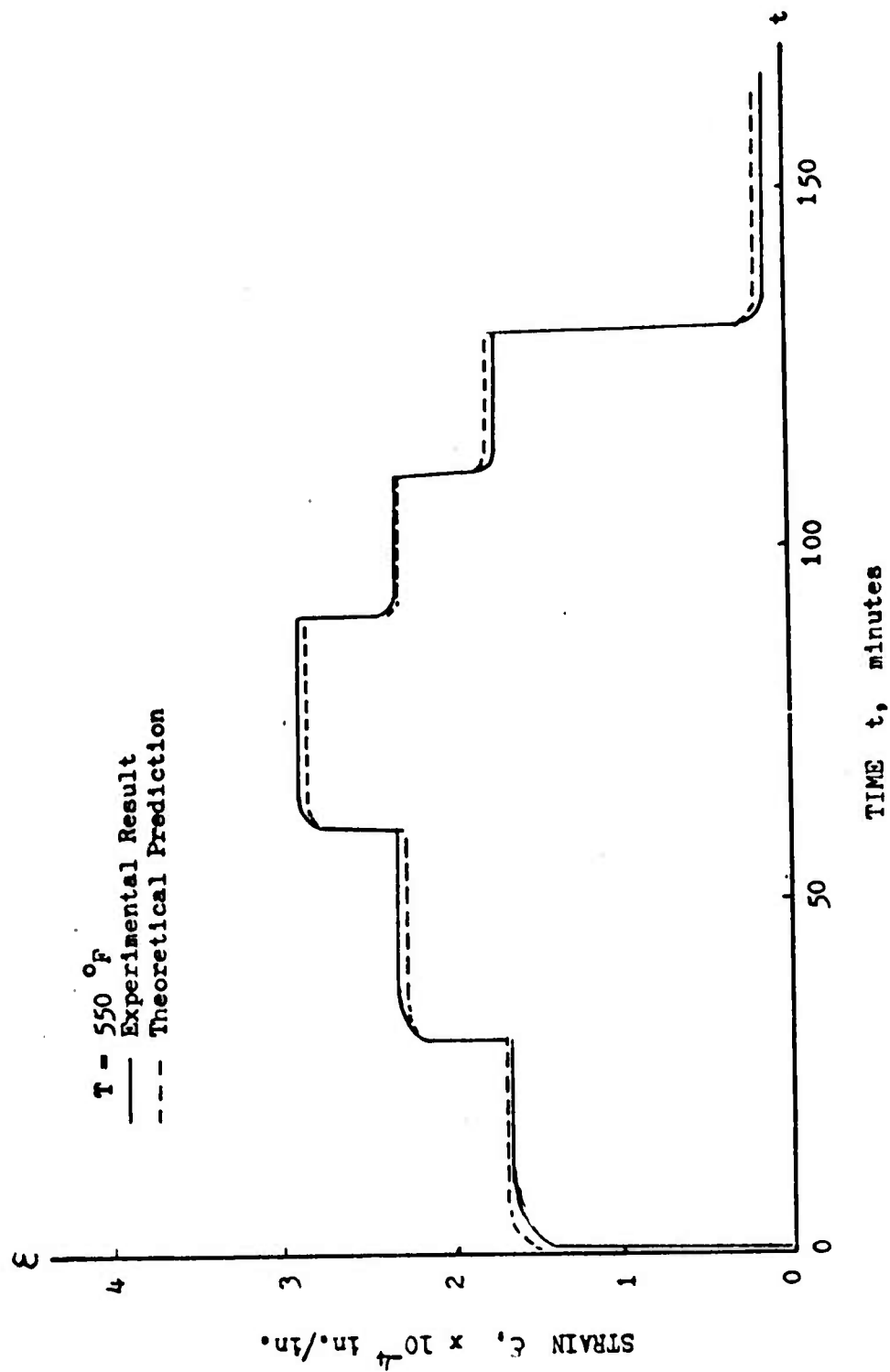


FIG. 30 Comparison of the Theoretical Prediction vs. Experimental Result

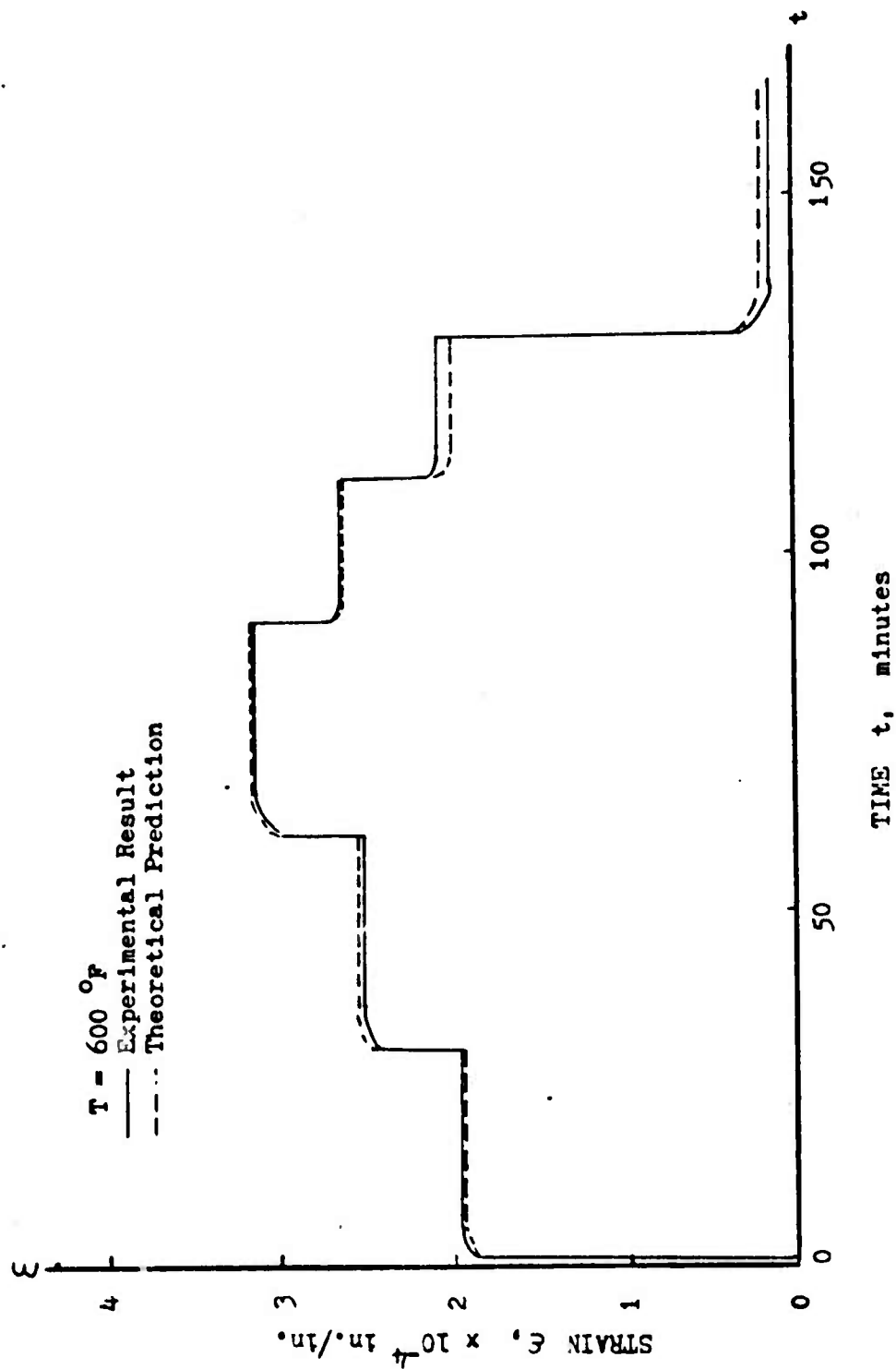


FIG. 31 Comparison of the Theoretical Prediction vs. Experimental Result

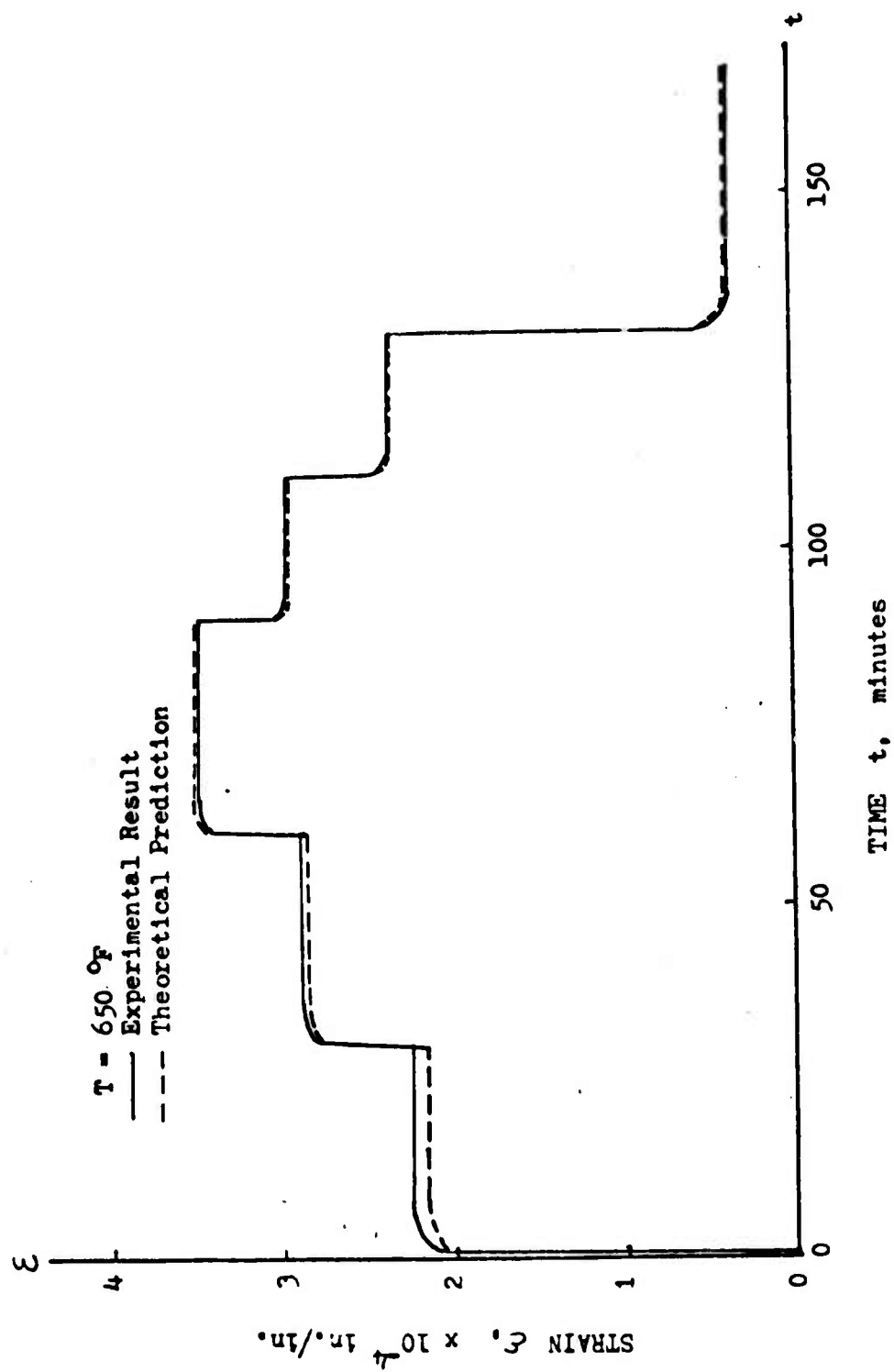


FIG. 32 Comparison of the Theoretical Prediction vs. Experimental Result

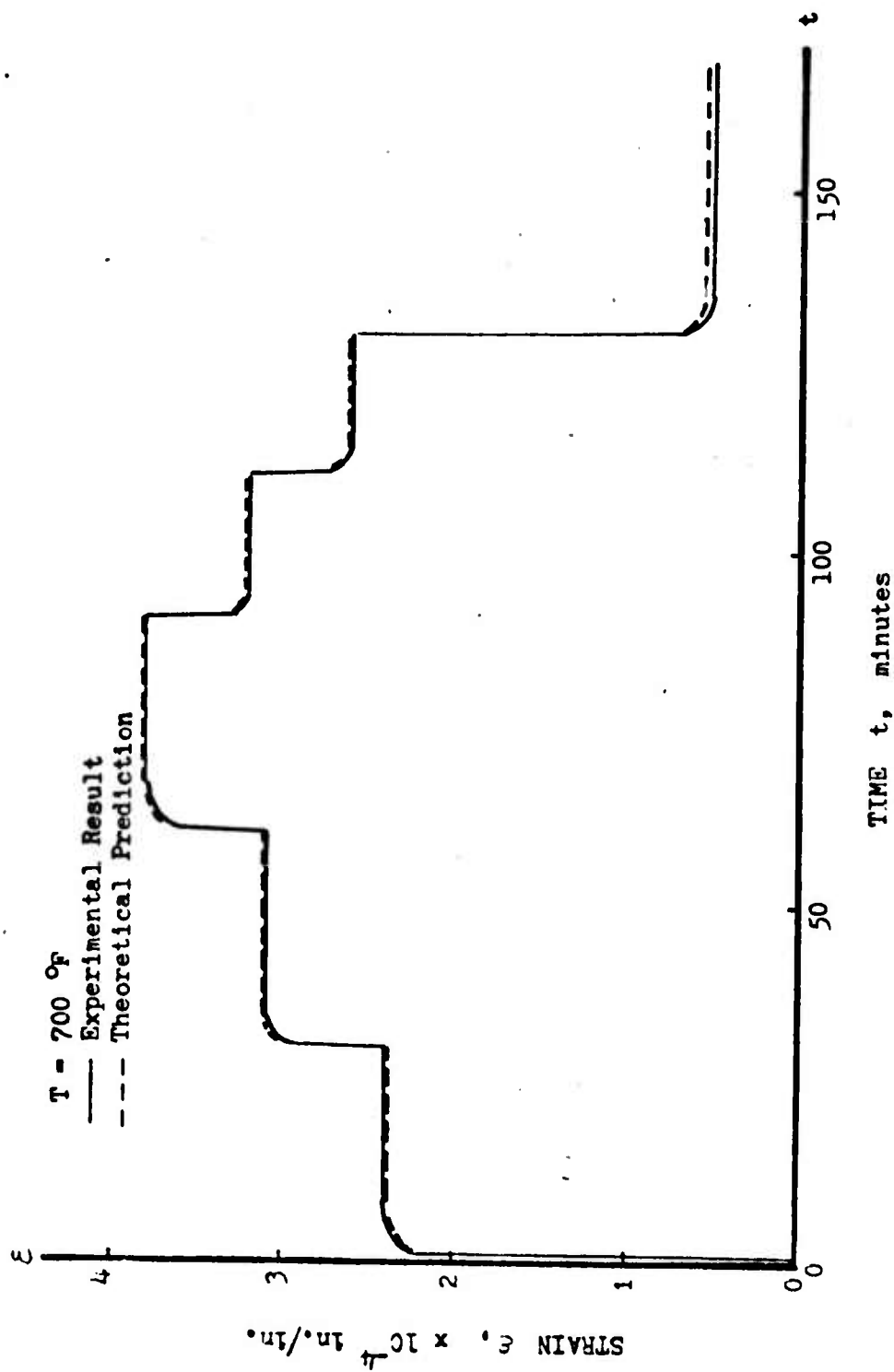


FIG. 33 Comparison of the Theoretical Prediction vs. Experimental Result

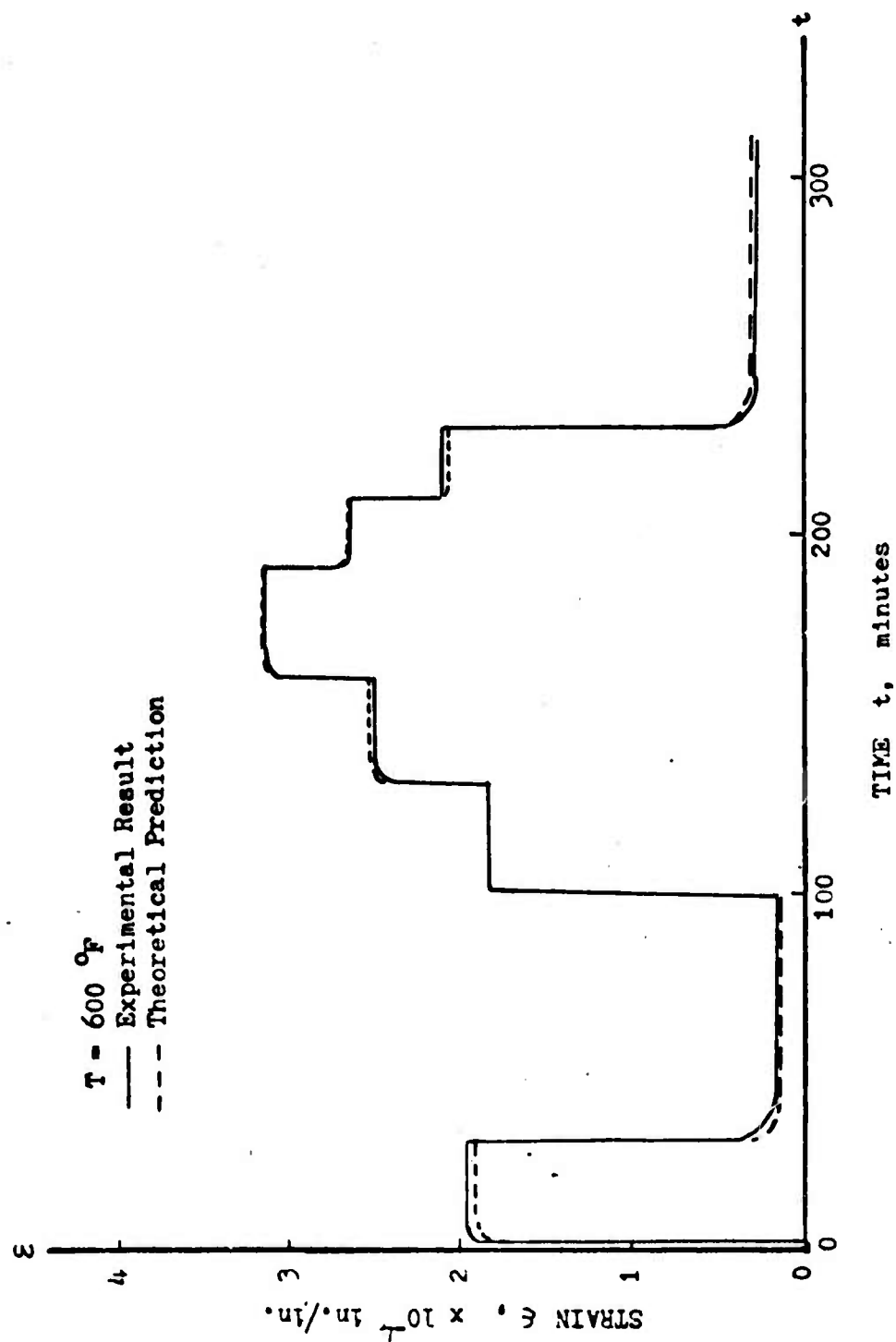


FIG. 34 Comparison of the Theoretical Prediction vs. Experimental Result

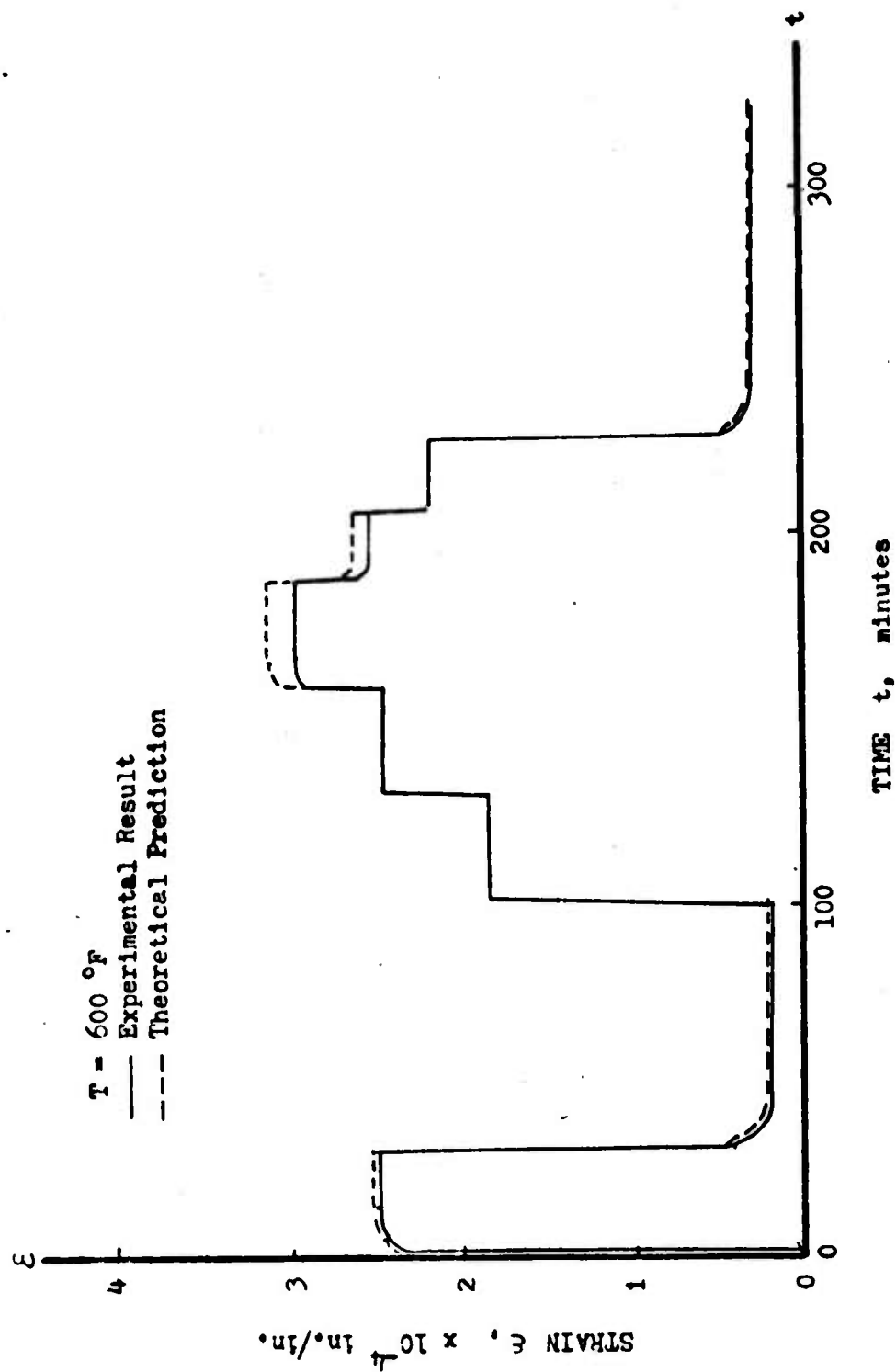


FIG 35 Comparison of the Theoretical Prediction vs. Experimental Result

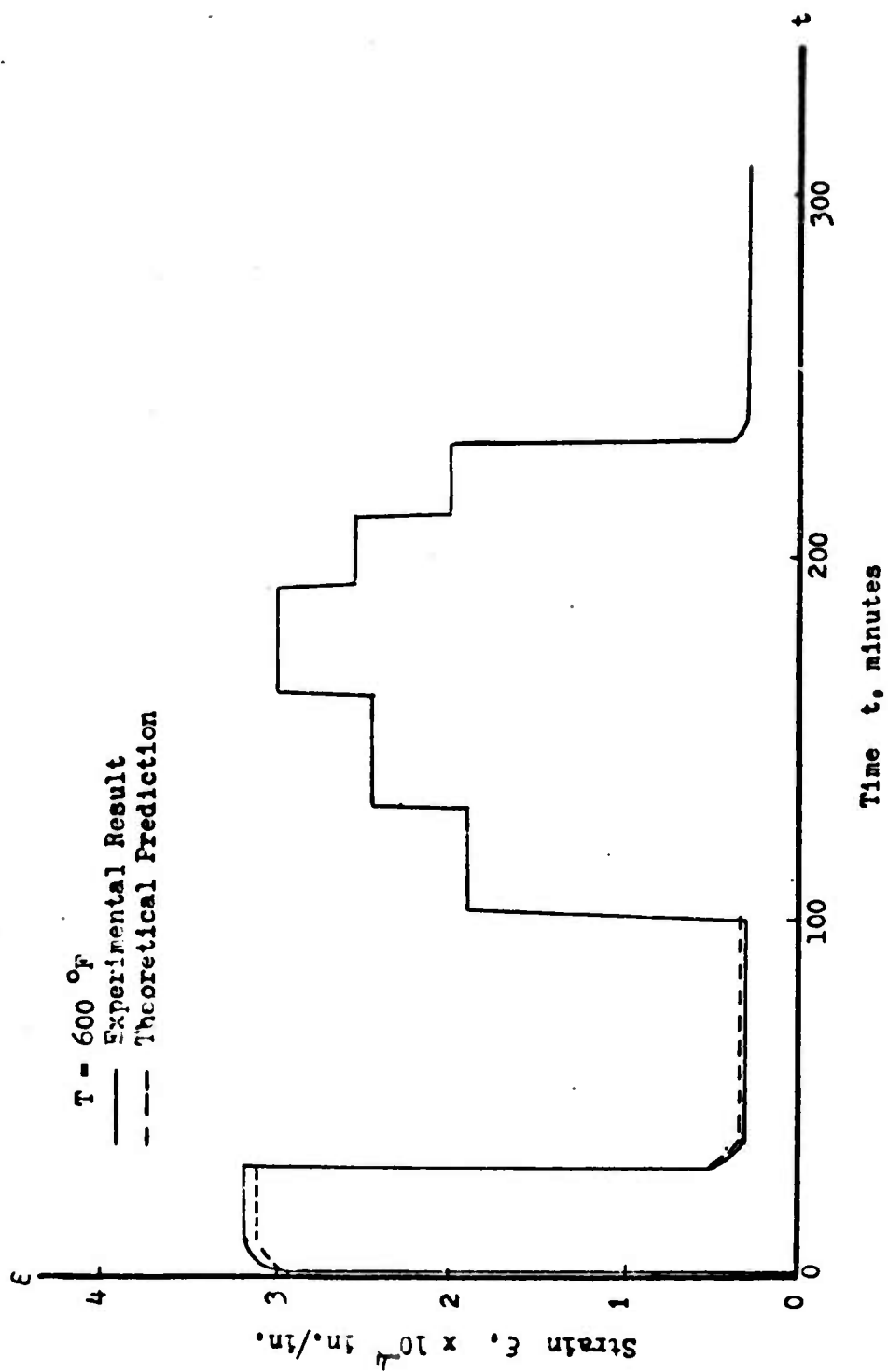


FIG. 36 Comparison of the Theoretical Prediction vs. Experimental Result

Tension Tests

Several tension tests under step loads at several temperatures were conducted. It was found that there is no measureable time-dependent strain and that the time-independent strain is almost completely recoverable. This is due mainly to the fact that the material is extremely brittle even at the elevated temperature (up to 700°F) and that the tensile strength is very small, less than 4% of the compressive strength.

From these tests the Young's modulus of the material was found. As shown in Figure 37, the Young's modulus depends on temperature.

$$\epsilon = \sigma/E_T$$

$$E_T = 12.1 \times 10^6 - 17.3 (T-75) \times 10^3$$

where T is °F.

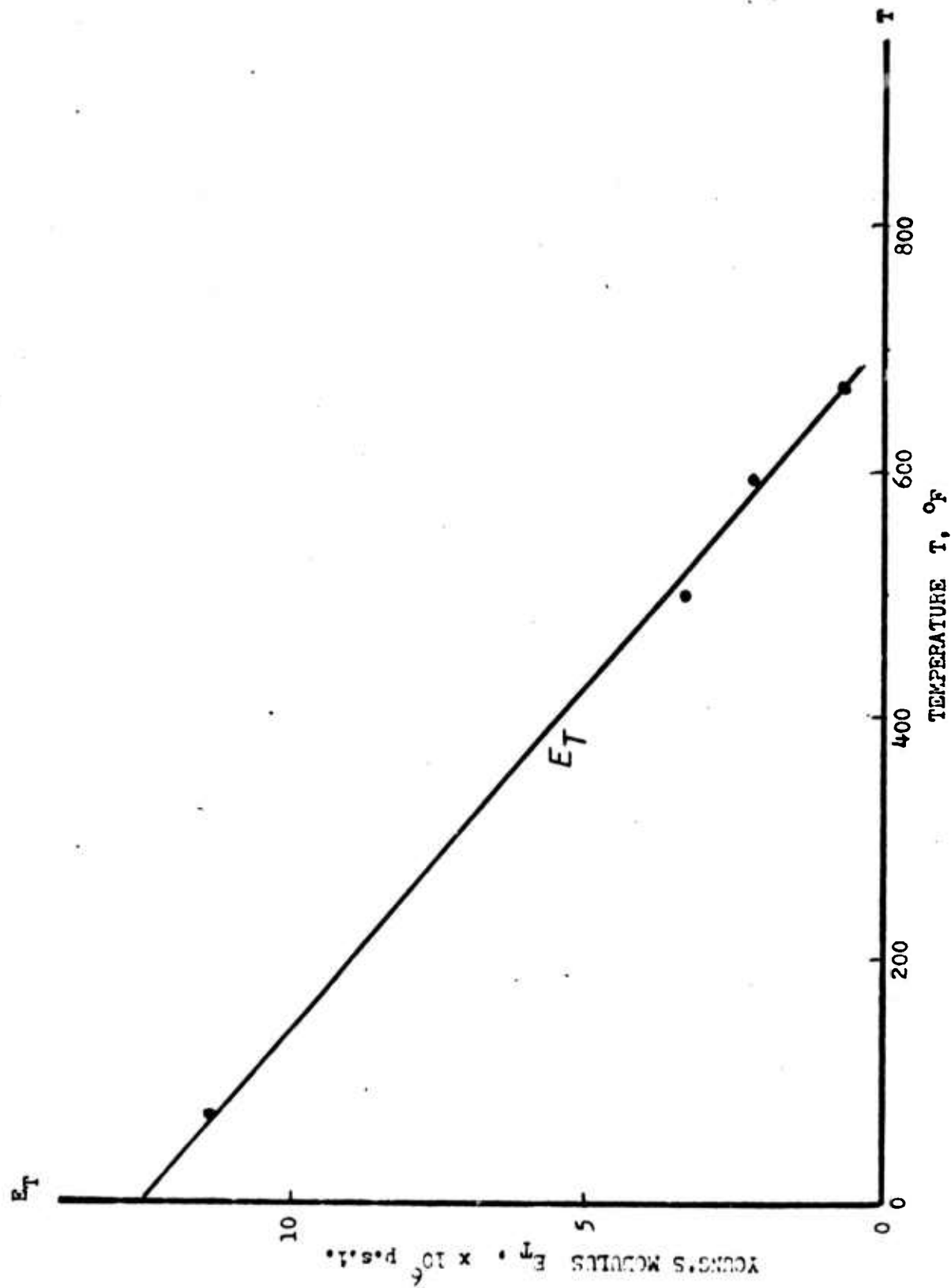


FIG. 37 Tensile Young's Modulus vs. Temperature for Charcoal Granite

3.6 Experimental Results of Dresser Basalt

Compression Tests

Ten compression creep tests under constant stresses at five temperatures were conducted. All the tests were loaded under constant stresses for 300 minutes and the specimens were unloaded. The test program and results are shown in Table 3. The strain-time curves for each test are shown in Figure 38 and Figure 39. From these creep curves, it indicates that at room temperature the strains of Dresser basalt under unconfined compression are time-independent, at least up to five hours after loading and at the stress up to 12,000 psi which is about 50 to 60 percent of the ultimate compressive strength of the material; at elevated temperatures (above 455°F), the strains are time-dependent. Also, the instantaneous strains upon application of loading are always larger than the instantaneous recovery strain upon unloading. This indicates that the instantaneous strains consist of recoverable and irrecoverable strains. The determination of the instantaneous strains during loading will be discussed later in this section.

The determination of the elastic modulus is made use of the instantaneous recoverable strains and the applied stresses at each test. The results are shown in Table 3 and Figure 40. The dependence of the elastic modulus upon temperature is clearly indicated. However, because of insufficient test data, no attempt is made here to develop an equation to express the relation between them.

The transverse strains under compressive stresses were also recorded for the first four specimens. At higher temperature, the strain gages were inoperative and henceforth, no transverse strains were available. The Poisson's ratio for each of the first four specimens, as determined from the instantaneous recoverable axial and transverse strains, is about 0.31.

TABLE 3. COMPRESSION CREEP TEST RESULTS FOR DRESSER BASALT

Specimen No.	Input Conditions		Strain Outputs				
			Elastic modulus (1)	Poisson's ratio (2)	$\epsilon = \epsilon_0 + Ct^n$		
	Stress 1000 psi	Temp. °F			$\epsilon_0, 10^{-6}$ in/in	$C, 10^{-6}$ in/in	n
BC-1	10	72	5.66	0.32	1880	-	-
BC-2	12	73	5.35	0.29	2360	-	-
BC-3	8	455	5.22	0.31	1650	20	0.126
BC-4	8	455	4.93	0.31	1750	22	0.126
BC-5	8	550	4.51	-	1950	41	0.144
BC-6	8	550	4.73	-	1900	40	0.144
BC-7	8	675	4.27	-	2120	51	0.173
BC-8	8	675	4.31	-	2120	52	0.173
BC-9	8	810	3.82	-	2450	80	0.195
BC-10	8	810	4.11	-	2320	72	0.195

(1) Determined from the instantaneous recoverable strains, $\sigma/\epsilon e$.

(2) Determined from the instantaneous recoverable axial and diametral strains.

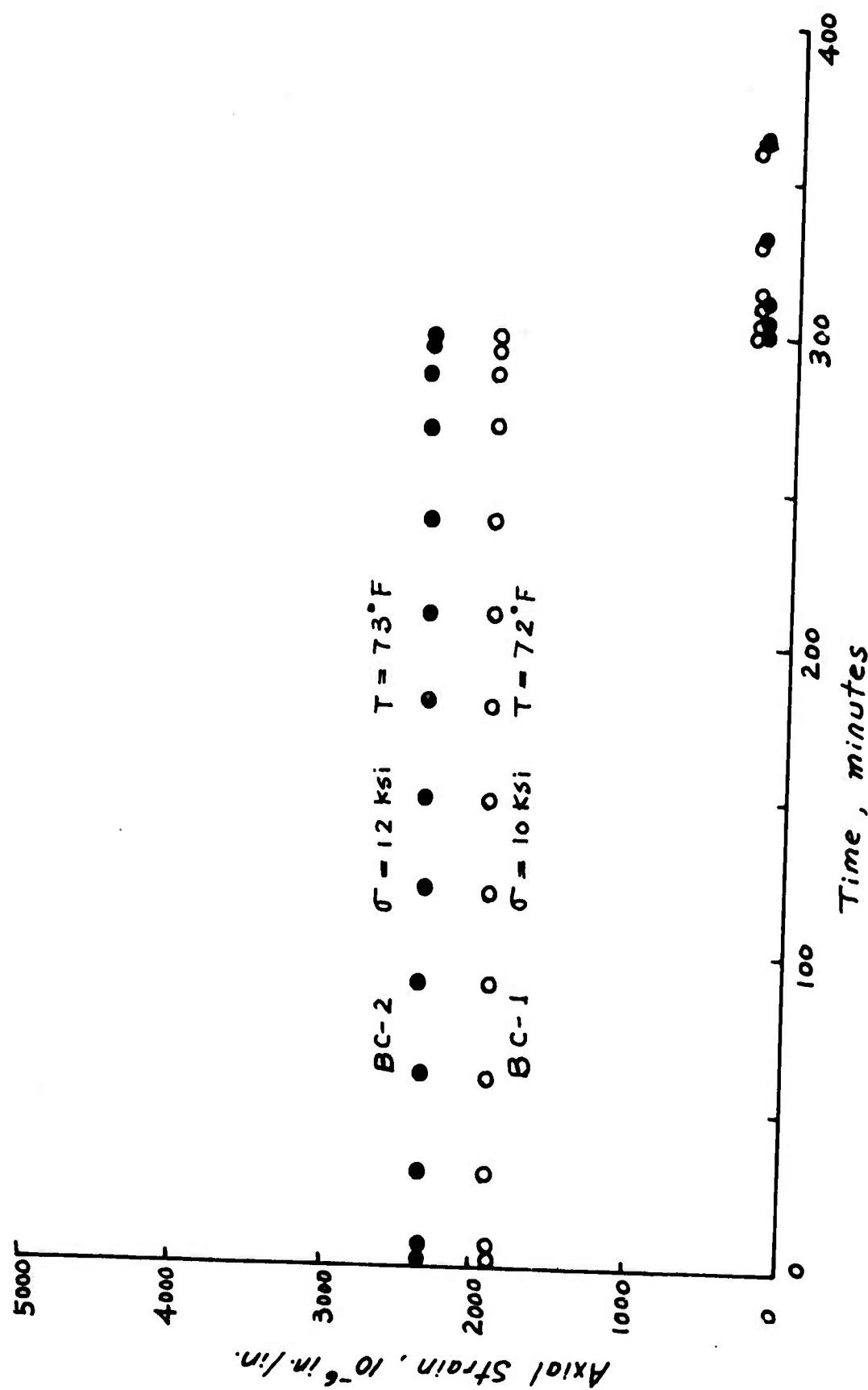


FIGURE 38 Creep Curves for Dresser Basalt Under Compressive Stresses

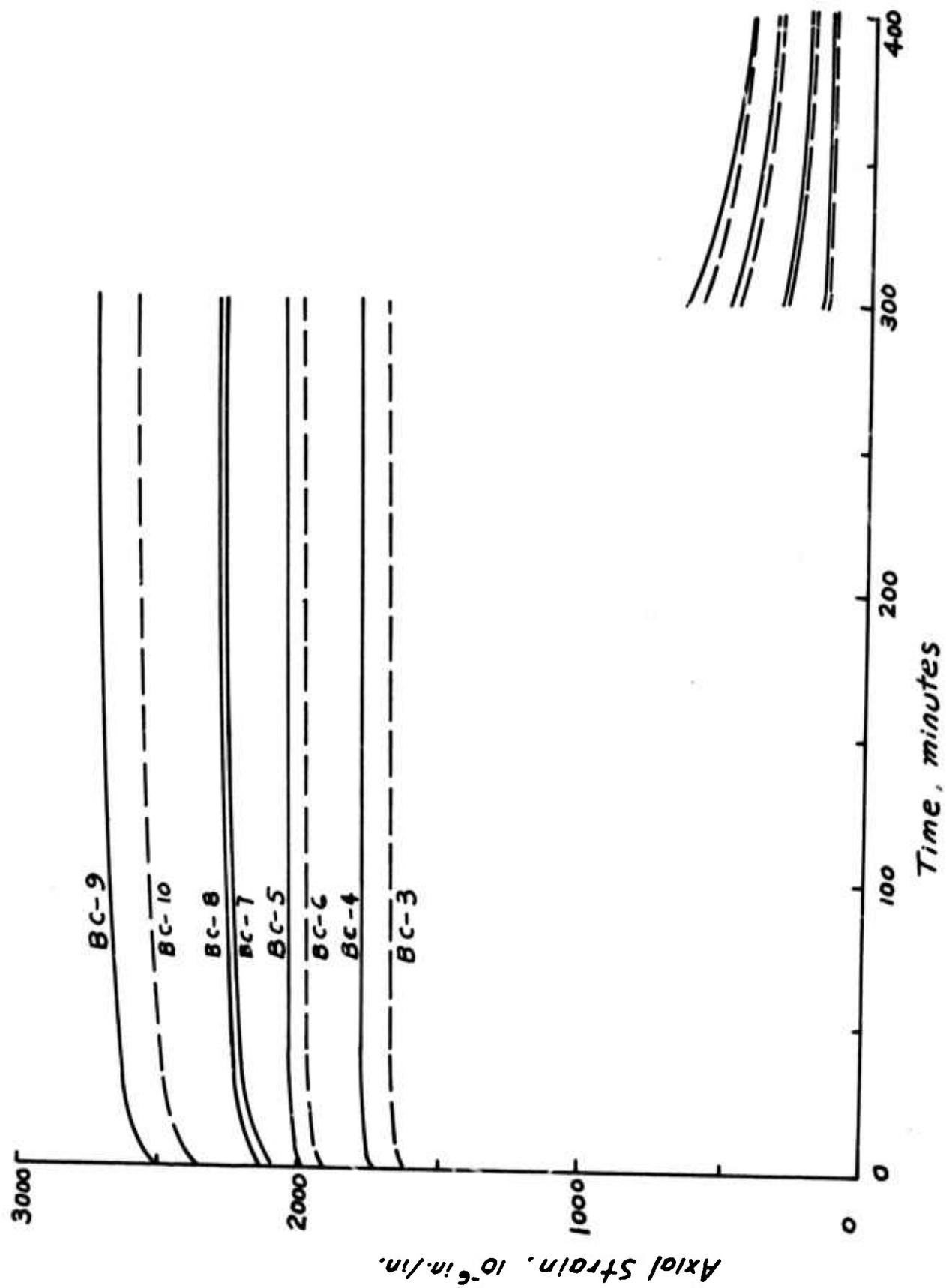


FIGURE 39 Creep Curves for Dresser Basalt Under Compressive Stresses

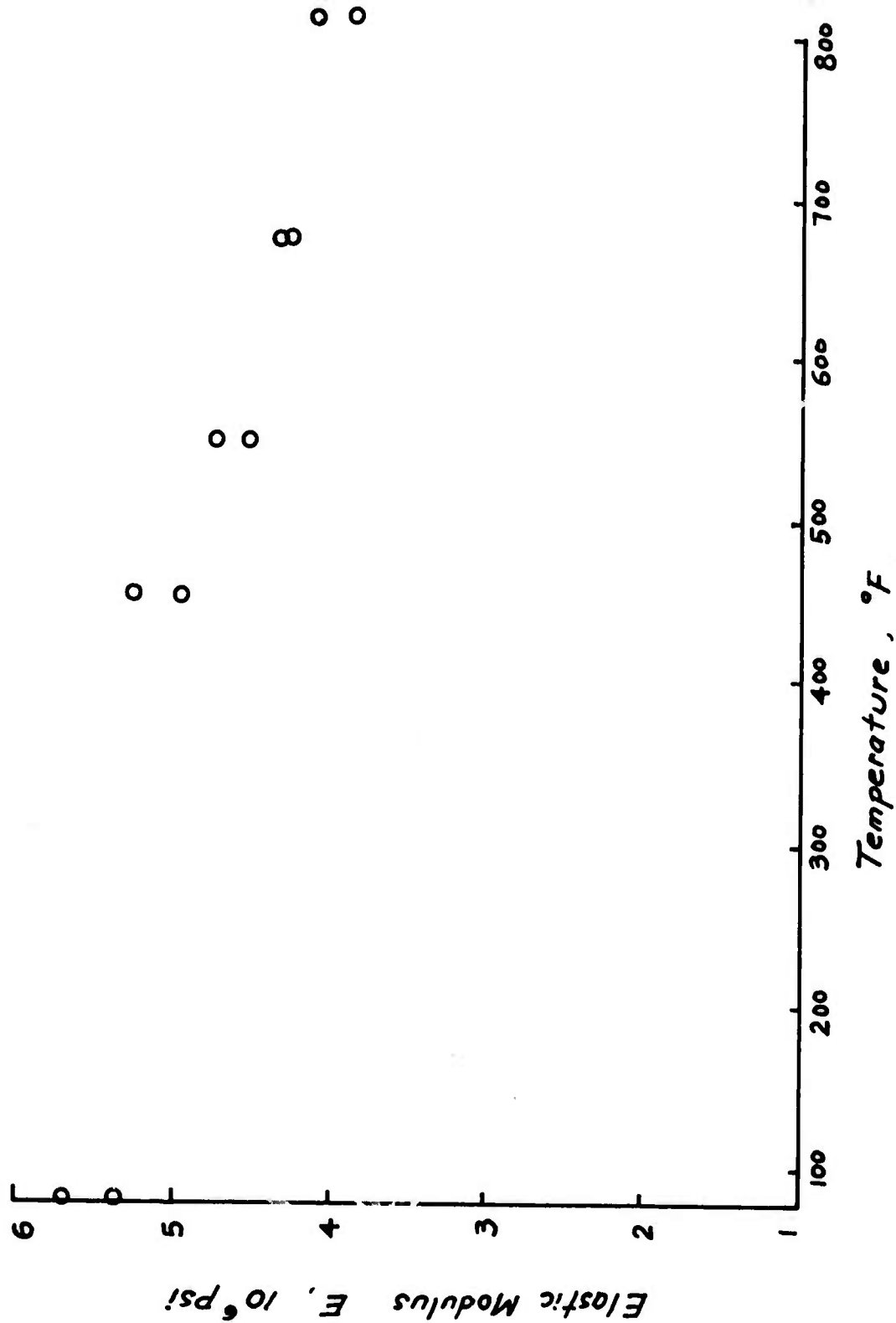


FIGURE 40 Compression Elastic Modulus of Dresser Basalt vs. Temperature

The log-log plots of the loading portion of the creep curves are shown in Figure 41. The nature that the creep curves can be approximated by straight lines indicates that the time-dependent behavior of Dresser basalt under unconfined compressive stresses can be represented by a power law time function.

$$\epsilon = \epsilon_0 + ct^n$$

The values of ϵ_0 , c and n of each test are summarized in Table 3. The dependence of ϵ_0 , c and n on temperature is clearly indicated.

Upon unloading, the total strains accumulated during the loading period were partially recoverable and partially irrecoverable and the recoverable strains consist of instantaneous recoverable strains and time-dependent recoverable strains. As shown in Figure 39, all these three types of strains are temperature dependent.

Tension Tests

Four constant stress tension creep tests were conducted at four temperatures. In addition, a constant stress creep test was conducted at room temperature. The test results as shown in Figure 42 indicate that Dresser basalt exhibits time-dependent behavior at elevated temperatures while at room temperature. The time-dependency is negligible. Results shown in Figure 42 also indicate that the material exhibits a certain amount of irrecoverable strain upon unloading from the constant stress creep tests. The amount of irrecoverable strains depend on the temperature.

3.7 Diametral Compression Beam Bending Test Results

Since the reliable tensile and compressive moduli of Dresser basalt are not available for temperatures between 75° to 400°, the diametral compression and beam bending tests were conducted on charcoal granite only where the compressive modulus and tension modulus can be obtained from Figure 19 and Figure 37 respectively.

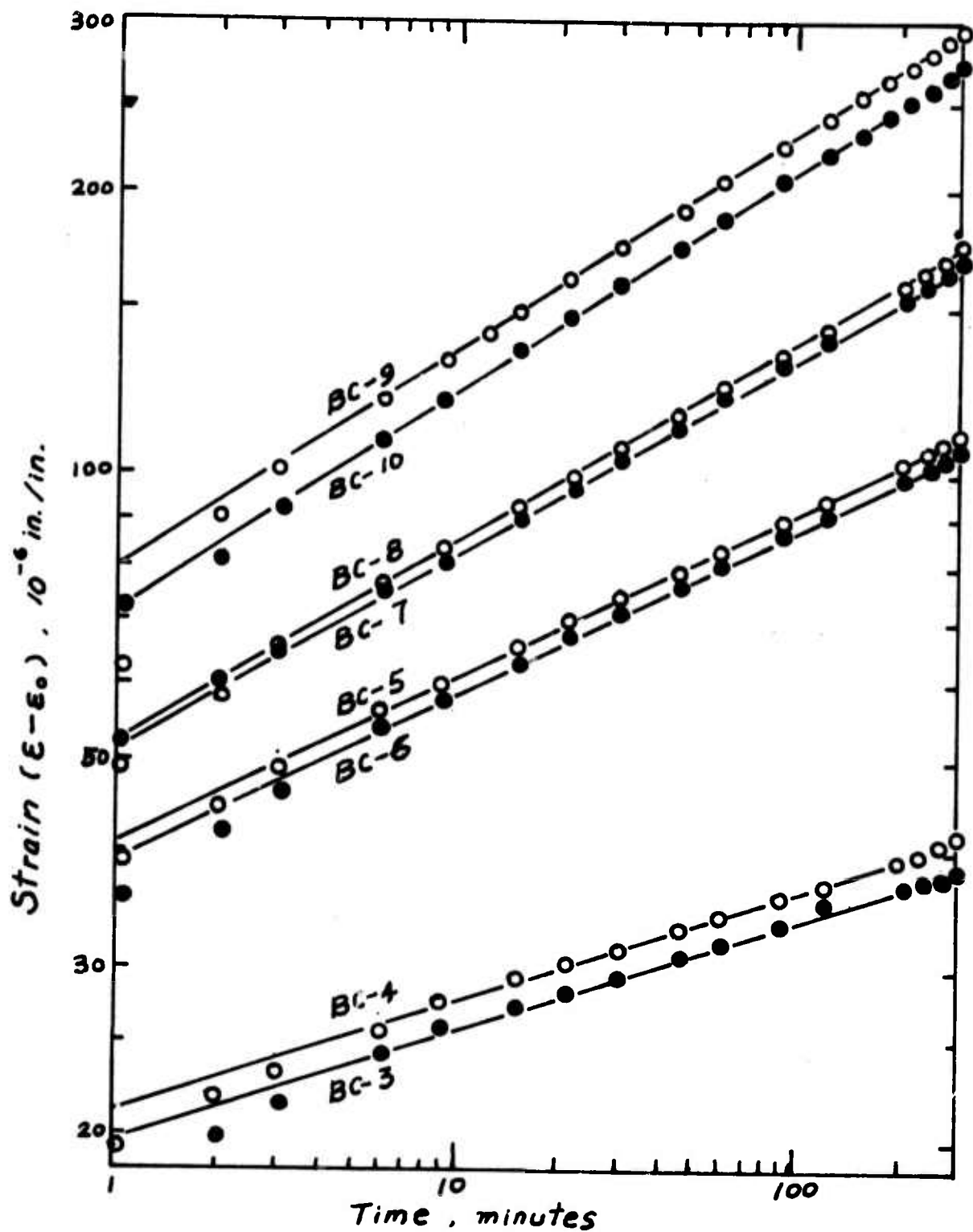


FIGURE 41 Log-Log Plots of Creep Curves for Dresser Basalt Under Compressive Stresses

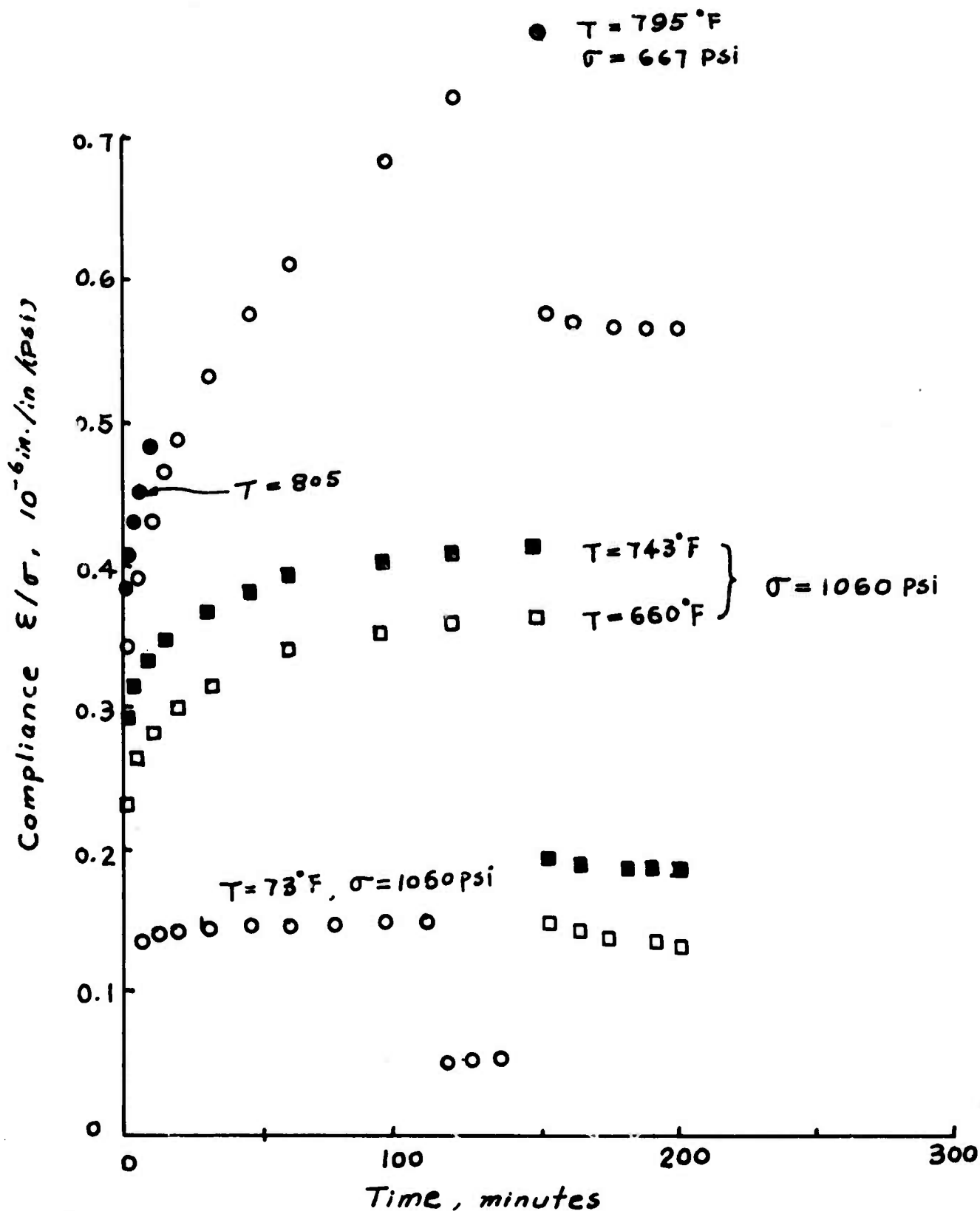


FIGURE 42 Tensile Creep Curves of Dresser Basalt

For the diametral compression tests on charcoal granite, the results of tensile strains and compressive strains at the center are shown in Figure 43 and Figure 44 for temperature at 200°F and 400°F. Figure 45 shows the tensile and compressive strains as resulted from the beam bending tests of charcoal granite at 200°F and 400°F.

In carrying out the theoretical predictions, the linear elastic solutions are chosen instead of the bilinear solutions. This is due to the fact that for temperatures between 75°F to 400°F, the elastic modulus of charcoal granite under compression and tension are nearly the same as the results shown in Figure 19 and Figure 37 indicate. Figure 19 shows that at the small stress (less than the threshold stress σ_0), the Young's modulus is smaller due to the "preconsolidated effect". The actual maximum compressive stresses in the diametral compression tests and the beam bending tests are estimated to be smaller than this threshold stress. Because of this, the actual moduli for tension and compression are approximately the same. Using $E_c = E_t = 7 \times 10^6$ psi, and $E_c = E_t = 5 \times 10^6$ psi at temperatures equal 200°F and 400°F, together with the Poisson's ratio equals 0.21, the linear elastic solutions of the strains at the corresponding positions were obtained and the theoretical results are shown in Figure 43, Figure 44 and Figure 45. The comparisons between the theoretical predictions to the experimental results are quite satisfactory.

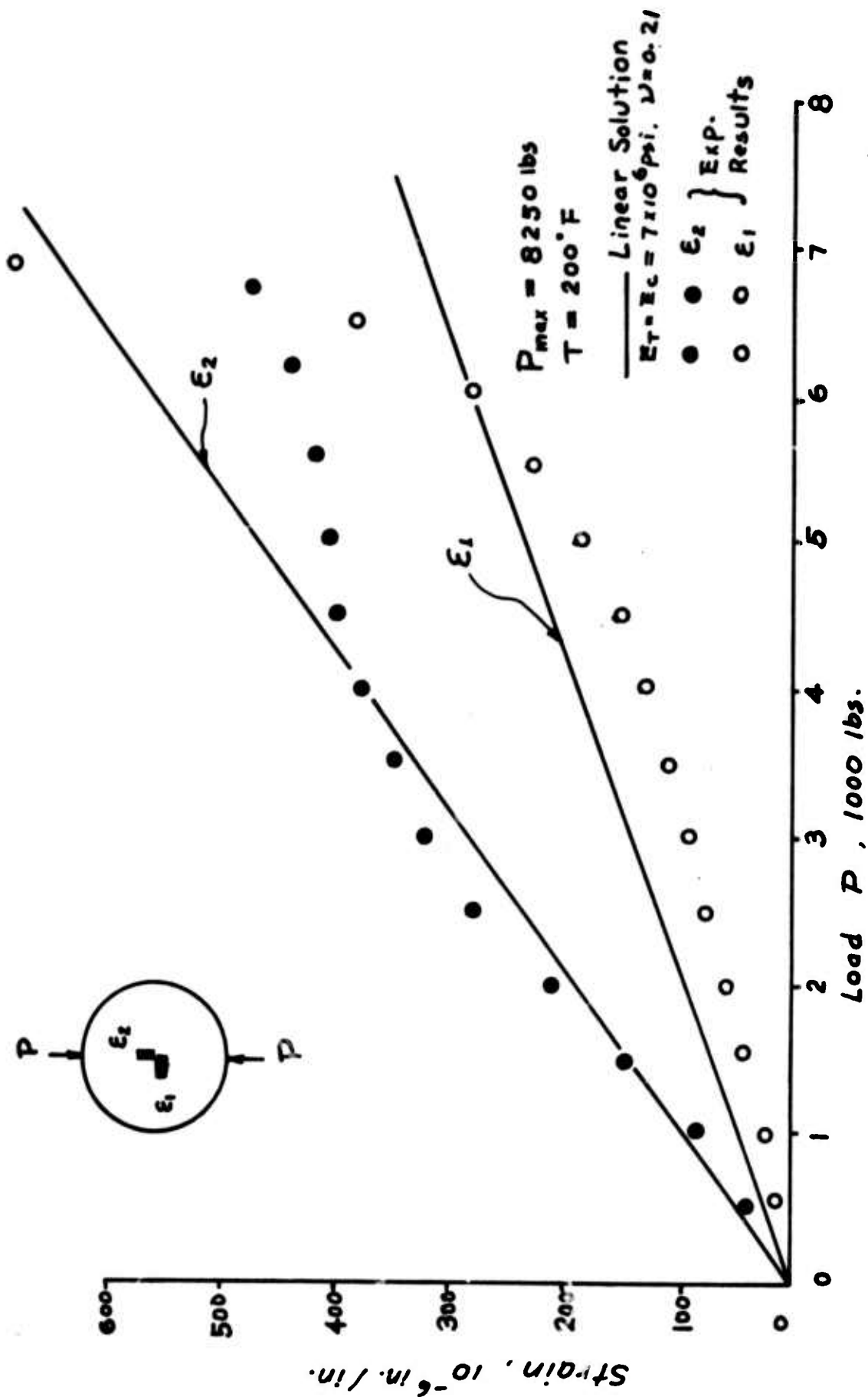


FIGURE 43 Diametral Compression Test Results (Charcoal Granite)

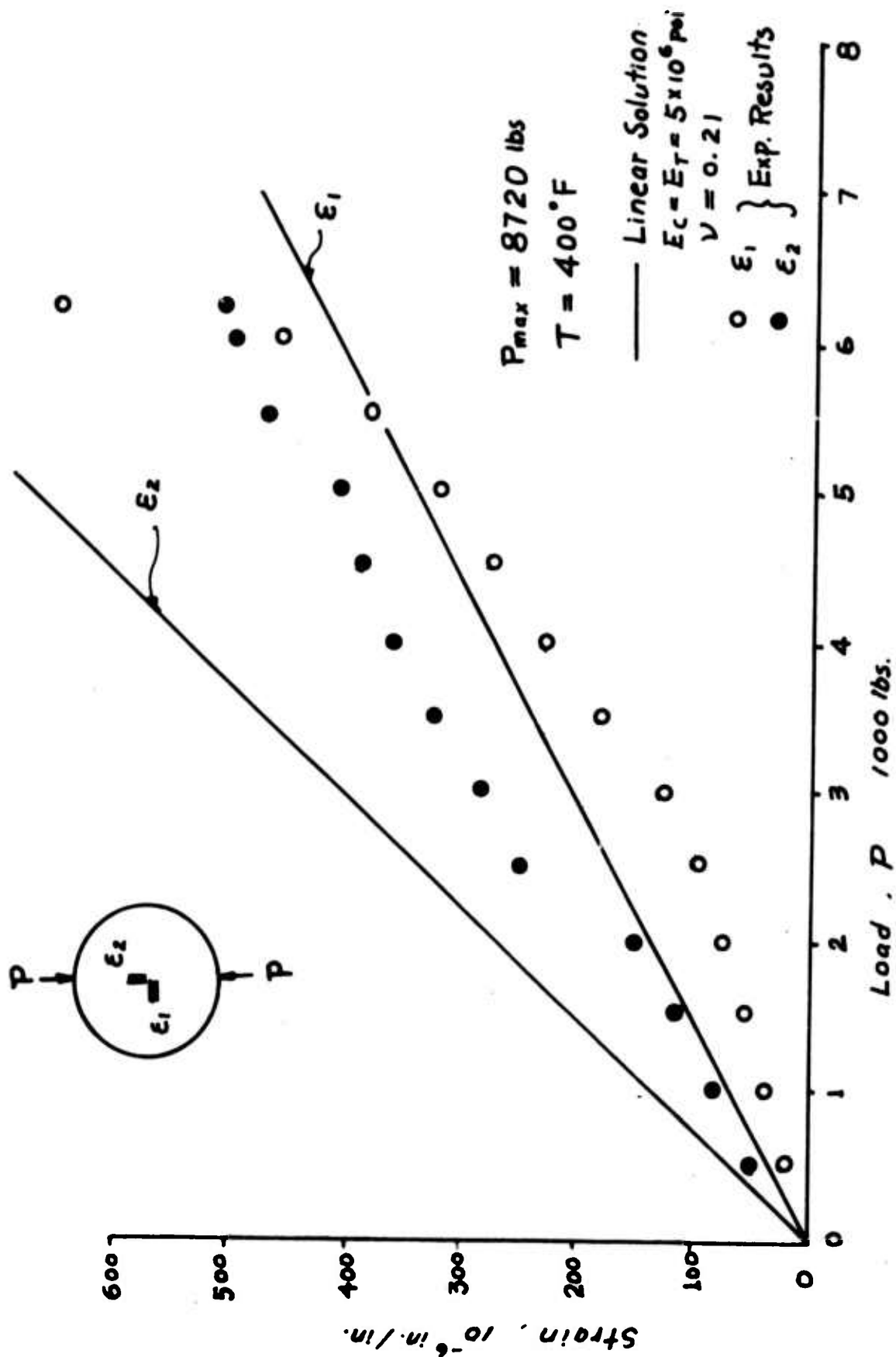


FIGURE 44 Diametral Compression Test Results (Charcoal Granite)

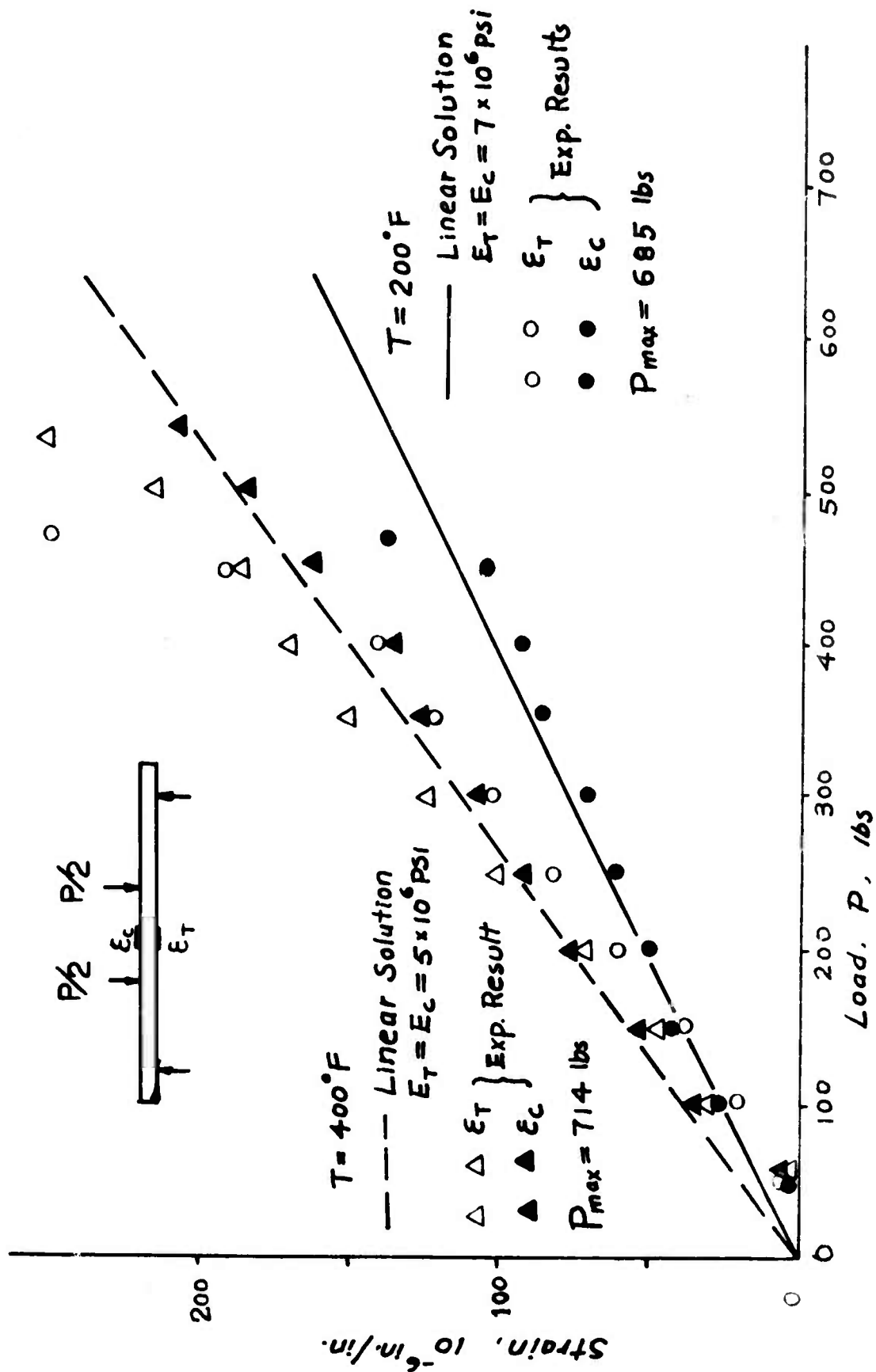


FIGURE 45 Beam Test Results (Charcoal Granite)

4.0 CONCLUSIONS

On the basis of results obtained from this study, the following conclusions are drawn:

1. A survey of literature on different tensile and compressive strengths and moduli of different rock types, indicates that the ratio of tensile modulus to compressive modulus ranges from 0.05 to 1.00. In order to solve problems involving these materials, the difference of moduli in tension and in compression must be taken into consideration. Henceforth, a bilinear elastic theory was developed. The bilinear elastic theory differs from the classical linear elastic theory in that two Young's moduli, one for tension and one for compression, are assumed for bilinear analysis while for linear analysis a common Young's modulus is used. It was proven that dilatational and deviatoric stresses and strains are interrelated, a fact which is not indicated in the classical theory of elasticity. This interrelation was investigated for pure shear stress state which indicates that applying pure shear stress gives rise to a nonvanishing axial strain and dilatational strain.
2. Three different boundary value problems, a beam under pure bending, a circular opening under internal pressure, and a disk under diametral compression, were analyzed. The results indicate that when $E_t < E_c$ the critical tensile stresses developed in these three problems are reduced. However, the critical tensile strain for a beam under bending is increased. These results point out the fact that when these three types of tests were used for the characterization of the "tensile strength" of bilinear materials, care must be exercised in the interpretation of the test results.
3. Results of unconfined compressive tests on charcoal granite at different temperatures indicate that at lower temperature (75°F to 500°F)

the stress-strain relations are time-independent; above that temperature, the stress-strain relations become time-dependent. The results also indicate that at lower stress, the stiffness of the material is relatively low and the stress-strain relations are nonlinear. As the applied stress increases, the slope of the stress-strain curves increase until threshold stresses are reached; beyond that stress, the stress-strain relations for each temperature become linear.

4. Results of uniaxial tension tests on charcoal granite at elevated temperature (up to 700°F) show that the material is almost elastic, no measureable time-dependent strain and no irrecoverable strain.

5. Results of uniaxial tension and compression tests on Dresser basalt indicate that the material exhibits creep at elevated temperature (about 450°F). The compressive Young's modulus of Dresser basalt is found to be dependent on temperature. The modulus decreases from about 5.5×10^6 psi to 4.0×10^6 psi for temperature increase from 73°F to 810°F.

6. The results of the maximum tensile strains and compressive strains measured during the diametral compression tests and beam bending tests on charcoal granite can be predicted fairly accurately by using linear elastic solutions. This is due to the fact that the compressive modulus at small stress (as defined by the slope of the stress-strain curves) is smaller and is nearly equaled to the tensile modulus. Although, at higher stress level (about 4,000 psi and higher) the compressive modulus is higher than the tensile Young's modulus. The ultimate tensile strengths of charcoal granite as determined from uniaxial tension tests, beam bending tests and diametral compression tests are about 800 psi, 1400 psi, and 1800 psi, for temperature ranged from 72°F to 400°F.

REFERENCES

- i. Griggs, D. T., "Creep of Rocks," J. Geophys. Res., 74, 3, 1939.
 "Experimental Flow of Rocks Under Condition Favoring Recrystallization," Geol. Soc. Am. Bull., p. 1001-1022, 1940.
2. Höfer, K., "Bertrag zur Grage der Standfestigkeit von Bergfesten in Kalibergbau," Freiberger Forschungsh, A100, 1958.
3. Obert, L. and Duvall, W. I., Rock Mechanics and the Design of Structures in Rock, John Wiley & Sons, Inc. 1967.
4. Heard, H. C., "The Effects of Large Changes of Strain Rate in the Experimental Deformation Rock," J. Geol., 71, 2, 1963.
5. Le Comte, P., "Creep and Internal Friction in Rock Salt," Doctoral Thesis, Harvard Univ., 1960.
6. Walsh, J. B., "The Effects of Cracks on the Compressibility of Rock," J. Geophys. Res., 70, 2, p. 381-389, 1965.
 "New Measurement of Linear Compressibility of Rock," J. Geophys. Res., 70, 2, p. 391-398, 1965.
 "The Effects of Cracks on the Uniaxial Compression Rocks," J. Geophys. Res., 70, 2, p. 399-411, 1965.
 "The Effects of Cracks in Rocks on Poisson's Ratio," J. Geophys. Res., 70, p. 5249-5257, 1965.
7. Hokao, Z., "Thermal Fracturing of Rocks By a Thermo-Drill," J. of the Faculty of Eng., University of Tokyo, 30, 3, 1970.
8. Byerlee, J. D., "Brittle-Ductile Transition in Rocks," J. Geophys. Res., 73, p. 4721-4750, 1968.
9. Fischer, R. L. and Cheung, J. B., "Thermoviscoelastic Properties of Rock at Elevated Temperatures," submitted for publication in the proceedings of the Intl. Conf. on Creep and Fatigue in Elevated Temp. Applications, Philadelphia, Pa.
10. Adams, L. H. and Williamson, E. D., "The Compressibility of Minerals and Rock at High Pressure," J. Franklin Inst., 195, p. 475-529, 1923.
11. Birch, F., "The Velocity of Compressional Wave in Rocks to 10 kb,"
 1, J. Geophys. Res., 65, p. 1083-1102, 1960.
 2, J. Geophys. Res., 66, p. 2199-2224, 1961.
12. Brace, W. F., "Brittle Fracture of Rocks," Paper presented at Int. Conf. on State of Stress in the Earth Crust, Preprints of Paper, Mem. RM-3538, Rand Co., 5, 1963.

13. Morgenstern, N. R., "Non-linear Stress-Strain Relations for a Homogeneous Sandstone," Int. J. Rock Mech. Sci., 6, p. 127-142, 1969.
14. Prager, W., "On Ideal Locking Materials," Trans Soc. Rheology, 1, p. 169-175, 1957.
 "On the Formulation of Constitutive Equation for Living Soft Tissues," 27, p. 128-132, 1969.
15. Haimson, B.C. and Tharp, T. M., "Reas Stresses Around Boreholes,"
16. Ambartsumyan, S. A. and Khachatryan, A. A., "The Basic Equation of and Theory of Elasticity for Materials with Different Tensile and Compressive Strengths," J. of Mechanics of Solids, 1, No. 2, (1970).
17. Herrmann, L. R., "Bilinear Elasticity with Application to Thick-Walled Cylinders," University of California, Institute of Eng. Research Report, (Feb. 1962).
18. Blatz, P. J. and Levinson, M., "Stress Induced Anisotropy in Pressurized Thick Walled Cylinders," California Institute of Technology, Graduate Aeronautical Laboratories Report GALCIT SM 62-6, (Jan. 1962).
19. Timoshenko, S. P. and Goodier, J. N., Theory of Elasticity, McGraw-Hill, 1970.
20. Greenspan, D., Introductory Numerical Analysis of Elliptic Boundary Value Problem, Harper and Row publisher, New York, 1965.
21. Conte, S. D., Elementary Numerical Analysis, McGraw-Hill, New York, 1965.
22. Wilson, E. L., "Structural Analysis of Axisymmetric Solids," AIAA J., 3, (1965).